Permafrost in Switzerland

2014/2015 to 2017/2018

Glaciological Report (Permafrost) No. 16–19

2019

Permafrost in Switzerland

2014/2015 to 2017/2018

Glaciological Report (Permafrost) No. 16–19

Swiss Permafrost Monitoring Network

Edited by

Jeannette Nötzli[1], Cécile Pellet[2] and Benno Staub[2]

PERMOS Office

[1]WSL Institute for Snow and Avalanche Research SLF

[2]Department of Geosciences, University of Fribourg

2019

Publication of the Cryospheric Commission of the Swiss Academy of Sciences (SCNAT)

ISSN 2296-6153 (Online)
ISSN 2296-6145 (Print)

Swiss Permafrost Monitoring Network (PERMOS)
c/o Department of Geosciences
University of Fribourg
Chemin du Musée 4
CH–1700 Fribourg
www.permos.ch
office@permos.ch

Citation

PERMOS 2019. Permafrost in Switzerland 2014/2015 to 2017/2018. Noetzli, J., Pellet, C. and Staub, B. (eds.), Glaciological Report Permafrost No. 16–19 of the Cryospheric Commission of the Swiss Academy of Sciences, 104 pp, doi:10.13093/permos-rep-2019-16-19.

Data availability

This report is based on the PERMOS data set published under DOI 10.13093/permos-2019-01.

Cover page

Drilling of a replacement borehole in rock glacier Corvatsch-Murtèl in September 2015. Photo: J. Nötzli.

Imprint

Project management and editing
Jeannette Nötzli, Cécile Pellet and Benno Staub

Authors

Jan Beutel	Computer Engineering and Networks Laboratory, ETH Zurich: Chapter 6
Reynald Delaloye	Department of Geosciences, University of Fribourg: Chapters 6–7
Christin Hilbich	Department of Geosciences, University of Fribourg: Chapter 4, Appendix C
Coline Mollaret	Department of Geosciences, University of Fribourg: Chapter 4, Appendix C
Jeannette Nötzli	WSL Institute for Snow and Avalanche Research SLF, Davos: Chapters 1–3, 8, Appendices A–B
Cécile Pellet	Department of Geosciences, University of Fribourg: Chapters 4–8, Appendix C
Marcia Phillips	WSL Institute for Snow and Avalanche Research SLF, Davos: Chapter 5

Site maintenance, data acquisition and preprocessing (PERMOS Partners)

- Department of Geography, University of Zurich (UZH): Tobias Bolch, Isabelle Gärtner-Roer, Johann Müller, Andreas Vieli, Samuel Weber
- Department of Geosciences, University of Fribourg (UniFR): Reynald Delaloye, Christian Hauck, Christin Hilbich, Martin Hölzle, Coline Mollaret, Cécile Pellet, Benno Staub, Julie Wee
- Institute of Earth Sciences, University of Applied Sciences and Arts of Southern Switzerland (SUPSI): Cristian Scapozza
- Institute of Earth Surface Dynamics, Faculty of Geosciences and Environment, University of Lausanne (UniL): Christophe Lambiel
- Institute for Geotechnical Engineering (IGT-ETH), Laboratory of Hydraulics, Hydrology and Glaciology (VAW–ETH) and Computer Engineering and Networks Laboratory (TIK-ETH), ETH Zurich: Sarah M. Springman (IGT), Daniel Farinotti (VAW), Luisa Pruessner (VAW), Jan Beutel (TIK)
- WSL Institute for Snow and Avalanche Research SLF, Davos (SLF): Jeannette Nötzli, Marcia Phillips

Review
PERMOS Scientific Committee
PERMOS Steering Committee
MeteoSwiss (Chapter 2)

Summary translation
Cristian Scapozza (Italian)

Printed by
Ebnöther Joos AG, print & publishing, CH–8135 Langnau am Albis

Published Reports

The PERMOS concept and annex were approved by the permafrost coordination group on November 18, 1999 and by the Cryospheric Commission of the Swiss Academy of Science (Expertenkommission Kryosphäre EKK; former Glaciological Commission) on January 14, 2000 and were published in 2000. Annual reports on «Permafrost in Switzerland» started in 1999. The reports listed below are available for download on the PERMOS website www.permos.ch or as hardcopy from the PERMOS Office.

Reporting period	*Report No.*	*Year*
1999/2000	1	2001
2000/2001 and 2001/2002	2/3	2004
2002/2003 and 2003/2004	4/5	2007
2004/2005 and 2005/2006	6/7	2009
2006/2007 and 2007/2008	8/9	2010
2008/2009 and 2009/2010	10/11	2013
2010/2011 to 2013/2014	12–15	2016
2014/2015 to 2017/2018	16–19	2019

Preface

While thinking about writing this preface, a melody is running in my mind. The repetitive lyrics of a song I occasionally heard on the French-speaking radio seem to be particularly well suited: « …c'est l'année la plus chaude de tous les temps… l'année la plus chaude de tous les temps… l'année la plus chaude de tous les temps… » (the warmest year ever). This song was composed by a French artist, Raphaël, in May 2017 and is part of an album rightfully entitled Anticyclone…

The present report covers the years 2015–2018, which was the warmest 4-year period ever measured in Switzerland and probably the warmest since earlier centuries. Despite some masking effects mainly caused by the inter-annual variability of snow conditions, permafrost is warming everywhere in the Swiss Alps. There is a very strong disequilibrium between the surface temperatures (the annual means are already rising above 0 °C at most locations surveyed in the PERMOS network) and the (still existing) permafrost conditions at depth. Permafrost temperatures are getting closer and closer to 0 °C, and consecutively permafrost is tending to degrade. This means that the permafrost is containing more and more pore water at the bounds between ice and rock particles of any size, and that it is gradually thawing, as attested, for instance, by the increasing active layer depths. Even if the climate stopped to warm, which is far from any modelled scenario, there would be no real chance to see this trend being reversed: the current disequilibrium is so important, that the permafrost will certainly continue to warm, degrade and progressively thaw for decades. And given the actual climate scenarios, it will do so in an even accelerated way (I do not like to write this sentence, but this is the reality).

PERMOS was launched with the major objective of insuring the best feasible long-term collection of data documenting the changes in permafrost conditions in the Swiss Alps. Two decades later, the objective of PERMOS could be adapted to: documenting the degradation of the permafrost in the Swiss Alps. 20 years ago, almost nobody fully realized, how challenging this task would be. How can a change of a few tenths of degrees near the melting point at depth be satisfactorily measured over decades? Measurement drifts and uncertainties are often larger than the actual temperature change. Who did think that so many rock glaciers would move several metres per year and that measuring a displacement rate larger than a centimetre per day would have become relatively common? Will PERMOS be able to document the future degradation of permafrost in steep rock walls? And there are so many other questions…

Besides the fundamental and very much acknowledged support of all the partner institutions, PERMOS can only function with the strong personal investment of so many persons who contribute directly or indirectly to the data acquisition. This has no monetary value (never appears in a budget) and I would like to take the opportunity to thank all of them so much! As I do for Jeannette, Cécile and formerly Benno for their great job in the Office!

May 2019, Reynald Delaloye

Summary

The present report on permafrost in the Swiss Alps covers the four hydrological years 2014/2015 to 2017/2018. The state of permafrost in the Swiss Alps and its changes are observed within the Swiss Permafrost Monitoring Network (PERMOS) based on ground temperature measurements near the surface and at depth, changes in ice content determined from geophysical surveys, and creep velocities of rock glaciers derived from terrestrial geodetic surveys.

The report covers the warmest 4-year period of hydrological years ever recorded since measurements began in 1864. In contrast, the winter conditions during the reporting period were both, extremely poor and rich in snow. There was very little and late snow in winter 2016/2017 (in some regions already in winter 2015/2016), whereas in winter 2017/2018 the snow arrived rather early and snow heights were far above average.

Ground surface temperature (GST) measurements reflect atmospheric conditions and the duration and thickness of the snow cover. They have been continously high since 2009 for all regions and sites. At locations that are influenced by a winter snow cover, mean annual GST were higher than during the previous reporting period but they did not reach the maxima from 2003. The active layer thickness increased for most sites during the reporting period with many new record values observed in summer 2015 and 2018. The ground temperatures measured in boreholes at 10 and 20 m depth show that the warming trend that started in the year 2009 was interrupted at the snow-influenced field sites following the snow poor winter 2017 (in some regions already after winter 2016). The warming trend resumed in the uppermost metres after the hot summer 2018. At depth, however, the cooling is still visible and the warm conditions have not yet arrived.

Electrical resistivities measured within the permafrost layer at five sites showed a similar overall decreasing trend since the beginning of the measurements, except at Les Attelas where no clear trend was observed. Unlike the ground temperatures and the rock glacier creep velocities, no significant interruption of the trend was observed in the electrical resistivities following the snow-poor winter 2016/2017. Terrestrial geodetic surveys of rock glaciers show a common general behaviour: permafrost creep velocities continuously increased during the years 2007 until 2015 and decreased in 2016 and 2017, which is consistent with the decrease in permafrost temperatures after the snow-poor winter 2016/2017.

In summary, all elements observed within the PERMOS network during the reporting period 2014/2015–2017/2018 show a warming trend since the year 2009, which was temporarily interrupted at snow-influenced sites following the snow-poor winter 2016/2017, despite the constantly above-average air temperatures. However, the continuously decreasing electrical resistivities point to a persisting loss in ground ice and continuously warming permafrost conditions. Continuously warm permafrost conditions were observed at sites with temperatures close to 0 °C and at locations in steep and snow-free rock walls.

Zusammenfassung

Der vorliegende Bericht über den Permafrost in den Schweizer Alpen umfasst die vier hydrologischen Jahre 2014/2015 bis 2017/2018. Der Zustand und die Veräderungen des Permafrostes in den Schweizer Alpen werden im Rahmen des Schweizerischen Permafrostmessnetztes (PERMOS) beobachtet, basierend auf Temperaturmessungen nahe an der Oberfläche und in der Tiefe, Veränderungen des Eisgehalts aus geophysikalischen Untersuchungen sowie Kriechgeschwindigkeiten von Blockgletschern aus terrestrischer geodätischer Vermessung.

Der Bericht umfasst die wärmste hydrologische 4-Jahresperiode seit Beginn der Messungen im Jahr 1864. Im Gegensatz dazu waren die Winter im Berichtszeitraum sowohl extrem schneearm als auch schneereich. Im Winter 2016/2017 gab es sehr wenig und späten Schnee (in einigen Regionen bereits im Winter 2015/2016), während im Winter 2017/2018 der Schnee früh kam und die Schneehöhen weit über dem Durchschnitt lagen.

Die Messungen der Bodenoberflächentemperatur (GST) spiegeln die atmosphärischen Bedingungen sowie Dauer und Dicke der Schneedecke wider. Sie waren seit 2009 für alle Regionen und Standorte kontinuierlich hoch. An Standorten mit einer winterlichen Schneedecke war die durchschnittliche jährliche GST höher als im vorhergehenden Berichtszeitraum, erreichte die Maxima von 2003 aber nicht. Die Auftautiefe hat für die meisten Standorte im Berichtszeitraum zugenommen und in den Sommern 2015 und 2018 wurden an vielen Standorten neue Rekordwerte gemessen. Die Bohrlochtemperaturen in 10 und 20 Meter Tiefe zeigen aufgrund des schneearmen Winters 2017 (in einigen Regionen bereits nach dem Winter 2016) an den Schnee-beeinflussten Standorten einen Unterbruch des im Jahr 2009 begonnenen Erwärmungstrends. Nach dem heißen Sommer 2018 setzte sich der Erwärmungstrend in den obersten Metern wieder fort. In der Tiefe dominiert jedoch noch die Abkühlung und der Erwärmungstrend hat noch nicht wieder eingesetzt.

Die an fünf Standorten im Permafrost gemessenen elektrischen Widerstände zeigen seit Beginn der Messungen einen rückläufigen Gesamttrend, mit Ausnahme von Les Attelas, wo kein eindeutiger Trend beobachtet werden kann. Im Gegensatz zu den Bodentemperaturen und den Kriechgeschwindigkeiten der Blockgletscher wurde bei den elektrischen Widerständen nach dem schneearmen Winter 2016/2017 kein signifikanter Unterbruch des Erwärmungstrends beobachtet. Die terrestrische Vermessung der Blockgletscher zeigt ein gemeinsames Muster: Die Kriechgeschwindigkeiten nahmen in den Jahren 2007 bis 2015 kontinuierlich zu und sanken in den Jahren 2016 und 2017. Dies stimmt mit der Abnahme der Permafrosttemperaturen nach dem schneearmen Winter 2016/2017 überein.

Zusammenfassend lässt sich sagen, dass alle im Berichtszeitraum 2014/2015–2017/2018 im PERMOS-Netzwerk beobachteten Elemente seit dem Jahr 2009 einen Erwärmungstrend aufweisen, der trotz konstant überdurchschnittlicher Lufttemperaturen an schneebedeckten Standorten nach dem schneearmen Winter 2016/2017 vorübergehend unterbrochen wurde. Die kontinuierlich abnehmenden elektrischen Widerstände deuten jedoch auf einen anhaltenden Verlust von Untergrundeis und eine kontinuierliche Erwärmung des Permafrostes hin. Kontinuierlich warme Permafrostbedingungen wurden an Standorten mit Temperaturen nahe 0 °C und an Standorten in steilen und schneefreien Felswänden beobachtet.

Résumé

Ce rapport sur le pergélisol dans les Alpes suisses couvre quatre années hydrologiques de 2014/2015 à 2017/2018. L'état du pergélisol dans les Alpes suisses ainsi que ses changements sont documentés au sein du réseau suisse d'observation du pergélisol (PERMOS) sur la base de mesures de la température du sol près de la surface et en profondeur, des changements de la teneur en eau liquide déterminés par des mesures géophysiques et des vitesses de fluage des glaciers rocheux dérivées des levés géodésiques terrestres (TGS).

Ce rapport couvre la période de quatre années hydrologiques la plus chaude jamais observée depuis le début des mesures en 1864. Au cours de cette même période, les conditions d'enneigement ont au contraire été extrêmement variable avec à la fois des hivers pauvres et riches en neige. Au cours de l'hiver 2016/17, il y a eu très peu de neige (dans certaines régions c'était déjà le cas durant l'hiver 2015/2016), alors qu'au cours de l'hiver 2017/2018 la neige est arrivée tôt et les hauteurs de neige étaient bien au-dessus de la moyenne.

Les mesures de la température à la surface du sol (GST) reflètent les conditions atmosphériques ainsi que la durée et l'épaisseur de la couverture neigeuse. Depuis 2009, elles sont continuellement élevées dans toutes les régions et sur tous les sites. Aux endroits qui sont influencés par une couverture neigeuse hivernale, la GST annuelle moyenne a été plus élevée qu'au cours de la période du rapport précédent, mais elle n'a pas atteint les maximums observés en 2003. L'épaisseur de la couche active a augmenté sur la plupart des sites au cours de la période couverte par ce rapport, avec de nombreux nouveaux records atteints au cours des étés 2015 et 2018. Les températures du sol mesurées dans les forages à 10 et 20 m de profondeur montrent que la tendance au réchauffement amorcée en 2009 a été interrompue aux sites influencés par une couverture neigeuse à la suite des hivers 2016 (dans certaines régions) et surtout 2017. La tendance au réchauffement a repris dans les premiers mètres après l'été chaud de 2018. Cependant, le refroidissement est encore visible en profondeur et les conditions chaudes de la surface n'ont pas encore atteint ces couches du pergélisol.

Les résistivités électriques mesurées dans le corps du pergélisol à cinq sites ont suivi la même tendance générale à la baisse depuis le début des mesures, sauf aux Attelas où aucune tendance claire n'a été observée. Les processus propres à chaque site ainsi que la variabilité interannuelle peuvent toutefois affecter ponctuellement cette tendance générale. Contrairement aux températures du sol et aux vitesses de fluage des glaciers rocheux, aucune interruption significative de la tendance n'a été observée dans les résistivités électriques à la suite de l'hiver pauvre en neige de 2016/2017. Les résultats des mesures TGS sur les glaciers rocheux montrent un comportement général commun: les vitesses de fluage du pergélisol n'ont cessé d'augmenter entre 2007 et 2015 et ont diminué en 2016 et 2017, ce qui correspond à la baisse des températures du pergélisol après l'hiver pauvre en neige de 2016/2017.

En résumé, tous les éléments observés par le réseau PERMOS au cours de la période couverte par ce rapport (2014/2015-2017/2018) montrent que la tendance continue au réchauffement observée depuis 2009 a été temporairement interrompue dans les sites influencés par la neige en raison d'un ou de deux hivers pauvres en neige et ce malgré des températures de l'air constamment au-dessus de la moyenne. Toutefois, la diminution continue de la résistivité électrique indique une perte persistante de glace et un réchauffement continu des conditions du pergélisol. Des conditions continuellement chaudes ont été observées dans le pergélisol aux sites dont la température avoisine 0 °C et dans les parois rocheuses abruptes sans neige.

Riassunto

Questo rapporto sul permafrost nelle Alpi svizzere concerne i quattro anni idrologici dal 2014/2015 al 2017/2018. Lo stato e l'evoluzione del permafrost nelle Alpi svizzere sono osservati nell'ambito della Rete svizzera di monitoraggio del permafrost (PERMOS) sulla base di misurazioni della temperatura vicino alla superficie del suolo e in profondità, della variazione del contenuto in acqua liquida determinata da prospezioni geofisiche, della velocità di reptazione dei ghiacciai rocciosi derivata da rilievi geodetici terrestri (TGS).

Il rapporto copre il quadriennio costituito dagli anni idrologici più caldi mai registrati dall'inizio delle misurazioni nel 1864. Per contro, le condizioni invernali in questo quadriennio sono state estremamente scarse e ricche di neve. L'innevamento è stato scarso e tardivo nell'inverno 2016/2017 (in alcune regioni già nell'inverno 2015/2016), mentre nell'inverno 2017/2018 la neve è caduta piuttosto precocemente e l'innevamento è stato superiore alla media.

Le misurazioni della temperatura della superficie del suolo (GST) riflettono le condizioni atmosferiche e la durata e lo spessore del manto nevoso. Dal 2009, GST è stata costantemente elevata per tutte le regioni e per tutti i siti. Nelle località che sono maggiormente influenzate dalla copertura nevosa invernale, GST media annua è stata superiore a quella del periodo del rapporto precedente, ma non ha raggiunto i valori massimi del 2003. Lo spessore dello strato attivo è aumentato per la maggior parte dei siti durante il presente quadriennio con molti nuovi valori record misurati nelle estati 2015 e 2018. La temperatura del suolo misurata in perforazione a 10 e 20 metri di profondità mostra che la tendenza al riscaldamento iniziata nel 2009 si è interrotta nei siti maggiormente influenzati dalla copertura nevosa a seguito degli inverni scarsamente innevati del 2016 (in alcune regioni) e, soprattutto, del 2017. La tendenza al riscaldamento è però ripresa nella parte superiore del suolo dopo l'estate calda 2018. Il raffreddamento è tuttavia ancora visibile in profondità, dove le condizioni calde non sono ancora arrivate.

La resistività elettrica misurata nel corpo del permafrost in cinque siti ha mostrato una simile tendenza generale di diminuzione dei valori dall'inizio delle misurazioni, ad eccezione degli Attelas, dove non è stata osservata alcuna tendenza chiara. A differenza delle temperature del suolo e delle velocità di reptazione dei ghiacciai rocciosi, nessuna interruzione significativa della tendenza è stata osservata nella resistività elettrica misurata dopo l'inverno scarsamente innevato 2016/2017. I risultati del monitoraggio TGS dei ghiacciai rocciosi mostrano un comportamento generale comune: la velocità di reptazione del permafrost è aumentata continuamente dal 2007 al 2015 e diminuita nel 2016 e 2017, il che è coerente con la diminuzione della temperatura del permafrost dopo l'inverno scarsamente innevato 2016/2017.

In sintesi, tutti gli elementi osservati all'interno della rete PERMOS durante il periodo 2014/2015–2017/2018 presentano una tendenza al riscaldamento dal 2009 che è stata temporaneamente interrotta nei siti maggiormente influenzati dall'innevamento a seguito di uno o due inverni scarsamente nevosi, e questo nonostante la temperatura dell'aria sia stata costantemente superiore alla media. Tuttavia, la diminuzione continua della resistività indica una perdita persistente di ghiaccio nel suolo e un riscaldamento continuo del permafrost. Condizioni di permafrost temperato costanti sono state osservate nei siti dove la temperatura è prossima a 0 °C, sulla base delle resistività geoelettriche, o in quelli situati su pareti rocciose ripide e prive di neve.

Contents

1 Introduction

This report on permafrost in the Swiss Alps presents the data and results obtained by the Swiss Permafrost Monitoring Network PERMOS during the four hydrological years 2014/2015 to 2017/2018. The reporting period corresponds to the PERMOS Agreement 2015–2018. PERMOS documents the state of permafrost and its changes based on field data measured in the Swiss Alps since 2000. The evaluation and adaptation of the observation strategy as well as the operationalisation and standardisation of the infrastructure, the project and data management as well as the reporting have been ongoing since the start of the network.

Today, PERMOS builds on substantial and long-term financial support from the joint partnership of MeteoSwiss in the framework of GCOS Switzerland, the Federal Office for the Environment (FOEN) and the Swiss Academy of Sciences (SCNAT). PERMOS is run by six Partner Institutions from Academia and is managed by the PERMOS Office. The Scientific Committee provides scientific advise on data acquisition and reporting strategies and the Steering Committee supervises the network. PERMOS is an important contribution to the National Climate Observing System (GCOS Switzerland) and is part of the Swiss cryosphere monitoring (www.cryosphere.ch). Within the international framework, PERMOS is an important contributor to the Global Terrestrial Network for Permafrost (GTN-P) of the Global Climate Observing System (GCOS), which is co-sponsored by the World Meteorological Organization (WMO), the Intergovernmental Oceanographic Commission of UNESCO (IOC-UNESCO), the United Nations Environment Programme (UN Environment), and the International Science Council (ISC). Within the five-tiered principle proposed for the Global Hierarchical Observing Strategy (GHOST, cf. Harris et al. 2001 for adaptation to permafrost observation) the national network mainly contributes to tiers 3 and 4. It provides observations to sample the range of environmental variation in permafrost thermal state as in tier 3 (regional observations at intermediate depths and regular time intervals) and aims to describe representative permafrost conditions based on the observation sites and elements as in tier 4 (ground thermal conditions to provide representative permafrost conditions).

The PERMOS observation strategy follows a landform-based approach because differences in the subsurface thermal regime due to topography and (sub-)surface conditions are considered more important in the small country than those due to varying climate conditions (Figure 1.1). The main landforms distinguished are rock walls (e.g., Birg at Schilthorn), crests (e.g., Jungfraujoch, Matterhorn-Hörnligrat, Schilthorn, Stockhorn), talus slopes (e.g., Flüela, Les Attelas, Lapires, Muot da Barba Peider), and rock glaciers (e.g., Murtèl-Corvatsch, Réchy, Schafberg, Valle di Sceru). The network observes three main elements: (1) ground temperatures near the surface and at depth, (2) changes in ice content, and (3) permafrost creep velocities. The three elements complement each other in order to deliver a comprehensive picture of changes in mountain permafrost in Switzerland.

Ground temperature (GT) measured at 16 borehole sites are the basis of the monitoring because they provide direct evidence of permafrost and its changes (Table 1.1, Figure 1.2, Chapter 3). They are complemented by temperature measurements near the ground surface (GST) to capture the influence of different surface cover types, topographic settings or snow characteristics. Temperature changes at depth integrate and filter the signal from the ground surface and reflect trends delayed, but more clearly. They are however often influenced by effects of 3D geometry and latent heat (Noetzli and Gruber 2009). When ice-rich permafrost is at temperatures

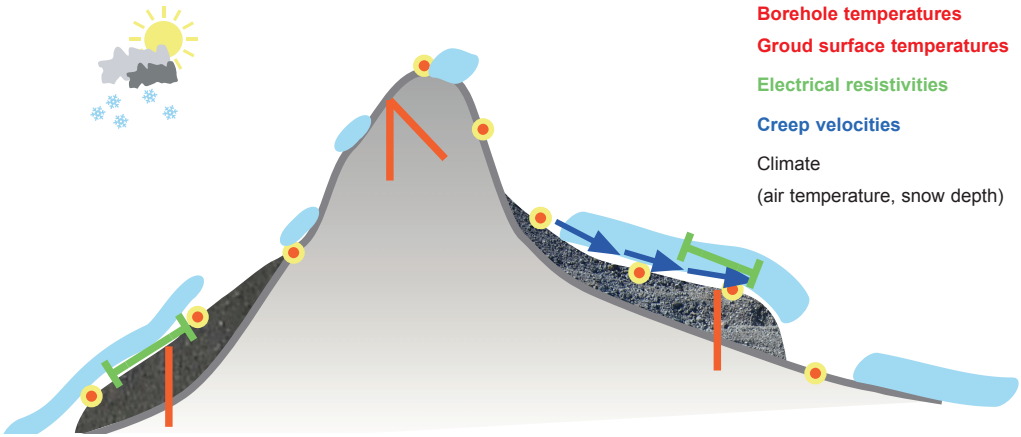

Figure 1.1: *Schematic sketch of the PERMOS observation strategy. The permafrost monitoring in the Swiss Alps builds on field measurements at sites with differing topographic settings and landform characteristics: ground temperatures near the surface and at depth, changes of electrical resistivities and creep velocities of rock glaciers.*

little below the melting point, only small or no changes can be observed because phase change is consuming up energy. This is a globally consistent picture (Biskaborn et al. 2019, Noetzli et al. 2018).

Electrical resistivity tomography (ERT) monitoring is performed at five borehole sites (Table 1.1, Figure 1.2, Chapter 4). Based on the differing electrical resistivities of frozen and unfrozen material and the calculation of their changes over time the changes in subsurface ice and unfrozen water content can be described. That way, important changes in permafrost can also be detected, where temperature changes are masked by latent heat effects.

The movement of rock glaciers is observed at 15 sites based on annual terrestrial surveys of a number of points on each landform (Table 1.1, Figure 1.3, Chapter 5). With increasing ground temperature and water contents, the creep velocities of rock glaciers generally also increase. This picture has been observed all over the European Alps (Delaloye et al. 2010). In addition, slope failures from permafrost areas are documented. Air photos taken at PERMOS sites allow the observation of creep velocities by photogrammetric analyses.

Two additional observation elements will be included for the period of the PERMOS Agreement 2019–2022 starting in 2019: 1) meteo data measured directly at the borehole sites and 2) permanent GNSS devices installed on rock glaciers. The latter complement the annual measurements to capture intra-annual signals. The observation strategy for the permanent GNSS devices was elaborated in a pilot study and is presented in Chapter 6.

As a result of the continuous evaluation and adaptation of the monitoring network, the Dreveneuse site will no longer be included in PERMOS from 2019. The site is located at around 1500 m asl. and is an example of low-elevation extra-zonal permafrost. Permafrost conditions have however no longer been observed since 2012. A final overview of the 14 years of continuous monitoring is given in Chapter 7.

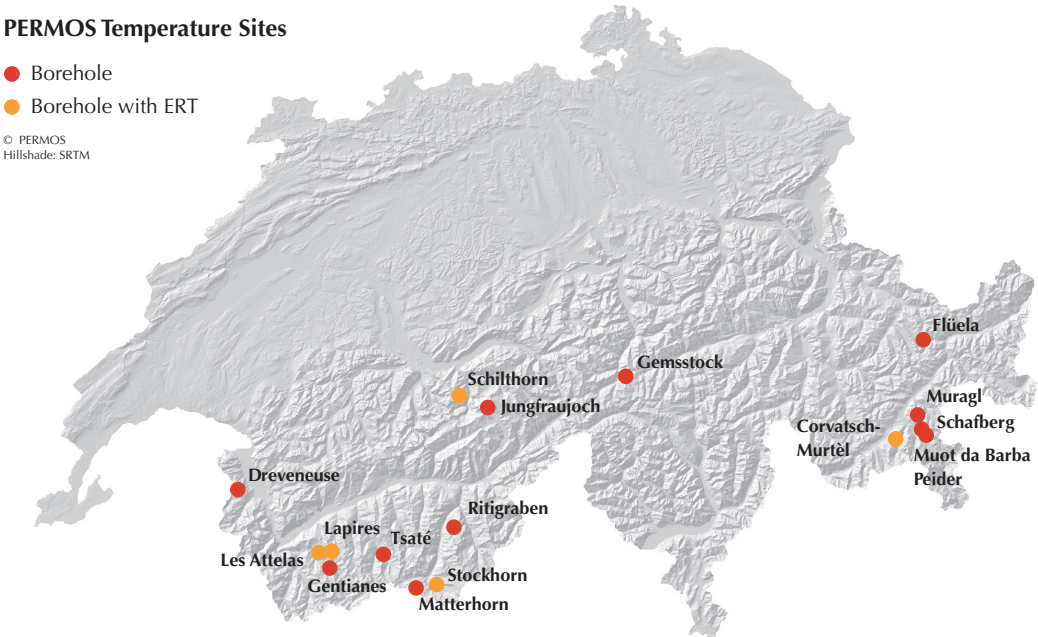

Figure 1.2: PERMOS temperature sites.

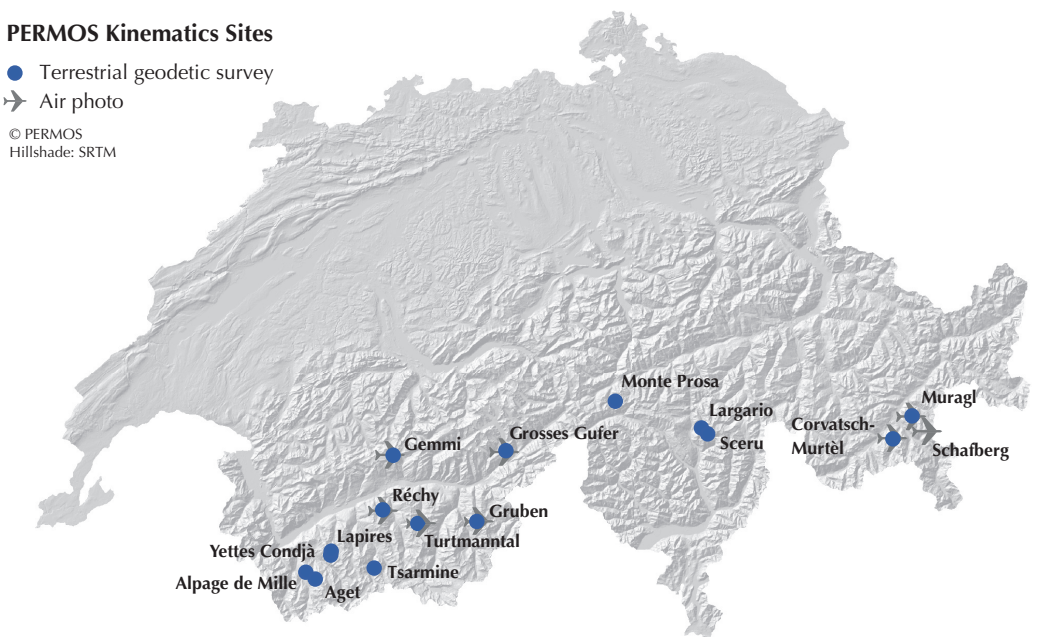

Figure 1.3: PERMOS kinematics sites.

Table 1.1 *Overview on the PERMOS sites, their main morphology and the type(s) of terrestrial measurements carried out. Sites are sorted regionally. BH=borehole, GST=ground surface temperature, RST=rock surface temperature, ERT=electrical resistivity tomography, TGS=terrestrial geodetic survey.*

Site	Institute(s)	Region	Morphology	BH	GST	RST	ERT	TGS
Jungfraujoch	SLF	Bernese Oberland	Crest	x				
Schilthorn	UniFR	Bernese Oberland	Crest	x	x	x	x	
Dreveneuse	UniFR	Chablais	Talus slope	x	x			
Corvatsch-Murtèl	UZH	Engadine	Rock glacier	x	x			x
Corvatsch-Murtèl	SLF	Engadine	Rock glacier			x		
Corvatsch-Murtèl	UniFR	Engadine	Rock glacier				x	
Corvatsch-Murtèl	ETHZ	Engadine	Rock glacier	x				
Flüela	SLF	Engadine	Talus slope	x				
Muot da Barba Peider	SLF	Engadine	Talus slope	x				
Muragl	ETHZ	Engadine	Rock glacier	x				
Muragl	UZH	Engadine	Rock glacier		x			x
Schafberg	SLF	Engadine	Rock glacier	x	x			
Aget	UniFR	Lower Valais	Rock glacier		x			x
Alpage de Mille	UniFR	Lower Valais	Rock glacier		x			x
Gentianes	UniL	Lower Valais	Moraine	x	x			
Lapires	UniFR	Lower Valais	Talus slope	x			x	x
Lapires	UniL	Lower Valais	Talus slope		x			
Les Attelas	UniL	Lower Valais	Talus slope	x	x		x	
Réchy	UniFR	Lower Valais	Rock glacier		x	x		x
Tsarmine	UniFR	Lower Valais	Rock glacier					x
Tsarmine	UniL	Lower Valais	Rock glacier		x			
Tsaté	UniL	Lower Valais	Crest	x	x			
Yettes Condjà	UniL	Lower Valais	Rock glacier		x			x
Monte Prosa	UniFR	Ticino	Rock glacier		x			x
Stabbio di Largario	SUPSI	Ticino	Rock glacier		x			x
Valle di Sceru	SUPSI	Ticino	Rock glacier		x			x
Gemmi-Furggentälti	UniFR	Upper Valais	Rock glacier		x			x
Grosses Gufer	UniFR	Upper Valais	Rock glacier		x			x
Gruben	UniFR	Upper Valais	Rock glacier		x			x
Matterhorn	SLF	Upper Valais	Crest	x				
Ritigraben	SLF	Upper Valais	Rock glacier	x				
Stockhorn	UniFR	Upper Valais	Crest	x	x		x	
Turtmanntal-Hungerlitälli	UZH	Upper Valais	Rock glacier		x			x
Gemsstock	SLF	Urner Alps	Crest	x		x		

The field work and site maintenance of the PERMOS network are carried out by the PERMOS Partner Institutions, which also carry the main work load of data acquisition:

- ETH Zurich: Institute for Geotechnical Engineering (IGT–ETH, until 2017), Laboratory for Hydraulics, Hydrology and Glaciology (VAW–ETH, from 2018) and Computer Engineering and Networks Laboratory (TIK–ETH)
- University of Applied Sciences and Arts of Southern Switzerland, Institute of Earth Sciences (SUPSI)
- University of Fribourg: Department of Geosciences (UniFR)
- University of Lausanne: Faculty of Geosciences and Environment, Institute of Earth Surface Dynamics (UniL)
- University of Zurich: Department of Geography, Glaciology and Geomorphodynamics Group (UZH)
- WSL Institute for Snow and Avalanche Research SLF, Davos (SLF)

2 Weather and Climate

Air temperature and snow cover are the weather and climate conditions, which have the largest influence on the inter-annual variations of the ground thermal regime and, hence, permafrost. Air temperature is an important factor for the energy balance at the ground surface at sites and in periods with little or no snow, that is during the summer period in debris slopes and rock glaciers and all year round in steep rock slopes. The snow cover insulates the ground from the atmospheric conditions, and therefore the time of the first snow fall, the duration and thickness of the snow cover and the time when the ground surface becomes snow free in spring are relevant.

The weather and climate conditions in the reporting years are compiled for hydrological years. They are based on the weather and climate information from MeteoSwiss (MeteoSwiss 2015, 2016, 2017, 2018, 2019) and snow data from the Intercantonal Measurement and Information System (IMIS) provided by the WSL Institute for Snow and Avalanche Research SLF. The timing and duration of the snow cover can additionally be determined based on continuous near ground surface temperature data (GST, cf. Chapter 3): the percolation of melt water provokes a sudden increase to 0 °C at the time when the snow cover is wet down to its base (start of the zero curtain). Then, GST remain almost stable (zero curtain) until the terrain becomes snow free and the temporal variability significantly increases.

2.1 Conditions in 2014/2015

In 2014, Switzerland experienced the second warmest autumn since the start of measurements in 1864 (cf. Figure 2.2). Only in the Southern Alps and the Engadine, autumn was wet and cloudy. The above-average temperatures continued in December and snow only fell in below-average quantities above around 1000 to 1500 m asl. At the end of the year, the weather changed to cold winter conditions with snowfall down to the lowlands north of the Alps. The first half of January was again extremely mild, but followed by a cold phase with widespread below-average temperatures and snowfall down to low altitudes until the end of February. Overall, winter 2014/2015 was mild with a surplus of 0.7 °C compared to the 1981–2010 norm. The regional distribution of snow depths remained constant during the entire winter: snow depth was almost twice as high as normal in the Gotthard region and the Southern Alps (excluding the southern valleys of Grisons). In the other regions they were about average.

Spring 2015 started sunny with high daily mean temperatures until mid-March. The month ended with snow and stormy conditions. In April the weather was sunny, mild and dry in the South, while May was very rainy. Snow depths, spring snow cover and timing of the melt out were about average at the permafrost observation sites (Figures 2.3 and 2.4). Summer 2015 was extremely warm: the fourth warmest June since the beginning of the measurement, was followed by the warmest July and the fifth warmest August. In all, summer 2015 was the second warmest in the 152-year history of measurements with a mean air temperatures about 2.5 °C above the 1981–2010 norm. The hot summer was followed by a cool beginning of autumn in September 2015.

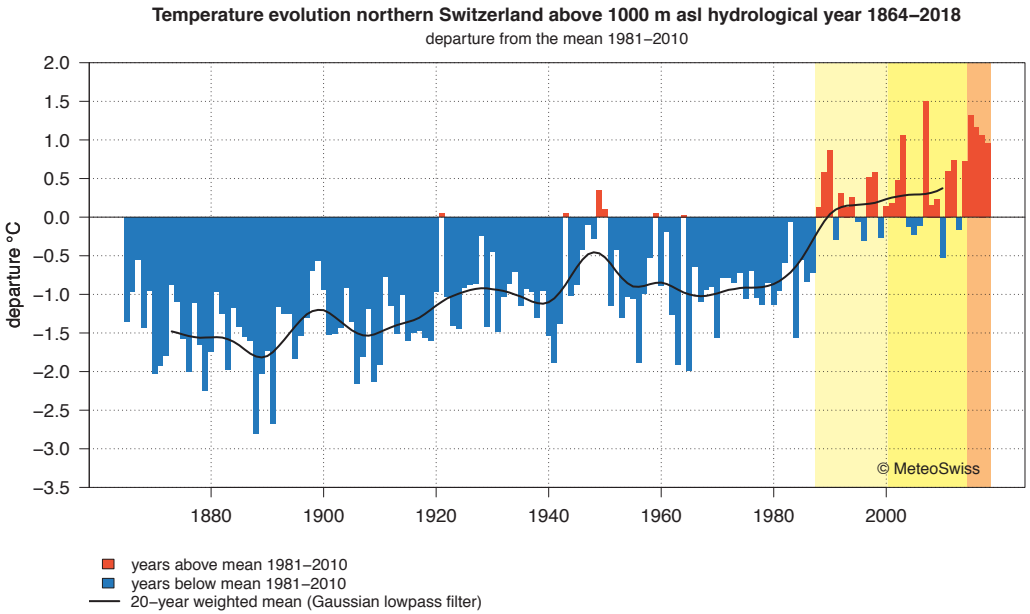

Figure 2.1: *Air temperature deviation from the norm 1981–2010 based on homogenised data series for Swiss stations above 1000 m asl. and hydrological years. The reporting period is highlighted in orange. The PERMOS Network started in the year 2000 (highlighted in yellow) and the longest time series from permafrost in Switzerland starts in the year 1987 (highlighted in light yellow). Adapted from MeteoSwiss (2019).*

2.2 Conditions in 2015/2016

October 2015 was somewhat colder than the norm 1981–2010 and first snowfalls occurred in the mountains (Figure 2.2). November and December were warmer than average and especially December was very dry. December was even the warmest ever measured with air temperatures 3.2 °C higher than the 1981–2010 norm, in mountain regions by up to 4–6 °C. Until the end of the year 2015, the mountains remained almost snow free, except for the Western Alps, where the November snow could persist. January and February 2016 were also about 2 °C warmer than average but with changeable weather. High precipitation was recorded in the northern and western parts of the Alps, whereas the Southern Alps remained dry in January. Despite the substantial precipitation in February and in March, the snow height reached average values only in the Western Alps, where the snow persisted throughout spring and led to a late melt out (Figures 2.3 and 2.4). Snow heights in the East and particularly in the South were lower than average.

Air temperatures in April 2016 were little above average in mountain regions. May was particularly wet and colder than average, which led to extensive snowfall events at higher altitudes and slowed down the snow melt above around 2500 m asl. In early summer, precipitation was still above average but air temperatures remained close to the norm. A wet June was followed by a warm July and August, which were both about 1 °C warmer

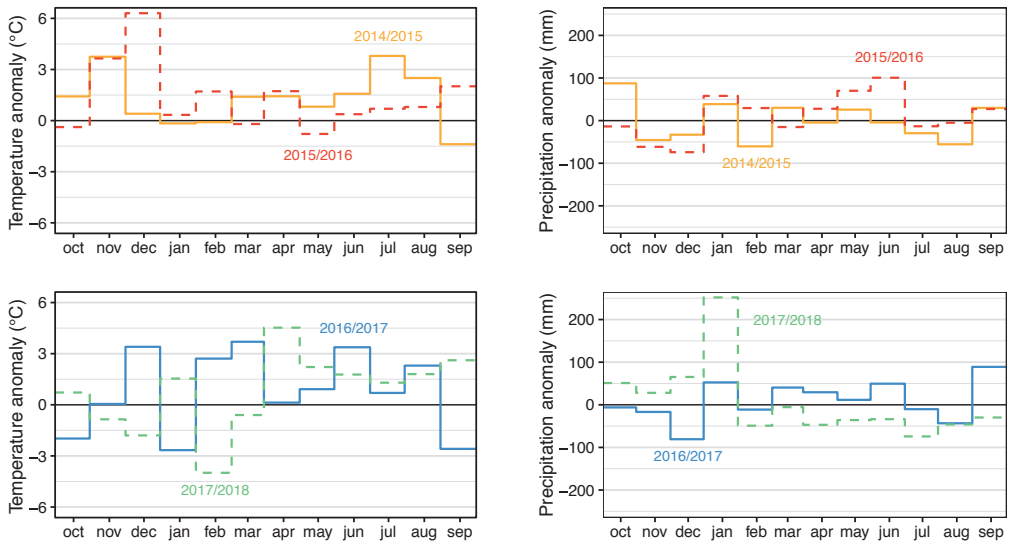

Figure 2.2: Mean monthly anomalies of air temperatures (left) and precipitation (right) from the long-term climatic mean (period 1981–2010) for the climate station at Weissfluhjoch and the reporting period. Data source: MeteoSwiss.

compared to the 1981–2010 period. The amount of summer precipitation was spatially variable, with only 50% of the average precipitation in the Valais. The last week of August was very warm followed by the third warmest September with temperatures 2.5 °C above average and only little precipitation.

2.3 Conditions in 2016/2017

October 2016 was rather cold in Switzerland, which led to the first snowfalls down to middle elevations. Large parts of the first half of November were cold as well and heavy snowfalls were recorded in the mountain regions. Due to persisting anticyclonic conditions, December was extremely dry and sunny. North of the Alps, December 2016 was the driest and the second warmest since the beginning of the measurements in 1864 (after December 2015). In the Western part of the Swiss plateau and the Valais, no precipitation was registered during the entire month. Due to the combination of high temperatures and lack of precipitation, a continuous snow cover only established late in January 2017, which was extremely cold. Conversely, February was very warm and record daily air temperatures were observed in many regions. Winter 2016/17 was the shortest (that is, the lowest number of days with a snow cover greater than 1 cm) since the beginning of the measurements in all regions of Switzerland and the one with the second lowest average snow height.

Spring 2017 was the third warmest since the beginning of the measurements in 1864 (+1.7 °C compared to the norm 1981–2010). This, together with the low snow heights, led to an early melt out of the snow cover (Figures 2.3 and 2.4). Summer 2017 was the third warmest ever measured (after 2003 and 2015, +1.9 °C). June was especially warm (+3.3 °C) with continuously high temperatures. It was followed by a slightly above average

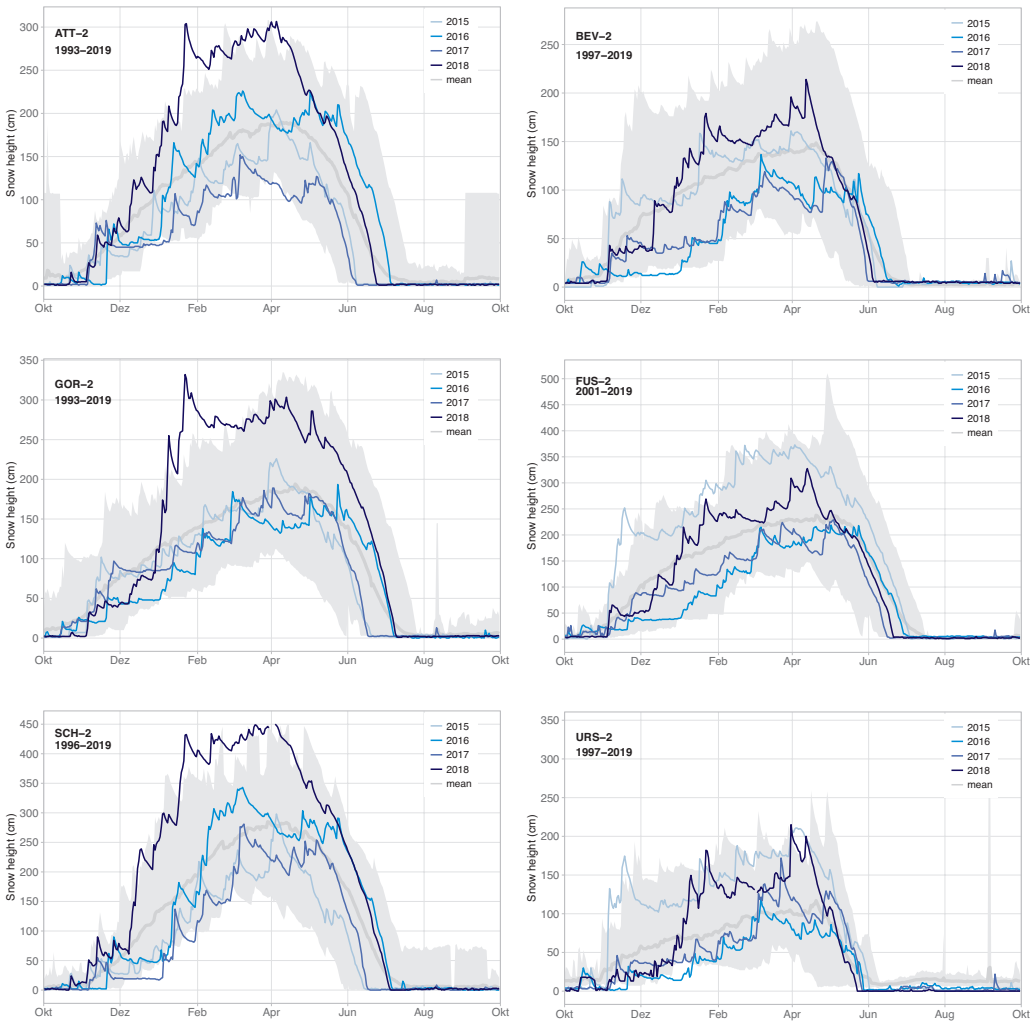

Figure 2.3: *Snow height at six IMIS stations during the four winters 2015–2018 compared to the mean (thick grey line), minimum and maximum (grey shaded area) of the previously measured data (before October 2014). Data were aggregated to daily means for plotting. The stations were selected to represent different permafrost regions in the Swiss Alps (cf. Table 1.1): Bernese Oberland: SCH-2, Urner Alps: URS-2, Engadine: BEV-2, Lower Valais: ATT-2, Upper Valais: GOR-2, Ticino: FUS-2. Data source: IMIS/SLF, www.slf.ch.*

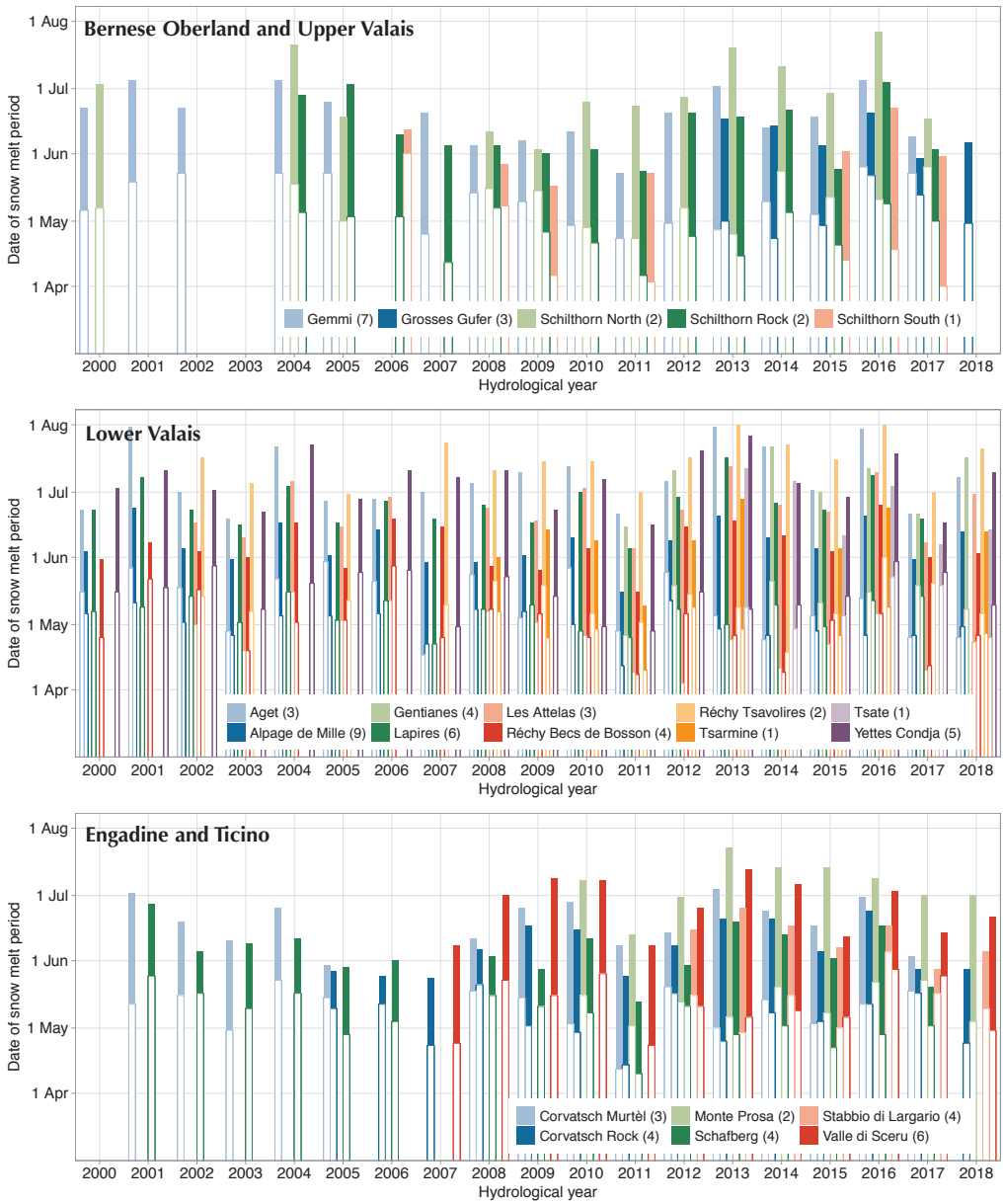

Figure 2.4: *Dates and duration of the snow melt period cacluated from ground surface temperature time series. The top and the bottom of the coloured bars indicate the mean of the start and the end of the zero curtain period for each site. All sites used for the calculation are located at elevations between 2300 and 2800 m asl. The number in brackets corresponds to the number of GST locations used for the site mean.*

July and a warm August. September 2017 was rather cold again, especially in the mountain areas, where fresh snow fell several times (a new record was established on Weissfluhjoch, where snowfalls occurred 15 times in September).

2.4 Conditions in 2017/2018

October 2017 was very dry and sunny due to persisting anticyclonic conditions, especially in the South. The first snowfalls occurred in November both at high and low elevation. December was also rich in snowfall, which yielded well above-average snow heights in all permafrost regions (+170% compared to the norm). In January 2018, another period of intense snow occurred (with record values all over the Alps and extreme snowfall only occurring every 75 years. During winter 2017/2018, air temperatures were in the order of the norm period 1981–2010, but with high variability: January was rather warm especially in the lower regions, whilst February was about 3 °C colder than normal. Until March, snow heights were above average, but they decreased very rapidly during a warm and dry spring, especially in April and May (Figures 2.3 and 2.4). Winter 2018 was extremely snow-rich but spring to autumn were extremely warm and dry with only about 70% of the normal precipitation.

After 2003 and 2015, the summer 2018 was the third warmest ever measured in Switzerland. Heat waves occurred north (end of July) and south (July) of the Alps for periods of 10–18 days. Following a dry spring, also summer 2018 was extremely dry and characterized by record amounts of sunshine. The dry and warm conditions persisted in September making 2018 the warmest ever measured summer semester (April–September).

2.4 Summary

The report covers the warmest 4-year period of hydrological years ever recorded since measurements began in 1864. All four hydrological years 2014/2015–2017/2018 are among the six warmest hydrological years ever measured at elevations above 1000 m asl. in Northern Switzerland (Figure 2.1). When considering calendar years, the years 2015 and 2018 marked new records of mean annual air temperatures. Also on a monthly or seasonal basis many record values were recorded. In contrast to the very high air temperatures, the thickness and duration of the snow cover during the reporting period were both, extremely poor and rich in snow. There was very little and late snow in winter 2016/2017 – in the eastern and southern part also in winter 2015/2016 – and in winter 2017/2018 the snow arrived rather early and snow heights were far above average.

3 Ground Temperatures

Long-term monitoring of permafrost primarily relies on ground temperatures (GT) continuously measured in boreholes because they are the only direct observations. Borehole temperature measurements are complemented by recordings of near ground surface temperatures (GST) because their changes are the main driving factor of changes in GT and, hence, changing permafrost conditions. GST measurements in the vicinity of the boreholes or on rock glaciers help to assess the spatial variability of the site and the representativeness of the borehole (Chapter 3.1).

The maximum annual thawing depth, the active layer thickness (ALT), is a reflection of the local snow and atmospheric conditions reigning during the current and previous year and is additionally influenced by local ground characteristics such as ground ice content or surface cover. The ALT is defined as the maximum depth of the 0 °C isotherm in the ground during one year and is determined from borehole temperature measurements (Chapter 3.2).

GT measured in boreholes down to a medium depth of around 10 m allow the observation of short-term and intra-annual temperature variations. At about 10 metres depth, temperatures no longer react to short-term (i.e., daily or weekly) fluctuations of atmospheric conditions but reflect the seasonal variations. Here, GT measurements reveal how air temperature and snow duration regulate ground temperatures at a regional to national scale. At about 10 metres depth, maximum temperatures occur in late winter because it takes about six months for a signal at the surface to penetrate to this depth. Further down at around 20 m depth, the seasonal signal is hardly visible and the time lag to the changes at the surface is in the order of years. Temperature changes at greater depth are governed by long-term changes at the surface and trends are reflected filtered and delayed (Chapter 3.2).

3.1 Ground surface temperatures

Ground surface temperature (GST) is measured at three main types of locations: (i) in steep bedrock, where the influence of topography is maximal and the relation to atmospheric conditions is direct (no thicker snow or debris cover is present); (ii) in gently sloping or flat bedrock, where a snow cover builds up during winter, and (iii) within coarse blocks or debris slopes, where often air circulation takes place in the uppermost layer. The temperatures are continously recorded with a temporal resolution of 1 to 3 hours. Miniature temperature loggers are placed little below the surface to avoid the influence of direct shortwave radiation and to capture a slightly filtered temperature signal. In bedrock, Geoprecision M-Log devices (www.geoprecision.de) are installed. In loose sediments, UTL–1 and UTL–3 (www.geotest.ch) or Maxim iButtons® (www.maximintegrated.com) are used.

In total, GST are measured at 23 PERMOS sites, each with 4 to more than 20 individual GST locations (Table 3.1). Half of the measurements are taken on rock glaciers or moraines (51%), a third in debris slopes (30%), and the rest in steep or flat bedrock (13%) or in soil or vegetation (6%). A relatively thick snow pack typically develops during winter at the GST locations with snow depth from about 0.5 to more than 3 m, except for the locations in near-vertical bedrock and a few that are wind-exposed. An early snow cover following a warm autumn

Table 3.1: Overview on the PERMOS GST sites, the start of the measurements, the elevation as well as the number of GST locations in different surface types.

Site name	year	n	max h (m asl.)	min h (m asl.)	bedrock steep	bedrock snow	debris	coarse blocks	other
Aget	1998	7	2915	2829	–	–	6	1	–
Alpage de Mille	1997	18	2450	2230	–	–	4	10	4
Corvatsch	2001	23	3300	2535	6	6	–	11	–
Dreveneuse	2004	6	1630	1565	–	–	–	6	–
Gemmi	1994	23	2653	2452	–	–	3	19	1
Gemsstock	2012	5	2931	2907	3	2	–	–	–
Gentianes	2010	10	2897	2864	–	–	6	2	1
Grosses Gufer	2012	5	2542	2389	–	–	5	–	–
Gruben	2012	5	2897	2817	–	–	–	5	–
Lapires	1998	23	2770	2375	–	–	6	12	5
Les Attelas	2001	13	2768	2640	–	–	9	3	1
Monte Prosa	2009	4	2530	2482	–	–	–	4	–
Muragl	2018	5	2533	2624	–	–	–	5	–
Rechy	1997	13	3140	2590	–	–	–	13	–
Schafberg	2000	8	2741	2722	–	–	–	8	–
Schilthorn	1998	31	2968	2410	1	6	24	–	–
Stabbio di Largario	2011	6	2469	2290	–	–	–	6	–
Stockhorn	2011	5	3383	3413	–	–	5	–	–
Tsarmine	2007	6	2600	2488	–	–	–	6	–
Tsate	2007	6	3065	3025	–	3	3	–	–
Turtmanntal-Hunger.	2010	14	2495	2859	–	–	–	22	–
Valle di Sceru	2006	10	2569	2460	–	1	3	6	–
Yettes Condjà	1998	13	2810	2600	–	2	2	8	1

and an early snow melt in spring leads high GST, while a late snow cover in autumn and a late snow melt result in a cooling of the ground surface. A detailed description of the GST locations was published in PERMOS (2013).

The parameters derived from the GST measurements are:

(i) the surface offset, which is the difference of the mean annual GST (MAGST) to the mean annual air temperature (MAAT),
(ii) the duration and timing of the snow cover (results are shown in Chapter 2),
(iii) the ground freezing index (GFI) and the thawing index (THI), which is the sum of all daily negative (resp. positive) temperatures measured during one hydrological year. The GFI and THI indicate how cold or warm a year was at the ground surface, and
(iv) MAGST calculated as running mean to represent inter-annual GST variations.

To calculate these parameters the GST time series were first aggregated to daily mean values. Then they were gap-filled using the approach by Staub et al. (2017), which also allows to estimate the resulting uncertainty for

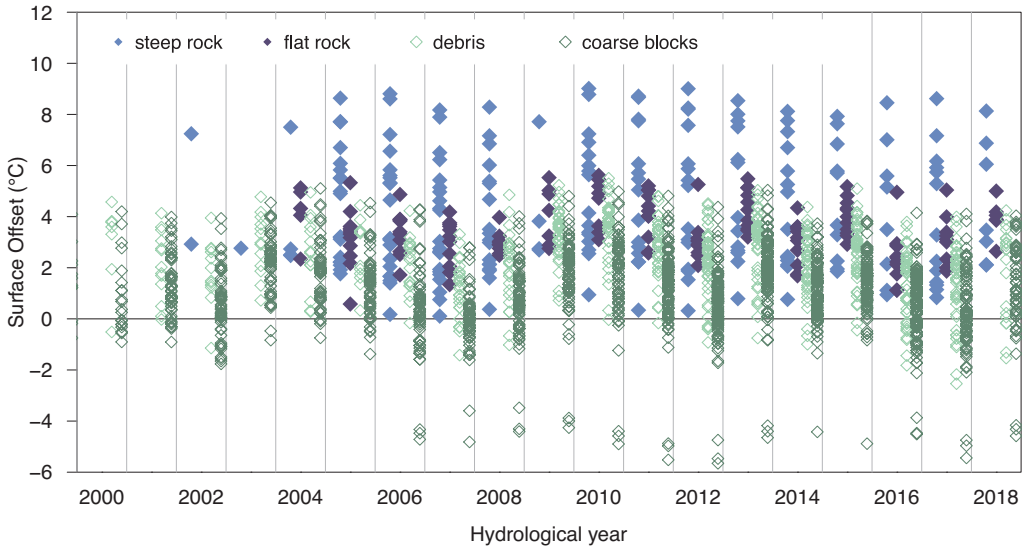

Figure 3.1: Calculated surface offset for mean annual ground surface temperatures for the hydrological years 2000–2018 and different surface types: steep rock (light blue), flat rock (dark blue), debris (light green) and coarse blocks (dark green).

aggregates and indices. The parameters (ii) to (iv) were calculated for each individual GST location and then averaged at the site scale using selected GST locations (see Appendix A with figures for each site and all GST locations used for the site mean). The selection takes into account the length and completeness of the time series (at least 5 years of data and 90% of all daily values). GST locations with special characteristics are not considered (e.g., strong air circulation, outside the main landform). Separate means were calculated for GST locations in bedrock in steep and snow influenced locations (e.g., Corvatsch or Schilthorn), on different landforms (e.g., Réchy) or with different aspects (e.g., Schilthorn) at one site.

(i) Surface offset

The surface offset was calculated for each GST location and all hydrological years (Figure 3.1) and with air temperature data from MeteoSwiss (stations Corvatsch and Jungfraujoch). The MAAT were extrapolated to the elevation of the GST locations using a constant lapse rate of 0.006 °C m^{-1}.

MAGST is generally higher than MAAT in GST locations in bedrock. In south-exposed near-vertical locations the surface offset amounts to up to 10 °C and in north-exposed locations MAGST is only slightly higher than MAAT. This is mainly a result of strongly varying shortwave incoming radiation between south- and north-exposed slopes. The MAGST can be considerably lower than MAAT in debris slopes and coarse blocky terrain with extreme values of surface offsets up to –6 °C for the ventilated talus slope at Dreveneuse (see Chapter 7).

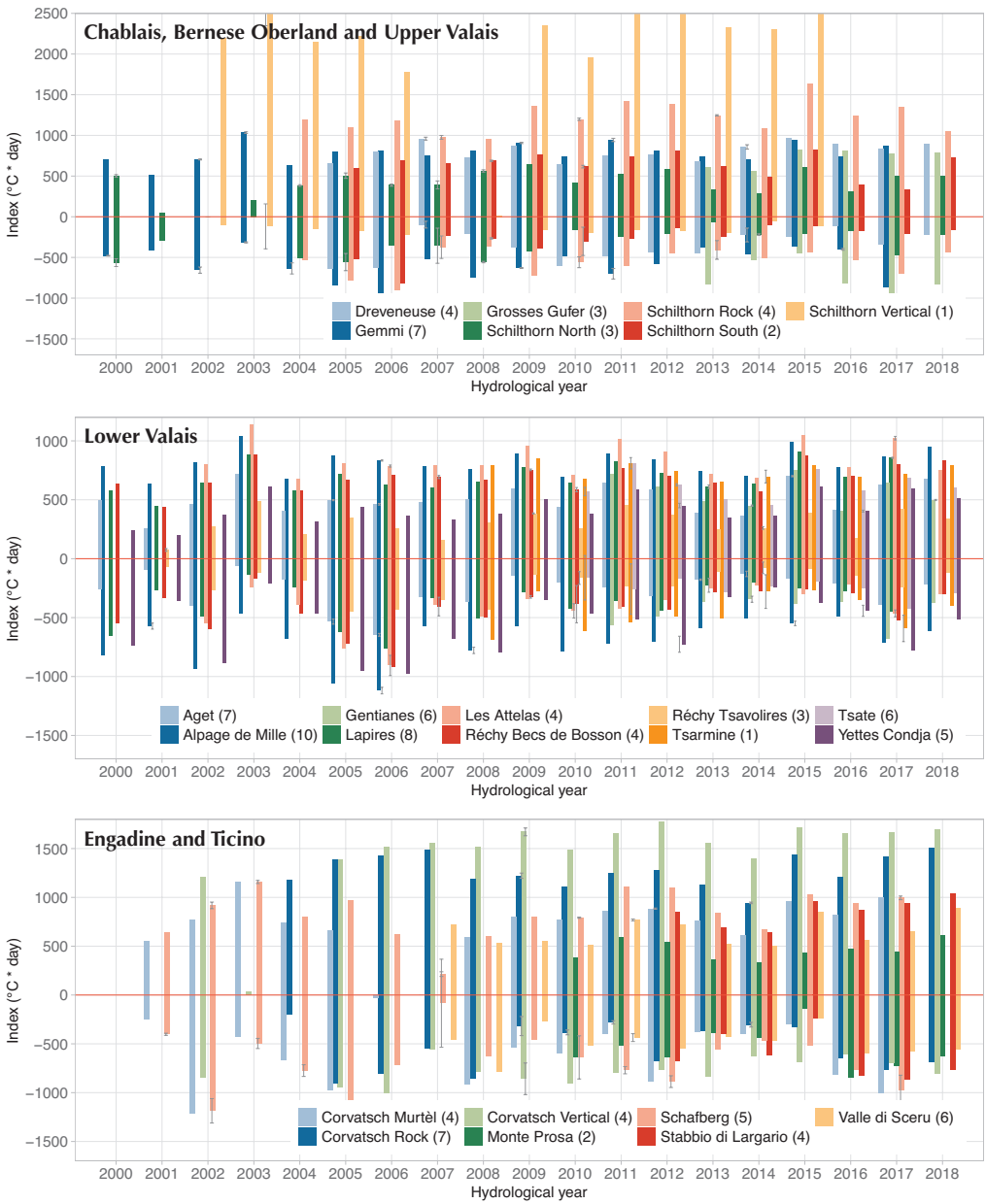

Figure 3.2: *Ground freezing and thawing index (GFI/THI) at GST sites: Upper Valais/Bernese Oberland/ Chablais (top), Lower Valais (middle) and Engadine/Ticino (bottom). The error bars show the estimated uncertainty from the filling of data gaps. The number in brackets denotes the number of GST locations used to calculate the site mean.*

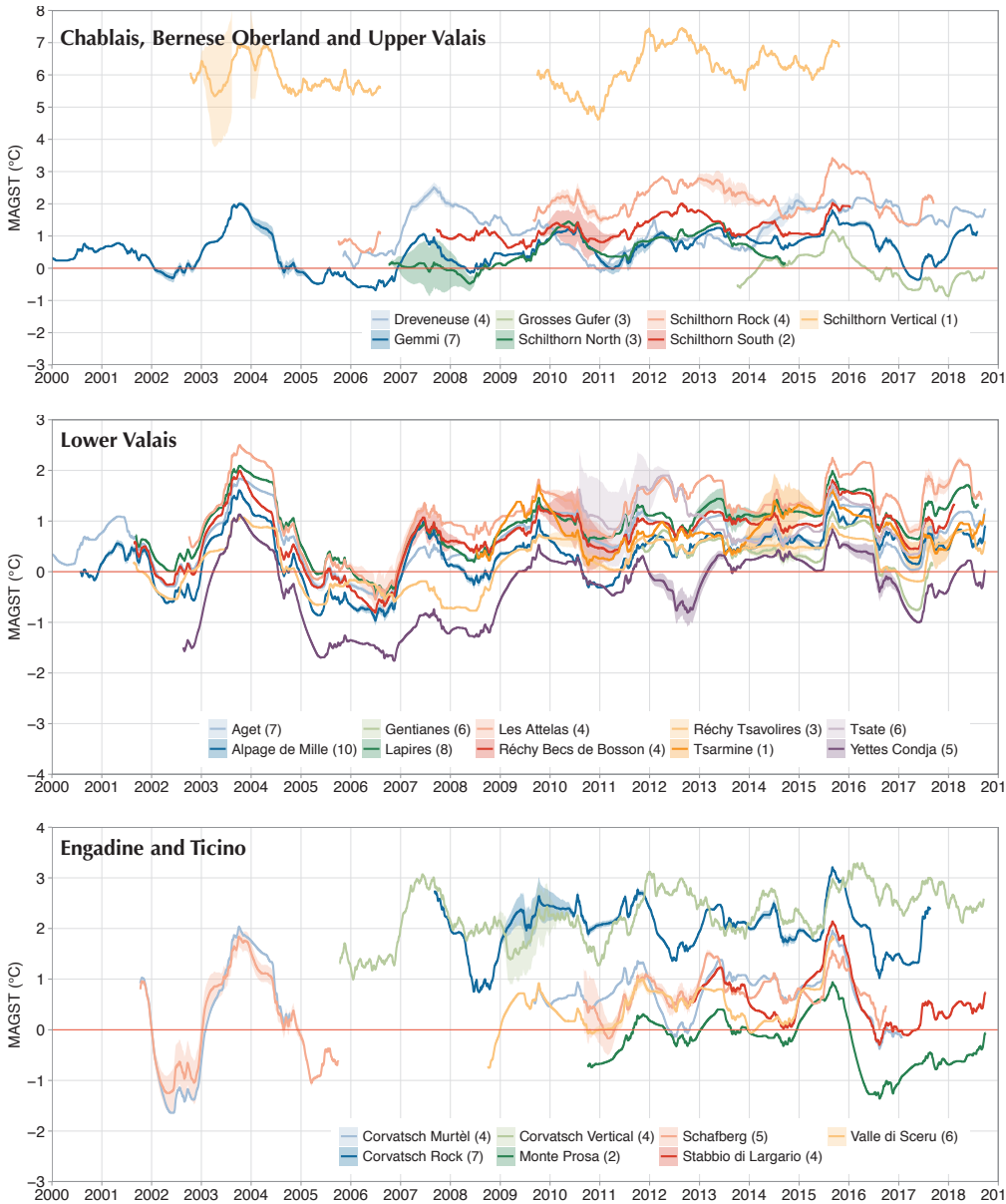

Figure 3.3: *Running annual mean of the ground surface temperature (MAGST) for the PERMOS sites distributed in different regions: Upper Valais/Bernese Oberland/Chablais (top), Lower Valais (middle) and Engadine/Ticino (bottom). The MAGST is calculated from gap-filled daily time series. The shaded areas illustrate the estimated uncertainty range resulting from gap-filling. The number in brackets denotes the number of GST locations used to calculate the site mean.*

(iii) Ground freezing (GFI) and thawing indices (THI)

In the hydrological year 2014/2015, the GFI was in the order of the three preceding years. The GFI was lower in the following three years, especially in the hydrological year 2016/2017 (Figure 3.2). The THI was slightly higher during the reporting period (i.e. warmer conditions) than in the preceding years, but still remained below the maxima observed after summer 2003. The highest THI was calculated for 2014/2015, because of the early melt-out and the high air temperatures in this hydrological year (cf. Chapter 2.1). The lowest THI values were obtained for 2015/2016 (cf. Chapter 2.2).

(iv) Mean annual ground surface temperature

The average MAGST for the PERMOS sites is shown in Figure 3.3 for three different regions in the Swiss Alps. MAGST are calculated using a 365-day running mean aggregated at the end of the period. That is, the MAGST plotted for a specific date reflects the mean of the 365-day period.

MAGST at locations where a thicker snow cover develops during winter show the combined influence of air temperature during the snow free period and the timing and duration of the snow cover (e.g. Gemmi, Aget, Yettes Condjà or Monte Prosa). The average MAGST for the sites remain at a comparably high level from 2009 onwards. The maximum recorded in the year 2003 was however not reached during the reporting period, although air temperature was clearly above average for all four hydrological years and new record values of daily GST were observed in summer 2015 and 2018 at several GST locations. The majority of site means reacts

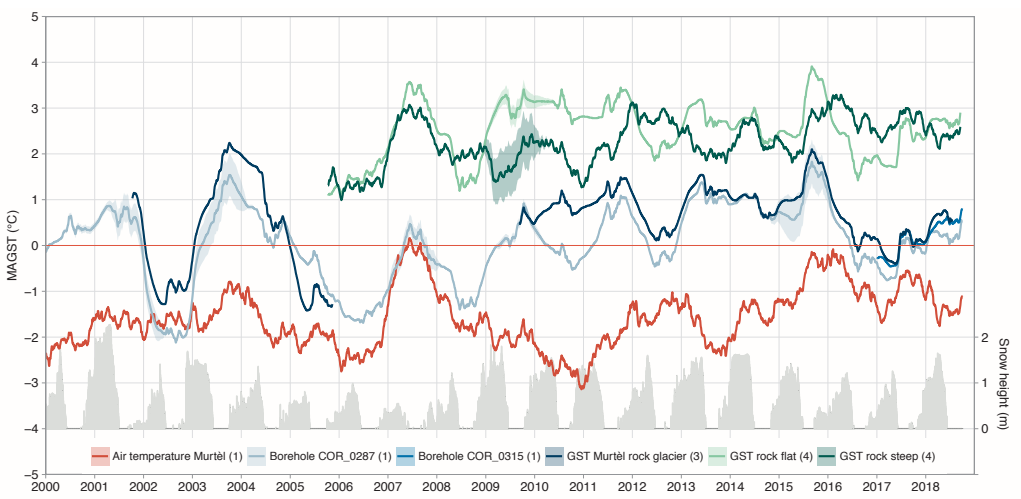

Figure 3.4: *Annual running means of ground surface temperatures at locations with different surface characteristics at the site Corvatsch-Murtèl compared to air temperature and snow height measured at the borehole site. For the different groups, the mean GST of several loggers was calculated: on rock glacier Murtèl, in flat bedrock, or in near-vertical bedrock. In addition, data from the uppermost thermistors in the boreholes COR_0287 (0.55 m) and COR_0315 (0.25 m) are shown. The snow height is displayed in grey at the bottom.*

similarly in terms of relative changes over time. Differences are typically related to different snow regimes (e.g., north and south exposition at the Schilthorn) or to site-specific processes (e.g., ventilated parts of talus slopes as observed at Dreveneuse or Lapires). For example in the hydrological year 2015/2016, the earlier snow cover in the Western Alps led to higher MAGST than in the Eastern and Southern Alps. In the East and South, winter 2016/2017 was the second consecutive winter with a late snow cover.

GST locations in near-vertical bedrock show a different behaviour because their temporal evolution predominantly follows air temperature and is not modified by a snow cover. Most of these time series only start in the year 2004 or later. But due to their high correlation with air temperature (Gruber et al. 2004) they are expected to be at record level with maxima in the hydrological years 2011/2012 and 2015/2016 following the hot summers in 2011 and 2015. This is supported by the correlation described below and by Figure 3.4.

The different behaviour of MAGST at sites with different surface types and snow regime is summarized in Figure 3.4 for the site Corvatsch-Murtèl. MAGST measured in steep rock, on flat bedrock, on the rock glacier Murtèl in coarse blocks as well as in the boreholes COR_0287 and COR_0315 (uppermost thermistor, see Chapter 3.2) are compared to the MAAT measured at the borehole site. The correlation coefficients (Pearson) obtained for the running MAAT with the running MAGST for the period 2006–2018 are 0.80 for the mean of GST locations in steep rock and only 0.27 for the uppermost thermistor in borehole COR_0287. The correlation coefficient for the mean of the snow influenced GST locations is in the same range as for the borehole COR_0287.

3.2 Borehole measurements

Borehole temperatures are measured at 16 sites in the Swiss Alps. The sites are located at elevations between 1580 m asl. (Dreveneuse) and 3400 m asl. (Stockhorn) with boreholes drilled in bedrock or in loose debris and blocks on rock glaciers, scree slopes, or moraines (see Table 1.1, Figure 1.4, Table B.1). At each site, 1–3 boreholes of 20–100 m depth are operated and ground temperatures are automatically logged with time intervals between 1 and 24 hours (daily recordings are a mean of several measurements during one day). The longest time series in mountain permafrost is measured in the 60 m deep borehole drilled in 1987 in rock glacier Murtèl-Corvatsch (GR) and reached 30 years during the reporting period, which is the typical length of a reference period for climate-related studies. Several time series now cover 15 years or more: Flüela, Gentianes, Lapires, Muot da Barba Peider, Muragl, Ritigraben, Schafberg, Schilthorn and Stockhorn.

3.2.1 Active layer thickness

As the ground in Alpine terrain typically consists of blocks, boulders or rock, methods to determine the active layer thickness (ALT) used in polar regions, such as probing or frost tubes, cannot be applied in mountain permafrost. ALT is calculated by linear interpolation between neighbouring thermistors in boreholes. Because freezing/thawing processes are not linear (latent heat effects), the results should be regarded as an approximation. The values obtained are more accurate the closer they are to the lower thermistor used for the interpolation, especially for ice-rich sites. Trends observed in the development of the ALT are however considered robust.

The ALT for the years 2015–2018 was determined for all boreholes wherever data availability and thermal conditions allow (Table 3.2, Figure 3.5). For several boreholes no ALT can be determined because they are not located in permafrost (GEM_0106, MUR_0199, DRE_0104), do not reach the surface (JFJ_0195), had considerable data

gaps in summer or autumn (MAT_0205, TSA_0104, SBE_0290) or the maximum ALT for the year 2018 occurred after the last manual data collection (ATT_0108, ATT_0208, MBP_0196, MBP_0296, SBE_0190). Figures showing ALT for all years and boreholes are provided in Appendix B.

ALT remained more or less constant or slightly increased during the reporting period in several boreholes with ice-rich subsurface: ATT_0108, ATT_0208, COR_0200, FLU_0102, GEN_0102, RIT_0102. A number of boreholes registered ongoing and gradual active layer deepening, for example COR_0287, LAP_1108, LAP_1208, SBE_0290, SCH_5198, SCH_5000, STO_6000 or STO_6100. New record ALT were observed at several sites after the very hot and dry summers 2015 and 2018, for example at Corvatsch-Murtèl, Lapires, Schilthorn or Stockhorn. No significant ALT decrease was observed during the reporting period.

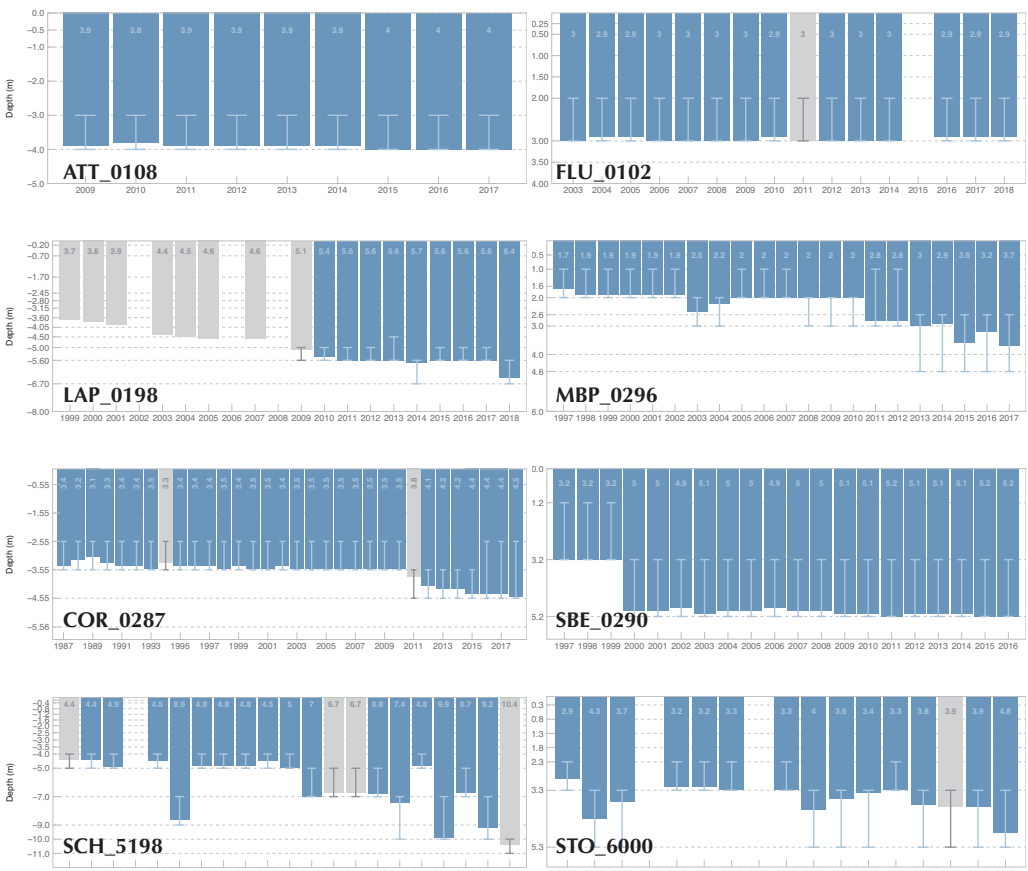

Figure 3.5: *Active layer thickness for selected PERMOS boreholes. The error bars indicate the depth of the thermistors used for the interpolation. Grey bars indicate years with reduced data quality.*

Table 3.2: Active layer thickness (ALT) interpolated from borehole temperature measurements in metres. Values given in grey and italic are best guess values because of data gaps or reduced data quality.

Name	2015		2016		2017		2018	
	ALT	Date	ALT	Date	ALT	Date	ALT	Date
Attelas 0108	4.0	29.08.	4.0	18.09.	4.0	26.08.	–	–
Attelas 0208	5.0	04.08.	5.0	29.09.	5.0	14.08.	5.0	17.09.
Corvatsch 0200	2.5	18.09.	–	–	–	–	–	–
Corvatsch 0287	4.4	01.09.	4.4	28.08.	4.4	25.09.	4.5	02.09.
Corvatsch 0315	–	–	3.4	10.09.	3.3	02.09.	3.4	24.09.
Flüela 0102	–	–	2.9	14.09.	2.9	01.09.	2.9	24.09.
Gentianes 0102	*4.5*	*02.11.*	*4.5*	*08.11.*	*4.3*	*07.11.*	–	–
Lapires 0198	5.6	16.08.	5.6	18.09.	5.6	02.09.	6.4	13.10.
Lapires 1108	5.3	23.11.	5.3	07.11.	–	–	–	–
Lapires 1208	4.7	16.08.	4.7	18.09.	4.7	01.09.	4.7	01.10.
Matterhorn 0205	–	–	*4.6*	*14.10.*	–	–	–	–
Muot da B. P. 0196	1.7	16.09.	1.4	16.09.	1.7	02.09.	–	–
Muot da B. P. 0296	3.6	07.09.	3.2	22.09.	3.7	06.11.	–	–
Ritigraben 0105	3.2	09.09.	3.7	14.09.	3.7	05.09.	3.9	27.09.
Schafberg 0190	2.6	09.09.	2.5	18.09.	2.5	09.09.	–	–
Schafberg 0290	5.2	07.09.	5.2	18.09.	–	–	–	–
Schilthorn 5000	8.9	21.12.	*9.5*	*24.08.*	8.8	15.10.	*9.8*	*04.11.*
Schilthorn 5198	9.9	17.11.	6.7	16.10.	9.2	04.10.	*10.4*	*17.12.*
Schilthorn 5200	2.9	27.09	*3.3*	*10.10.*	3.2	26.10.	*2.9*	*20.10.*
Stockhorn 6000	3.8	15.09.	*3.9*	*17.09.*	3.9	15.09.	4.8	08.10.
Stockhorn 6100	5.0	24.12.	5.0	27.10.	5.0	24.12.	5.3	29.10.
Tsaté 0104	7.9	09.10.	–	–	–	–	–	–

3.2.2 Borehole temperatures

Temperatures measured in the boreholes during the reporting period are depicted in Figure 3.6 and detailed figures with ground temperatures for all boreholes are included in Appendix B.

The pronounced warming trend reported since the year 2009 (PERMOS 2016) continued in most of the boreholes for the year 2014/2015 as a result of the record warm year 2015 (see Chapter 2). Then one or two winters (depending on the region) with very late and thin snow covers led to an interruption of the warming trend for sites that are influenced by a snow cover. This interruption has already been visible at 10 m depth after winter 2015/2016 in Eastern Switzerland. In winter 2016/2017, the snow arrived very late in all regions and a temperature decrease down to 20 m depth was recorded for many of the borehole sites. The strongest cooling was observed at colder and snow-rich sites in Eastern Switzerland, such as Corvatsch-Murtèl or Muot da Barba Peider. A significant decrease in ground temperatures was also observed at Stockhorn and Les Attelas in Canton Valais. At locations where the ground temperatures are close to 0 °C, for example Schilthorn or Schafberg, as

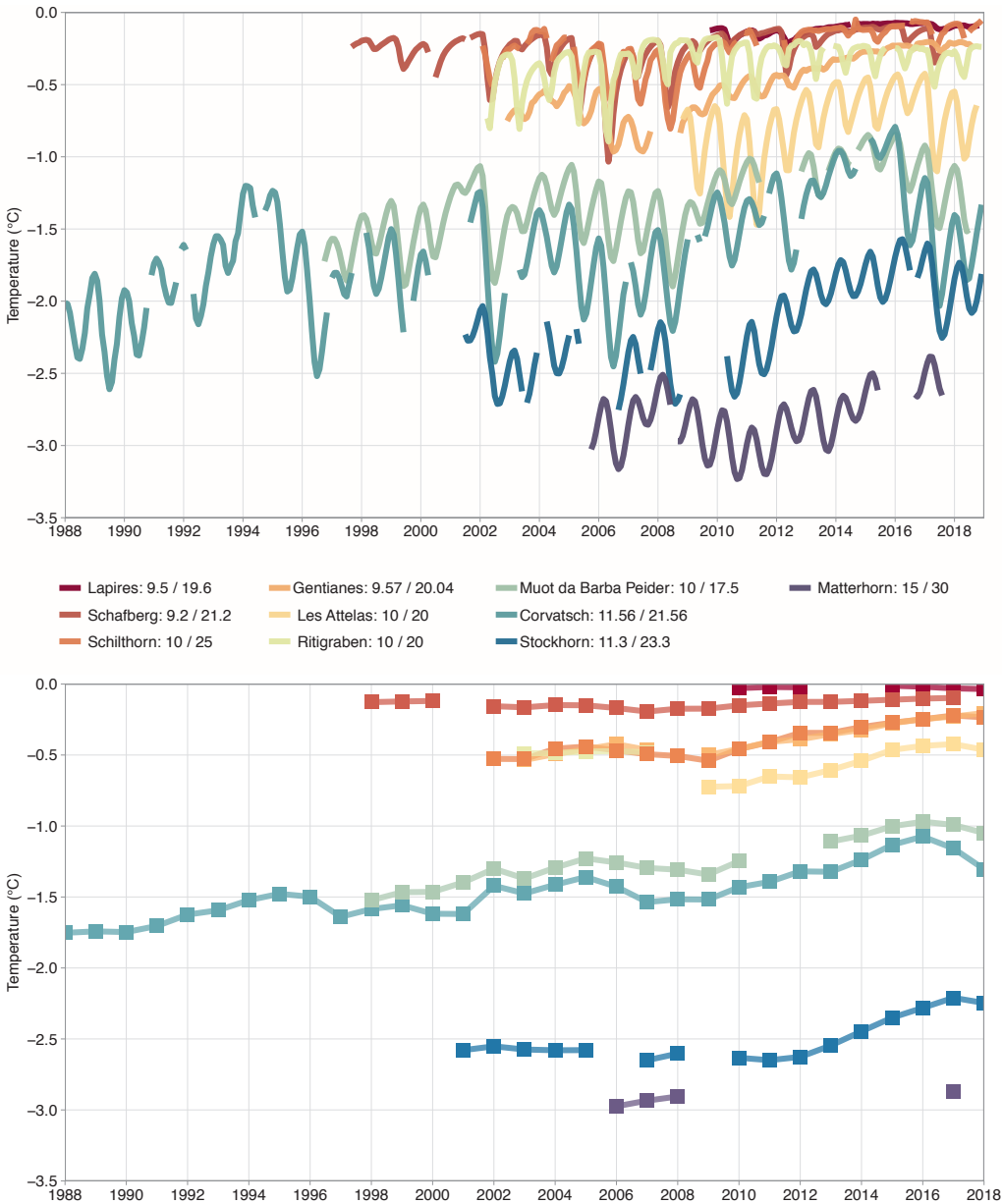

Figure 3.6: *Ground temperatures measured in selected boreholes at ca. 10 m depth (monthly means, top) and ca. 20 m depth (means of the hydrological year, bottom). The exact depths in metres are given in the legend.*

well as in locations in steep bedrock, such as Jungfraujoch or Gemsstock, no cooling of the permafrost could be observed. This cooling phase was however only temporary and the warming of the permafrost has resumed in the uppermost metres after the hot summer 2018 when the high GST have started to penetrate to depth. At the end of the reporting period the cooling is still visible at 10 m depth or even dominating at 20 m depth, especially where the temperature decrease was most pronounced. The heat of summer 2018 is slowly penetrating to depth.

3.3 Borehole replacement

Due to the limited expected lifetime of several of the borehole instruments as well as considerable shearing due to permafrost creep at rock glacier sites, the risk of loosing parts or the complete time series of several of the boreholes is continuously increasing. This is particularly true for the oldest borehole COR_0287 on Murtèl-Corvatsch, which has been running for more than 30 years. The shearing caused by the rock glacier movement makes a re-calibration or replacement of the thermistor chains, and hence, a validation of the measured temperatures impossible. The cables are likely considerably stretched and only about one quarter of the thermistors are still functional, most of them at depths shallower than 20 m. Similarly, the boreholes SCH_5000 at Schilthorn and TSA_0104 at Tsaté increasingly show problems with data quality and the thermistor chains are blocked.

Table 3.3: Replacement boreholes drilled during the reporting period to secure exisiting time series. Double thermistor depths for redundancy are marked in bold.

Borehole PERMOS site Drilling date Instrumentation date	Coordinates (CH1903)	Depth (m)	Distance to old BH (Name, dist in m)	Thermistor type and depths (m)
COR–0315				YSI 44031
Corvatsch-Murtèl	783149	60.5	COR_0287	Chain 1: 0.25, 0.5, 0.75, 1, 1.5, 2,
Sep/Oct 2015	144734		5 m	2.5, **3**, 3.5, 4, 4.5, **5**, **10**
06.01.2016	2666			Chain 2: **3.01**, **5.01**, 6, 8, **10.01**, 12,
				14, 16, 18, **20**
				Chain 3: **20.01**, 25, 28, 30, 32, 34,
				36,38, 40, 42, 45, 50, 55,
				58, 60
TSA_0117				YSI 44031
Tsaté	608500	20	TSA_0104	Chain 1: 1, 3, 5, 6, 6.5, 7, 7.5, 8,
16.–18.08.2017	106415		1 m	8.5, 9.5, **10, 12.5**, 15, **20,**
28.09.2017	3050			**20.1**
SCH_5318				YSI 44031
Schilthorn	630343	30	SCH_5000	Chain 1: 0.5, 1, 1.5, 2, 3, 4, **5**, 6, 7,
24.09.2018	156416		5 m	8, **10**, **15**, **20**
(Summer 2019)	2910			Chain 2: **5.01**, 9, **10.01**, 11, 12, 13,
				14, **15.01**, 16, 17, **20.01**,
				25, 30

Figure 3.7: *Drilling work for new boreholes at the PERMOS sites Corvatsch-Murtèl (top), Tsaté (bottom left) and Schilthorn (bottom right). Photos: J. Nötzli, C. Lambiel, C. Pellet.*

The PERMOS Scientific Committee considered the three boreholes described above to be in most critical condition and a timely replacement crucial. Replacement boreholes were drilled in 2015 (Corvatsch-Murtèl, UZH), 2017 (Tsaté, UniL) and 2018 (Schilthorn, UniFR) to ensure the continuation of the time series for long-term monitoring (Figure 3.7). The timely replacement of the boreholes allows for an overlap and comparison of the old and new measurements according to the GCOS Monitoring Principles as well as a validation of the old time series.

To secure the continuation of the time series, the new data should be as similar to the existing time series as possible. Drill sites were therefore chosen in close proximity of the existing boreholes. A minimum borehole depth of 20 metres for the PERMOS Network was established in earlier evaluation rounds. Thermistor chains were custom built with Yellow Springs Instruments 44031 thermistors on individual, switched wires to minimize

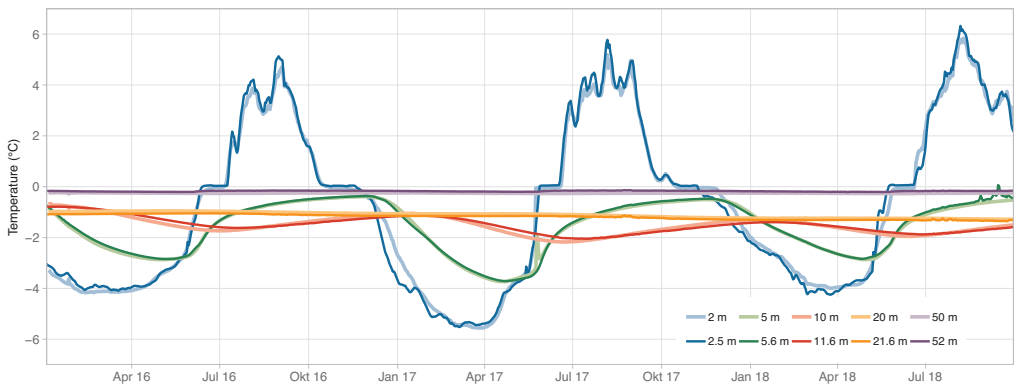

Figure 3.8:
Comparison of measured ground temperature time series in the old (COR_0287) and new (COR_0315) boreholes in rock glacier Corvatsch-Murtèl at selected depths since the start of the measurements in the new borehole in January 2016. The temperatures measured in the newer borehole are displayed with thicker lines and lighter colors.

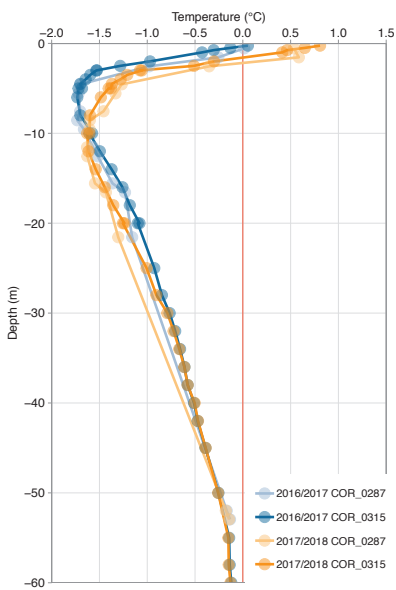

Figure 3.9:
Comparison of temperatures profiles measured in the old (COR_0287) and new (COR_0315) boreholes in rock glacier Corvatsch-Murtèl for the hydrological years 2016/2017 and 2017/2018.

the risk of losing all thermistors simultaneously in case the cables are damaged. The thermistor chains were offset calibrated at 0 °C in an ice-water bath. The thermistor spacing was adapted from the standard described by the PACE project (Harris et al. 2001) to account for blocky surface layers, zones of special interest and for an expected increase in ALT. The depths that are most important for the long-term monitoring are doubled for redundancy in case of drift or loss of a thermistor: at 5, 10 and 20 metres. This was achieved either by overlapping chains (Corvatsch, Schilthorn) or small thermistor spacing (Tsaté). The exact thermistor depths for the three boreholes are given in Table 3.3. All sites were instrumented with a Campell Scientific CR1000 logger and are accessible remotely via mobile communication.

A comparison of old and new data has only been done for the Corvatsch boreholes so far. At Tsaté, the old logger is broken and no reliable data is available. On Schilthorn, the instruments will only be installed in Summer 2019. The comparison of the about three years of measurements shows a very high agreement of the old and new time series both in their temporal evolution (Figure 3.8) as well as for the mean annual depth profiles (Figure 3.9). The accordance of the borehole temperature in the two boreholes is considered very good and the re-drilling of the Corvatsch borehole COR_0287 successul for the continuation of the important time series.

3.4 Summary

GST measurements reflect atmospheric conditions and the duration and thickness of the snow cover. They are high since 2009 for all regions and sites. At locations that are influenced by a winter snow cover, MAGST were higher than during the previous reporting period but they did not reach the maxima from 2003. In near-vertical bedrock MAGST closely follow air temperatures relative to their changes over time and they were continuously above average. ALTs increased for most borehole sites during the reporting period and remained more or less constant for some of the boreholes. New record ALT were observed in summer 2015 and 2018 at many boreholes sites.

The ground temperatures show a continued warming trend that started in the year 2009 and was interrupted following the snow-poor winter 2017 (and 2016 in some regions). The warming resumed in the uppermost metres after the hot summer 2018. The warmest 4 year period ever measured for air temperatures led to warm ground surface and ground conditions in the permafrost regions in Switzerland. However, there was no continuous increase in ground temperatures because of the important modifying influence of the winter snow cover and years with an exceptionally late snow cover.

During the reporting period three replacement boreholes were drilled to ensure the continuation of ground temperature time series: Corvatsch-Murtèl, Tsaté and Schilthorn. In all three boreholes, the old thermistor chains were blocked, preventing recalibration or replacement. The comparison of the old and new time series on Corvatsch-Murtèl show a very high agreement, both in their changes over time and in their vertical profile.

4 Electrical Resistivities

To deliver a comprehensive picture of the permafrost state and changes in the Swiss Alps, electrical resistivities have been operationally monitored at five sites for more than 10 years. Electrical resistivity values enable the observation of freezing and thawing processes occurring within the subsurface. By performing resistivity measurements at different locations along the ground surface and with variable spacing between the measuring electrodes, electrical resistivity values on a 2-dimensional grid are obtained, so-called electrical resistivity tomography (ERT, Figure 4.1).

ERT measurements are complementary to the borehole temperatures and GST measurements since they allow for a 2-dimensional characterization of the subsurface composition. When repeated over time, freezing and thawing processes can be identified. This is especially relevant when permafrost temperatures are close to 0 °C. Then, additional heat transfer from the atmosphere does not result in further temperature increase but is «masked» by phase changes, which can be detected by ERT measurements. Decreasing electrical resistivities indicate an increase of the liquid water to ice content ratio in the ground (i.e. less ice). Conversely, increasing electrical resistivities indicate a decrease of the liquid water to ice content ratio (i.e. more ice). Furthermore, using ERT measurements, these changes can be detected down to large depths (several tens of metres at the profiles included in the PERMOS Network).

4.1 Monitoring Strategy

Within the PERMOS Network, ERT measurements are currently carried out at five field sites, where stainless steel electrodes and fixed cables are permanently installed. Typically, measurements are performed once a year

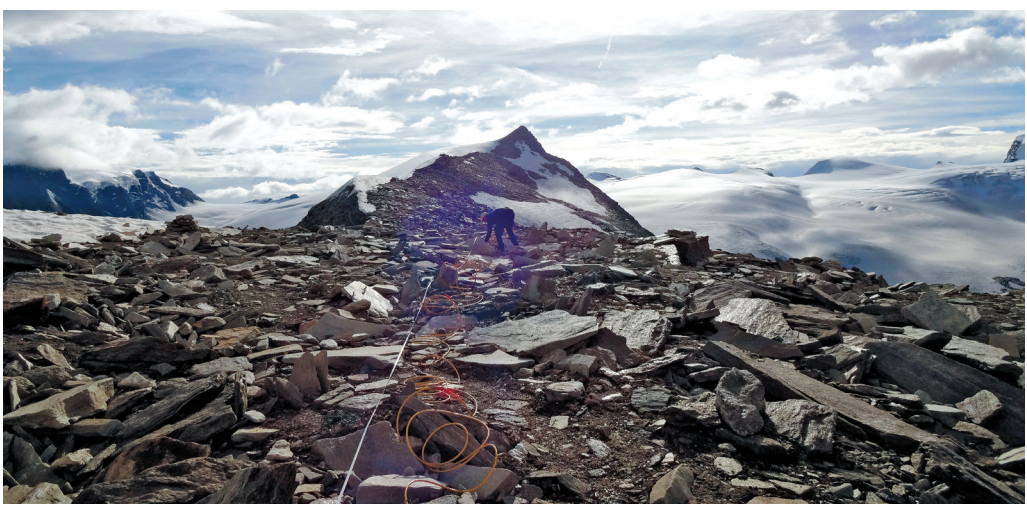

Figure 4.1: ERT measurement on the Stockhorn plateau at 3400 m asl. Photo C. Pellet.

at the end of the summer in order to capture the active layer thickness variations as well as potential signs of ground ice degradation.

The quality of the measured data prior to the inversion is assessed using a systematic procedure, which accounts for the contact resistance between the electrode and the ground, the physical plausibility of the measured values and the data consistency at each measurement depth (see Mollaret et al. 2018 for a more detailed description). For the datasets with more than 80% of data remaining after this filtering procedure, the distribution of the specific electrical resistivity for a finite element grid is computed using similar constraints and model set-up (so-called inversion). In addition to the standard processing of the ERT data, both the measured apparent resistivities and the inverted specific resistivities are systematically stored in the PERMOS database.

4.2 ERT Results for 2015 to 2018

Between 2015 and 2018 measurements of the 2-dimensional distribution of electrical resistivities in the ground has been continued at the five permanently installed profiles, which include two talus slopes (ATT and LAH), two bedrock sites (SCH and STO) and one rock glacier (MCO, Figure 4.2). All permanent ERT profiles are located

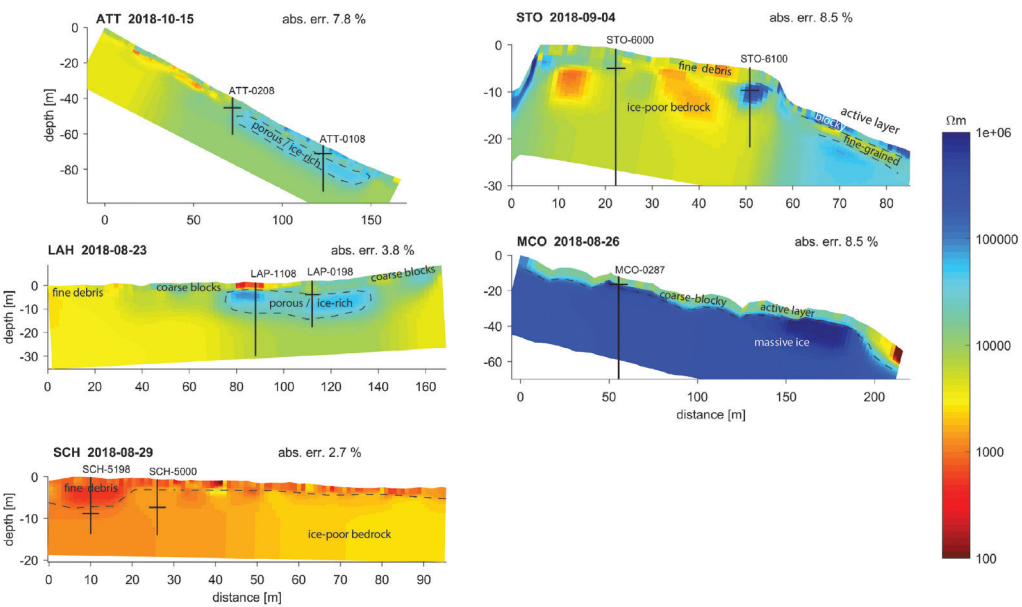

Figure 4.2: *Tomograms showing the resistivity distribution in 2018 at the five PERMOS ERT profiles. The vertical lines represent the borehole location and the horizontal lines the depth of the thaw layer at this date. The interpretation of the ground composition based on the ERT data is indicated.*

close to the PERMOS boreholes (vertical lines in Figure 4.2) to allow a joint analysis of the borehole temperatures with the temporal changes in resistivities.

Figure 4.2 shows tomograms and their interpretation for all PERMOS sites at selected dates at the end of the summer 2018. Resistivity values obtained at the different sites span over three orders of magnitude and highlight the considerable variability of alpine permafrost conditions ranging from fine-grained debris and weathered bedrock at Schilthorn (SCH, ~1 kΩm) to massive ice in a coarse-blocky rock glacier Corvatsch-Murtèl (MCO, ~1000 kΩm). Conversely, at Attelas (ATT), Lapires (LAH) and Stockhorn (STO) the resistivity values are relatively similar (~10–20 kΩm). Note that depending on the lithology, porosity and subsurface temperature, similar resistivity values can represent very different subsurface characteristics. For instance, values around 20 kΩm represent porous ice-rich permafrost at Attelas and Lapires, compared to ice-poor bedrock permafrost at Stockhorn and unfrozen coarse-blocky material at Corvatsch-Murtèl.

At Attelas and Lapires, the ERT tomograms show clearly defined and very localised permafrost areas. These areas are consistent with the site specific process driving the permafrost occurrence (ventilation effect within the talus slope yielding colder condition at the bottom of the slope, see also Delaloye and Lambiel 2005) and are confirmed by the borehole temperature measurements. At Corvatsch-Murtèl, the ERT measurement reveals a relatively homogeneous massive ice body extending all along the profile, which is consistent with the available temperature and geomorphological observations. Finally, at Schilthorn and Stockhorn the ERT measurements are indicative for ice-poor bedrock permafrost, which is supported by the borehole temperatures. Important lateral variations can be observed (especially at Stockhorn), which are attributed to variable ground properties such as lithology or degree of fracturation and weathering of the bedrock.

At Attelas, Lapires and Corvatsch-Murtèl the thaw depths derived from the respective borehole temperatures (horizontal lines in Figure 4.2) are well represented by vertical resistivity contrasts. However, at the ice-poor bedrock site Schilthorn and somewhat less at Stockhorn the resistivity contrasts characteristic of the thaw depths are masked by the significant resistivity variations due to the variable ground properties.

Based on the interpretation of the ERT tomograms (see Figure 4.2) a representative permafrost layer was delimited at each site. Figure 4.3 shows the evolution of the mean inverted resistivities of these permafrost layers at a selected date in August or September (see Table 4.1). Given that the geology of the subsurface does not change over the time scale considered, the observed changes in resistivity can be attributed to variations in ice and unfrozen water contents. Therefore, a decrease in resistivity with time points to an increase in unfrozen water content and/or a decrease in ice content, whereas an increase in resistivity may be caused by ice aggradation and/or drained pore water.

At Schilthorn, a continuous decreasing trend of permafrost resistivities has been observed since 1999. During the 2015–2018 period, each year reached a new lowest record resistivity value. At Corvatsch-Murtèl and Stockhorn, the resistivities also exhibit a decreasing trend over the last five years. The effect of the permafrost cooling that occurred during the winter 2016/17 is not visible in the resistivity data although the permafrost temperatures at 10 m and 20 m depth have been affected for more than two years (see Figure 3.6). The resistivities measured within the talus slope at Lapires show a decreasing trend since 2006, which stopped in 2017 and 2018, most probably due to the permafrost temperature decrease observed in winter 2016/2017. Finally, at Attelas resistivi-

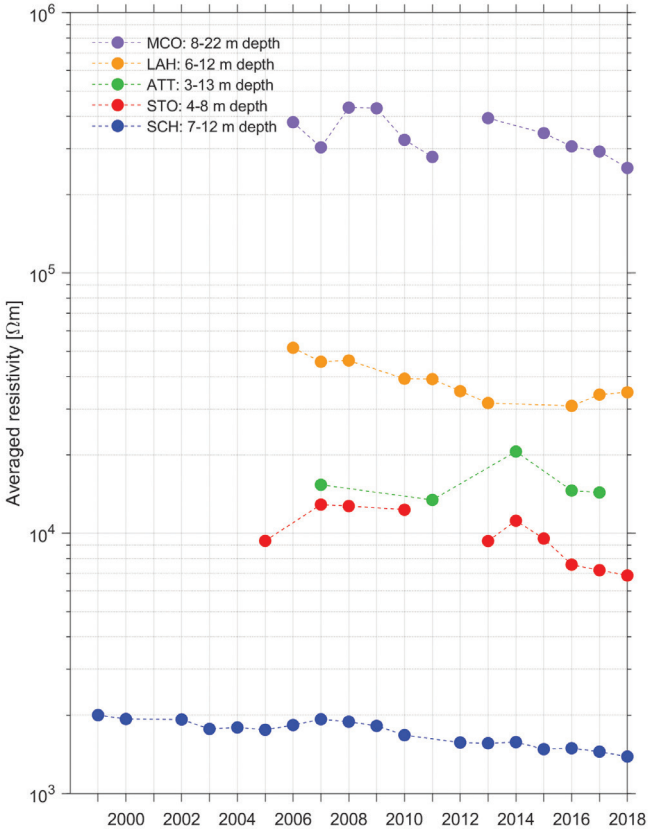

Figure 4.3:
Average inverted electrical resistivities of the permafrost layer at the reference date in August or September for different sites. The depth range of the permafrost layer that has been used for averaging is indicated in the legend.

ties show no clear trend, which can partly be explained by the irregular date of measurement as well as the short period of measurement (see Table 4.1). It is worth noting that similarly to Lapires the resistivities measured in 2017 are relatively close to the values of 2016, which could also result from the marked 2016/2017 winter cooling. The changes in resistivities discussed here are strictly limited to selected permafrost zones within the tomograms. However, changes also occurred in other parts of the 2-dimensional profile. For a more complete overview, all tomograms as well as the changes of resistivity compared to the first measurements over the entire profile are included in Appendix C.

Table 4.1: Reference ERT annual measurement date and average inverted electrical resistivities (Res) of the permafrost layer.

	Attelas		Lapires		Corvatsch-Murtèl		Schilthorn		Stockhorn	
Year	Res	Date	Res	Date	Res	Date	Res	Date	Res	Date
	kΩm	dd.mm	kΩm	dd.mm	kΩm	dd.mm	kΩm	dd.mm	kΩm	dd.mm
1999	–	–	–	–	–	–	2.00	15.09	–	–
2000	–	–	–	–	–	–	1.9	28.08	–	–
2001	–	–	–	–	–	–	–	–-	–	–
2002	–	–	–	–	–	–	1.9	15.08	–	–
2003	–	–	–	–	–	–	1.8	23.08	–	–
2004	–	–	–	–	–	–	1.8	23.08	–	–
2005	–	–	–	–	–	–	1.8	03.09	9.4	02.09
2006	–	–	51.6	29.08	379.3	17.08	1.8	24.08	–	–
2007	15.4	25.08	45.6	27.08	303.8	30.08	1.9	29.08	12.9	24.08
2008	–	–	46.1	19.08	432.1	09.09	1.9	25.08	12.7	21.08
2009	–	–	–	–	429.2	23.08	1.8	28.08	–	–
2010	–	–	39.2	24.08	–	–	1.7	28.08	12.3	25.08
2011	13.4	30.09	39.1	15.08	279.1	16.08	–	–	–	–
2012	–	–	35.1	24.08	–	-–	1.6	19.08	–	–
2013	–	–	31.6	13.09	393.3	22.08	1.6	28.08	9.3	11.09
2014	20.6	30.09	–	–	–	–	1.6	29.08	11.1	29.08
2015	–	–	–	–	344.6	07.09	1.5	26.08	9.5	09.09
2016	14.6	23.09	30.9	31.08	306.3	26.08	1.5	01.09	7.6	14.09
2017	14.3	25.09	34.1	22.08	292.9	24.08	1.5	29.08	7.2	07.09
2018	–	–	34.8	23.08	253.1	26.08	1.4	30.08	6.9	04.09

4.3 Summary

Repeated ERT measurements allow for the borehole-independent observation of freeze and thaw processes in the subsurface. The yearly measurements performed at the end of summer enable the documentation of the cumulative effect of freeze and thaw processes over the full year. Resistivities measured within the permafrost layer at five alpine permafrost sites exhibit a similar overall decreasing trend since the beginning of the measurements, except at Attelas where no clear trend is currently observed. Site-specific processes and properties may punctually affect this general trend. For example, talus slopes are more sensitive to snow-poors winters due to the combined effect of conductive cooling and reinforced air circulation, which strengthens the cooling effect of winter air temperature (LAH in 2017 and 2018 and ATT in 2017).

5 Kinematics

Creeping mountain permafrost landforms, such as rock glaciers, are key indicators of the impact of climate change in mountain permafrost areas. Their dynamics reveal indirect information on the ground thermal condition and its evolution as well as on the composition of the subsurface and the processes active therein. Inter-annual changes in the creep behaviour have been shown to follow mainly an exponential relation with multi-annual ground surface temperature forcing (Staub et al. 2016), whereas the largest part of the movement is taking place within one or several shear horizons at 10–30 m depth (see Figure 5.1 and Arenson et al. 2002, Buchli et al. 2013). Within the PERMOS Network, continuous long-term data series of permafrost creep are currently obtained at 15 rock glacier sites (18 rock glacier lobes) in order to provide a basis for the understanding and investigation of ongoing processes and dynamics.

5.1 Monitoring strategy

Similarly, to the global PERMOS strategy, the kinematic monitoring strategy follows a landform-based approach. Seasonal, inter-annual and long-term variations in rock glacier kinematics (see e.g. Delaloye et al. 2010, PERMOS 2016) may be captured using a combination of aerial survey (AS) and terrestrial geodetic surveys (TGS, by total station or differential GNSS). Changes in geometry (i.e. horizontal velocities and vertical changes) are analysed in detail to quantify permafrost creep and to detect signs of potential permafrost degradation such as vertical thinning due to ice melt or rock glacier destabilization.

TGS were included into the PERMOS monitoring strategy in 2008 and are currently carried out at 18 rock glacier lobes distributed in four topo-climatic regions in the Swiss Alps. Surveys are performed at least once a year at the same time in the season (usually in late summer) for a number of selected boulders on each rock glacier (10–100 points). The measured coordinates (x, y) and elevation (z) are used to quantify the horizontal (Δxy) and vertical (Δz, ratio of slope) changes of each point. Trajectories and flow fields are then generated and creep rate time series for single measurement points and/or representative zones of the rock glacier are determined.

Figure 5.1: Front of the rock glacier Tsarmine (Val d'Arolla, VS) in January 2017. The shear horizon is clearly visible (see also Delaloye and Lambiel 2017). Photo: UniFR

A pilot study was launched in the year 2012 to evaluate the use of permanently installed GNSS sensors for long-term permafrost kinematics monitoring. The experience showed such sensors can be reliably operated and the data obtained allows the investigation of temporal patterns of creep displacements with unprecedented level of detail. Permanent GNSS sensors (one per instrumented site) will therefore be operationally integrated within the PERMOS Network from 2019. The monitoring strategy for this new element together with some exemplary results are presented in Chapter 6.

5.2 Permafrost creep

Terrestrial geodetic surveys have been continued during the period and currently cover 18 rock glaciers (Table 1.1 and Figure 1.5) located within four distinct topo-climatic regions in the Swiss Alps. Results show that, although the creep velocities measured at the different sites span over three orders of magnitude (Figure 5.2), a common general behaviour can be highlighted (Figure 5.3).

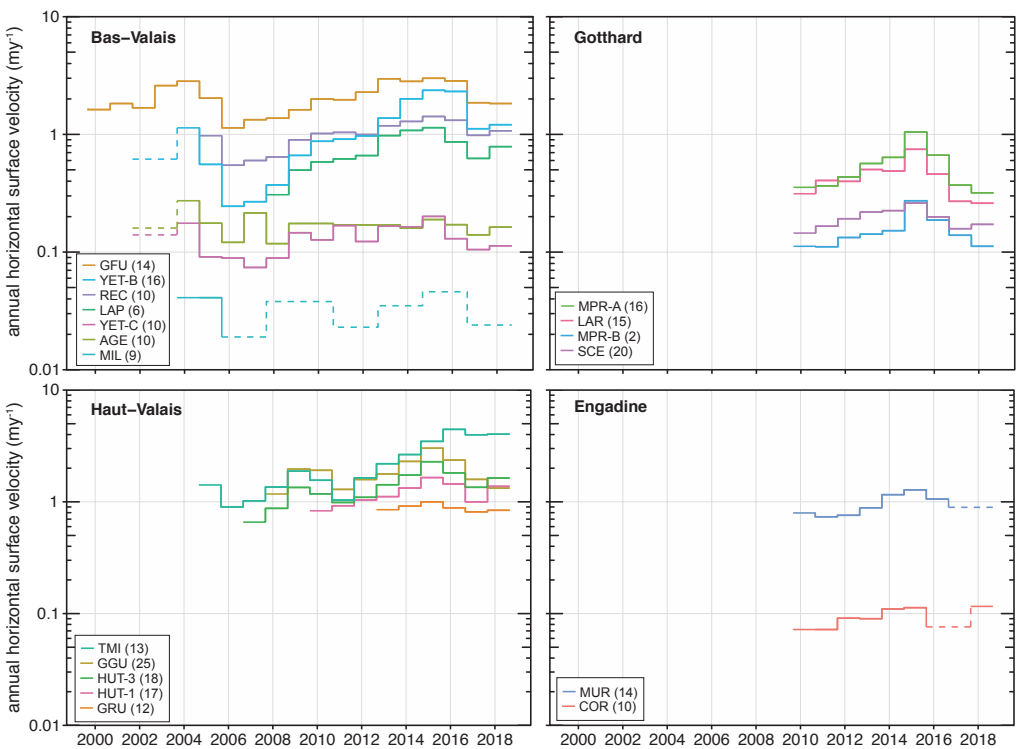

Figure 5.2: *Mean annual horizontal surface velocities (my^{-1}) for the number of reference points in brackets at 18 rock glacier lobes from 2000 to 2018 derived from terrestrial geodetic surveys. The rock glaciers are divided into four topo-climatic regions in Switzerland. The dashed lines represent velocities measured over two years.*

Following the extraordinary high horizontal velocities in 2003 and 2004, the creep velocities dropped until 2006 before increasing again until 2015. In 2015, new velocity records were reached at all sites. Especially the increase in the Gotthard and Southern Alps area is marked, where creep velocities increased by up to 80% compared to the previous year (Monte Prosa B, see Table 5.1). This new general velocity peak coincided with the absence of winter cooling due to an early development of the snow cover during the winter 2014/2015 (see Chapter 2). Following the velocity peak, a general decrease of the surface velocity was observed in 2016 and 2017. The pronounced drop in velocity in 2017 (–28% in average over the Swiss Alps) can be linked to the observed general permafrost cooling occasioned by the extremely snow-poor winter 2016/2017 (see Chapter 2). In 2018, the creep velocities generally start to increase again although very different regional signals were recorded (+11% and +9% in Bas- and Haut-Valais, –7% in the Gotthard area and +19% in Engadine, Table 5.1).

However, over the last years two rock glaciers have no longer followed the typical relationship of creep velocity and ground temperature. The Aget rock glacier shows an atypical deceleration (to be confirmed in the coming years). The Tsarmine rock glacier is entering a destabilization phase and dramatically accelerated during the past 5 years (see Table 5.1). This is the only rock glacier of the PERMOS Network that accelerated in 2016 and hardly decelerated in 2017. For both rock glaciers with atypical behaviour local factors currently outrival the climatic forcing as the main driving factor of creep velocity.

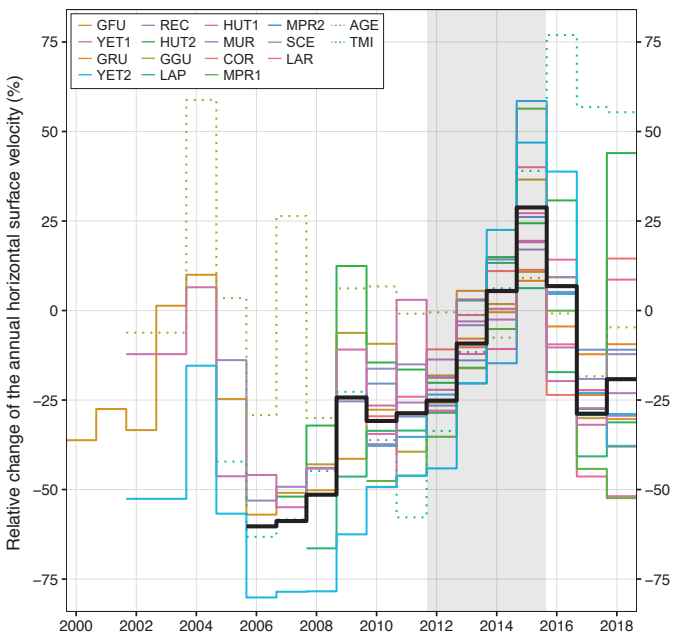

Figure 5.3: *Mean annual horizontal surface velocity (in %) relative to the reference period 2012–2015 (grey area) at 17 rock glacier lobes from 2000 to 2018 derived from terrestrial geodetic surveys. Rock glaciers showing an atypical evolution are shown in dotted lines and the black line corresponds to the mean of the Swiss Alps (excluding the two atypical rock glaciers).*

*Table 5.1: Relative change of the mean horizontal surface velocity (reference values) of PERMOS rock glaciers compared to the respective previous year in percent. The * represents velocities measured over two years.*

Site	2009	2010	2011	2012	2013	2014	2015	2016	2017	2018
Aget	+48	0	–3	0	0	–6	+18	–10	–18	+16
Gemmi	+18	+23	–1	+19	+30	–5	+6	–5	–35	–2
Lapires	+62	+17	+6	+7	+48	+11	+5	–24	–28	+26
Réchy	+40	+13	+2	-4	+19	+9	+10	–7	–25	+9
Yettes Condjà B	+78	+32	+4	+6	+42	+46	+18	–2	–52	+8
Yettes Condjà C	+64	–13	+32	–27	+3	–1	+23	–35	–19	+8
Mean Bas-Valais	+52	+12	+7	0	+29	+9	+13	–14	–30	+11
Grosses Gufer	+67	–2	–33	+23	+12	+30	+31	–22	–33	-16
Gruben						+8	+9	–12	–8	+3
Hungerlitälli 1			+11	+12	+7	+19	+24	–12	–31	+38
Hungerlitälli 2	+54	–12	–16	+11	+30	+22	+32	–21	–26	+21
Tsarmine	+39	–17	–34	+58	+34	+31	+31	+28	–11	+1
Mean Haut-Valais	+53	–10	–18	+26	+21	+20	+25	–8	–22	+9
Largario			+30	–2	+26	–3	+53	–38	–41	-4
Monte Prosa A			+3	+19	+30	+13	+64	–39	–44	-14
Monte Prosa B			–1	+20	+7	+7	+80	–32	–26	-19
Sceru			+14	+16	+14	+3	+16	–24	–21	+9
Mean Gotthard			+12	+13	+19	+7	+53	–31	–33	–7
Corvatsch-Murtèl			–8	+3	+17	+31	+10	–17		–16*
Muragl			0	+26	–1	+22	+3		–33*	+53
Mean Engadine			–4	+15	+8	+27	+7	–17	–33	+19
Mean Swiss Alps	**+52**	**+5**	**0**	**+12**	**+22**	**+13**	**+25**	**–17**	**–28**	**+7**

5.3 Slope failure from permafrost areas

The data in the PERMOS permafrost rock fall database is collected from different sources reporting observations. These include mountain guides, climbers, hut wardens, pilots, rescuers, local/cantonal hazard managers and the media. There is no active search for data, so only data delivered from these contributors is registered and there is likely an observer-bias caused by factors influencing the number of people in the mountains (e.g. weather conditions). This particularly concerns the observation of smaller events of a few 1000-10'000 m^3. Large rock slope failures are generally well documented and are often registered by the Swiss Seismological Service.

Rock slope failures occurring in the Swiss Alps between 2015 and 2018, above 2200 m asl. and with an estimated volume of at least 1000 m^3 are shown in Figure 5.4. Most volumes shown are roughly estimated, except at a few sites such as Pizzo Cengalo, where they were quantified using terrestrial laser scanning. Events with little reliable information are not shown. The observation period included two summer heat waves (2015 and 2018). The majority of events were near-surface failures involving a few thousand cubic metres. Permafrost ice was observed in the detachment areas right after the failure in several cases.

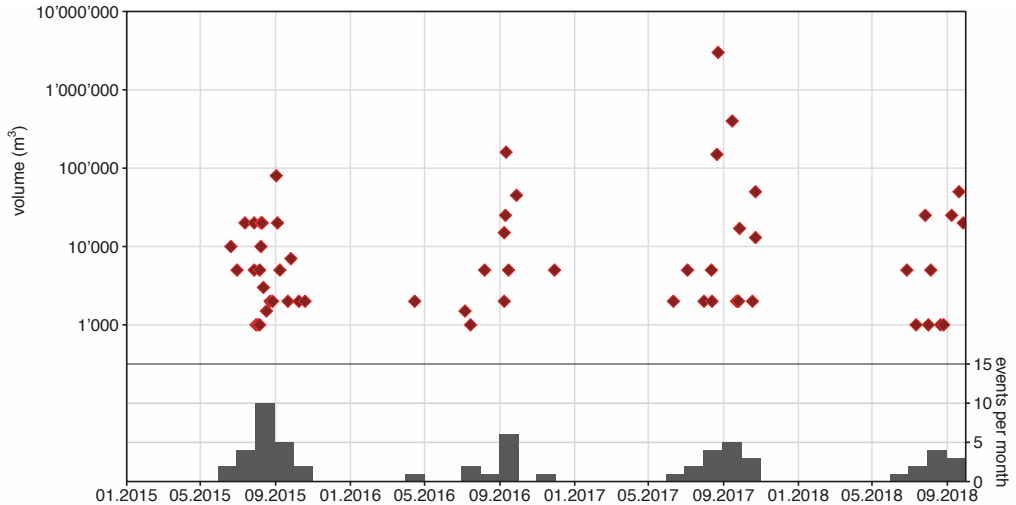

Figure 5.4: Rock slope failures registered in the PERMOS rock fall database from 2015 to 2018. Events with a volume exceeding 1000 m^3 and with a starting zone above 2200 m asl. are shown.

During the 2015 heat wave, 23 rock slope failures were documented. The largest one occured at the Grande Dent de Veisivi (Valais) with a volume of around 80'000 m^3. The rock fall activity peaked between the end of July and mid-September 2015. Sixteen events were smaller than 10'000 m^3. In the course of 2016, 12 events were reported. The largest one occurred at Pizzo Cengalo (Grisons) with a volume of 160'000 m^3. There was a short peak of activity in the second week of September 2016. Most events were smaller than 10'000 m^3.

The year 2017 was marked by the catastrophic Pizzo Cengalo rock slope failure. On August 23 2017 a volume of 3.1 million m^3 detached from the NE flank of Pizzo Cengalo at an elevation of ca. 3200 m asl. and claimed 8 lives. The rock avalanche eroded an entire glacier (about 600'000 m^3). A debris flow emanating from the rock-ice deposit minutes later caused huge damage to infrastructure in the village of Bondo. This cascading event was preceded by a rock slope failure of around 120'000 m^3 two days earlier. On September 15, a further 400'000 m^3 collapsed from the destabilized Northeast flank of Pizzo Cengalo. Nine other events in the Swiss Alps were smaller than 10'000 m^3 and three ranged between 10'000 and 50'000 m^3. In all, 15 rock slope failures were registered in 2017. There was a short peak of activity at the end of September. In 2018, 12 events were documented, with 7 smaller than 10'000 m^3. The largest ones, around 25'000–30'000 m^3, occurred at Linard Pitschen (Grisons), Grand Cornier and Petit Grépillon (Valais). There was no peak of activity and the events occurred between the end of June and mid-October 2018.

On 2 July 2018, a series of debris flows were triggered at the front of the Ritigraben rock glacier during intense rainfall (Figure 5.5). The debris flows reached the Vispa river, damming it, and caused damage to the sewage treatment station of St. Niklaus.

Figure 5.5: Front of the Ritigraben rock glacier before (left) and after (right) the debris flows of 2 July 2018. Photos: SLF time lapse camera.

5.4 Summary

Repeated TGS measurements enable the accurate observation and quantification of seasonal and inter-annual variations of rock glacier kinematics. The yearly measured coordinates are used to quantify permafrost creep as well as geometry changes for single measurement points and/or representative zones of the rock glacier. After more than 10 years of monitoring, results show that despite strong site-specific variations a common general behaviour can be highlighted. The permafrost creep velocities contiuously increased during the years 2007 until 2015 and decreaed in 2016 and 2017 along with the decrease in permafrost temperatures after the extremely snow-poor winters. Among the 18 rock glacier lobes currently monitored within the PERMOS network, two are starting to show atypical behaviour with trends that differ from the regional signal and no longer follow the relationship to ground temperature.

Several slope failures originated from permafrost areas during the reporting period. Outstanding was the rock fall at Pizzo Cengalo on August 23, 2017, which caused several cascading events including large debris flows, caused damages at infrastructure down in the valley and claimed 8 lives.

6 Permanent GNSS

The overall goal of the PERMOS kinematic strategy is the systematic long-term monitoring of permafrost creep to provide baseline data on the behaviour of permafrost related landforms in the Alps. This is currently achieved by terrestrial geodetic surveys (TGS), which provide annual to multi-annual displacement rates at spatially distributed points over entire landforms (see Chapter 5). A pilot study launched within the framework of PERMOS in 2012 showed that the observation of seasonal variations of permafrost creep using permanent GNSS devices is feasible. Permanent GNSS devices will be operationally included within the PERMOS network starting in 2019 to complement the current kinematic measurements with intra-annual variations at selected points. This chapter presents the monitoring strategy as well as exemplary results from the pilot study.

6.1 Monitoring strategy

Permanent GNSS devices complement the annual TGS and the repeated aerial image surveys to capture the seasonal, inter-annual and long-term variations in rock glacier kinematics at selected PERMOS kinematic sites. Due to resource constraints and/or specific site characteristics (e.g. avalanche-prone), implementing permanent GNSS measurements at all PERMOS kinematic sites is not possible. The feasibility (i.e. field work/instrument safety, accessibility/feasibility, long-term potential etc.) and relevance (i.e. amplitude of displacement, expected creep patterns including long-term development etc.) are therefore carefully evaluated by the responsible institution and subsequently discussed and approved by the PERMOS Scientific Committee before the integration within the network.

Figure 6.1: Permanent GNSS device installed on the Monte Prosa A rock glacier. Photo: J. Wee

Table 6.1: Overview of all PERMOS permanent GNSS monitoring sites.

Site	Region	Elevation (m asl.)	Start	Institution
Gemmi	Lower Valais	2482	2016	UniFR
Grosses Gufer	Upper Valais	2492	2018	UniFR
Gruben	Upper Valais	2823	2012	ETH-TIK / UniFR
Largario	Ticino	2356	2014	ETH-TIK / SUPSI
Monte Prosa A	Ticino	2475	2017	UniFR
Muragl	Engadine	2610	2012	ETH-TIK / UZH
Murtèl-Corvatsch	Engadine	2670	2015	ETH-TIK / UZH
Réchy	Lower Valais	2697	2016	UniFR

Permanent GNSS devices are installed at locations that are representative for the entire landform. To capture the effects caused by climate forcing and to guarantee long-term operation, permanent GNSS devices should not be installed in destabilised areas or zones in the process of settling (which may be necessary if the observations are targeted for other purposes such as natural hazard prevention and hazard management). The exact setup of the instrumentation (e.g. using a local reference or not) depends on the pattern and scale of motion of the specific landforms as well as on the baseline distance to other reference positions and has to be evaluated individually for each site. Additionally, a real-time remote access to the Permanent GNSS sensor is highly recommended to ensure control over the data and station health.

The sensing system must be able to provide reliable daily ENH position data. Typically, these position data collected at the Permanent GNSS sensors and at given reference locations are then post-processed using double- (or triple-) differencing techniques in combination with other GNSS data products. The daily ENH positions are referenced in a stable geodetic datum (preferably CH1903+/LV95) and reference frame (Bessel ellipsoidal). They also undergo basic quality checks and, if applicable, the data are corrected relatively to the local permanent base station. The processed time series of daily ENH positions are subsequently used to calculate 2D and 3D displacements (velocities), azimuth and inclination of the observed motion for the analysis of the seasonal patterns of permafrost creep.

From the year 2019, permanent GNSS measurements at 8 field sites within four topo-climatic regions in the Swiss Alps will be operationally included in the PERMOS network (see Table 6.1). In addition to these selected sites, many other comparable measurements exist in Switzerland not only on rock glaciers but also on landslides, glaciers, bedrock ridges, etc. (see e.g. Cicoira et al. 2019, Weber et al. 2019, Wirz et al. 2014).

6.2 Exemplary data

The Permanent GNSS devices that are integrated in the PERMOS network have been operated in the Swiss Alps since 2012 in the framework of various projects such as the «PERMOS permanent GNSS pilot project», the PermaSense project run by ETHZ, UZH and BAFU, and research projects from UniFR and UniL.

Figure 6.2 shows the evolution of monthly creep velocity at the Réchy/Becs-de-Bosson and Muragl rock glaciers measured by permanent GNSS as well as the creep velocity obtained from annual differential GNSS survey at

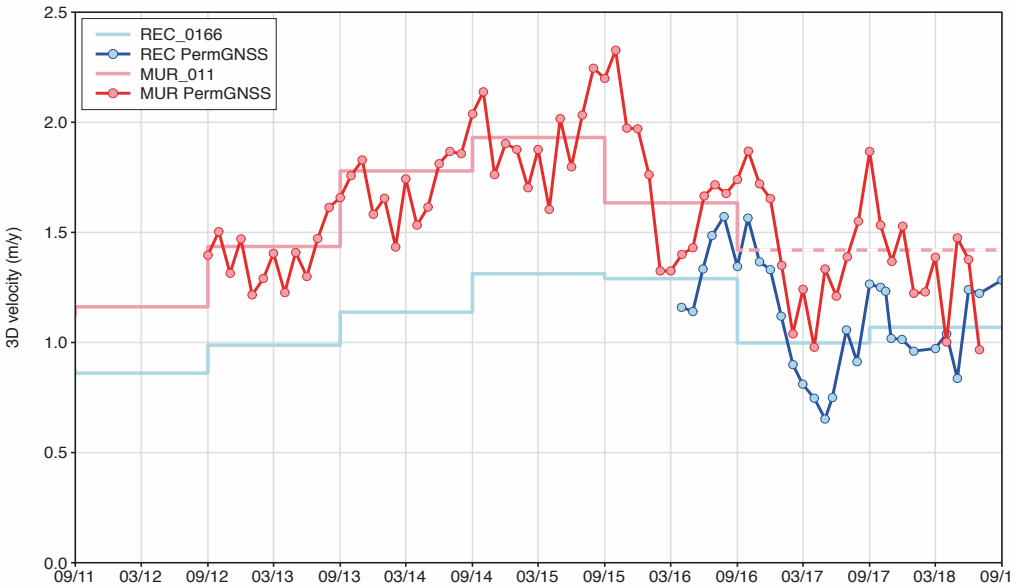

Figure 6.2: Evolution of the annual (light) and seasonal (dark) creep velocity at the Réchy (blue) and Muragl (red) rock glaciers. The dots represent monthly velocities and the dashed line the velocity measured by TGS over two years.

the nearest TGS observation point. Both sites show similar seasonal velocity pattern with lowest velocities at the end of winter (around April) and peak velocities in September-October. This general pattern is also observed at the other permanent GNSS sites (see Table 6.1). However, the summer development may strongly differ from one site to another and the amplitude between minimum and maximum velocities may vary from about 1:1.1 to 1:10 (e.g. Delaloye and Staub 2016, Wirz et al. 2016).

Low inter-annual variations in the relative contribution of the winter and the summer season to the total annual displacement rates are also observed. For example, the marked velocity decrease at Muragl during the winters 2015/16 and 2016/17 can be linked to extremely snow-poor conditions, which led to an important cooling of the ground (see Chapter 2 and 3). On the other hand, the relatively warm winters 2012 to 2015 combined with above average summer temperatures yielded a general increase of the creep velocity with maximum velocities observed in September 2015.

In addition to the seasonal and inter-annual velocity pattern, Figure 6.2 shows highly variable monthly velocities, which are especially visible during winter. The reliability and significance of these small variations (typically +/- 0.1–0.2 my^{-1}) are difficult to assess to date. They depend on a wide range of factors such as the accuracy of the measurement (including external effects as the snow pressure on the mast in winter time), the stability and anchorage of the boulder in the terrain, specific deformation in the active layer and the processing of the data. Hence, these short-term variations may be caused by factors other than the rock glacier motion (permafrost creep) and have to be interpreted with caution.

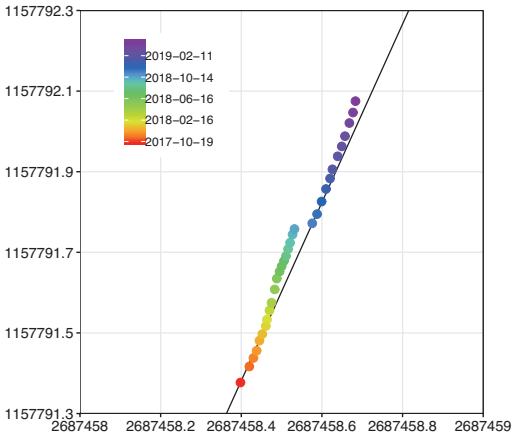

Figure 6.3:
Horizontal trajectory measured by the permanent GNSS device at Monte Prosa A from October 2017 until April 2019. The dots represent monthly mean positions and the black line represents the average trajectory.

Figure 6.3 shows the trajectory of one boulder on the Monte Prosa A rock glacier (Figure 6.1) measured by permanent GNSS. One can clearly see a progressive deviation of the trajectory of the boulder in spring/summer 2018 and a sudden back-movement during a severe rain/snow event on 30 October 2018. After the readjustment in autumn 2018, the progressive deviation resumed during winter 2018/2019 and is ongoing again at the time of writing this report. This deviation with sudden back-movement is most likely caused by the movement of the boulder alone, which is partly disconnected from and therefore not entirely representative for the movement of the rock glacier.

Both examples (Figures 6.2 and 6.3) illustrate the difficulties in interpreting continuous time series obtained from surface boulders for the observation and understanding of rock glacier creep processes at depth.

6.3 Summary

Permanent GNSS devices allow the observation of seasonal variations of permafrost creep and complement the annual surveys that are currently part of PERMOS. The sensing systems used provide reliable daily ENH positions from which velocities can be derived after a thorough data post-processing. Although uncertainties exist, such as the distinction of the movement of individual boulders from the creep of the entire landform, valuable information can be obtained from these measurements.

Although the monthly creep velocity exhibit site-specific variability, a similar seasonal behaviour of the permafrost creep velocities can be highlighted. Velocity minima are reached at the end of winter (April–May) and followed by an acceleration during the snowmelt season. Velocity maxima are usually achieved in autumn or early winter (September-December) and followed by a deceleration during winter (Figure 6.2, and Delaloye and Staub, 2016). Under changing climatic conditions, some of the currently observed rock glaciers may show changes in their seasonal pattern (timing and amplitude) in the following 10–20 years. Therefore, long-term observation of the seasonal pattern is crucial and falls well within the goal of the PERMOS Network.

7 Final Data from Dreveneuse

The Combe of Dreveneuse is located in the Valais Prealps between 1450 and 1800 m asl. and includes several scree slopes with varying aspects. This site has been explored since 2003 by Delaloye (2004) and Lambiel (2006) using a vast array of methods to describe and survey the occurrence of permafrost. Two drillings (5 and 15 m depth) were performed in November 2004 in the mid- and lower sections of one of the scree slopes located in Dreveneuse d'En Bas. There was no permafrost at that time, but sporadic occurrences were observed later on and the site was included in the PERMOS network as representative of extra-zonal low elevation permafrost occurrence in 2010.

The 14 years of continuous monitoring showed that in the middle of the slope permafrost conditions occurred only sporadically in a thin layer at around 11 m depth and have no longer been observed since 2012. In the lower section of the slope, permafrost similarly occurred sporadically but much closer to the surface in a thin layer at around 2 m depth. Because of the very sporadic occurrence of extra-zonal permafrost it was decided that the borehole site Dreveneuse will no longer be part of the PERMOS network from 2019 onwards.

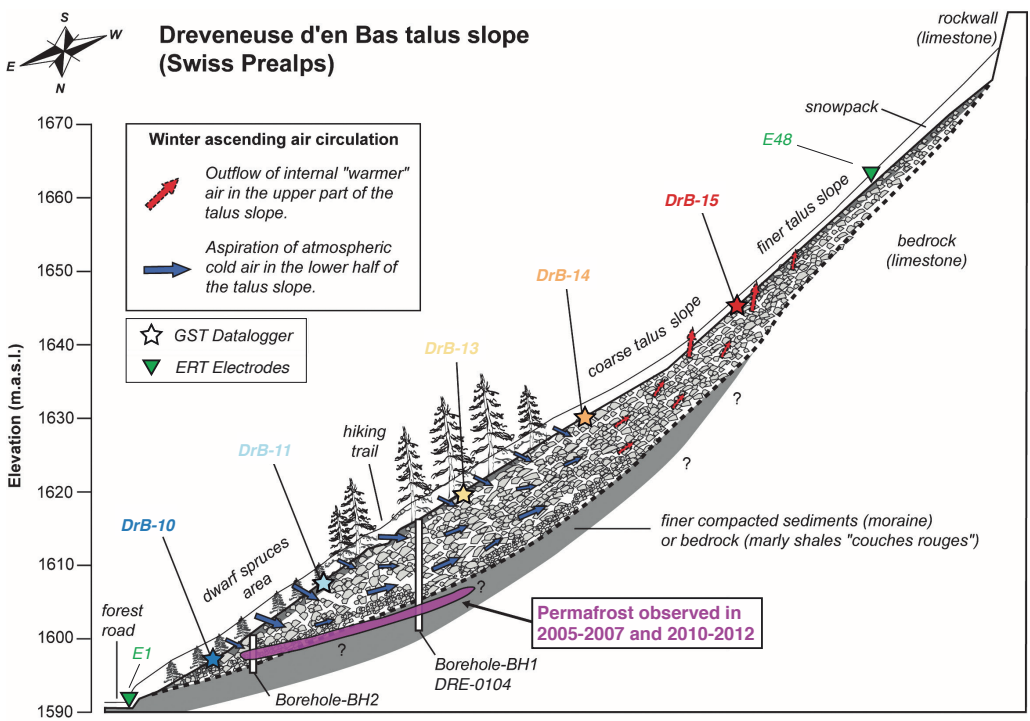

Figure 7.1: *Main characteristics of the Dreveneuse d'en Bas talus slope for the winter ascending air circulation phase. The limit between the porous blocky material and the substratum is based on borehole data and geophysical measurements (figure adapted from PERMOS 2010).*

The continuation of the monitoring at Dreveneuse is of interest for research, but does not fit into the scope of PERMOS, which is to provide a baseline of the evolution of permafrost in Switzerland and its changes. The UniFR will however continue the monitoring efforts at Dreveneuse. This chapter gives an overview of the data series collected at Dreveneuse since 2004 as a final report for this field site.

7.1 Air circulation mechanism

The Dreveneuse d'En Bas talus slope consists of limestone blocky and pebbly clasts, which are covered by a singular forest of dwarf trees in the lowermost third, where permafrost exists due to a complex ventilation system (PERMOS 2010). Although the site is located below the lower limit of discontinuous mountain permafrost (around 2400 m asl. in the Alps), internal air circulation in the scree slope enables cold ground conditions. Air circulation processes have been widely observed at both high and middle elevation in debris accumulations like talus slopes or relict rock glaciers (e.g., Delaloye and Lambiel 2005, Morard et al. 2008, Wakonigg 1996).

The temperature gradient between the air and the ground temperature causes air to circulate inside the large interconnected pore space between the coarse blocks of the talus slope. In winter, the relatively warm and light air from inside the talus ascends to the upper part, which leads to cold air aspiration in the lower part of the slope even through a snow cover (Figure 7.1). Typically, the outflow of warm air in winter leads to snowmelt windows in the upper part of the talus slope (Figure 7.2), whereas the aspiration of external air builds a cold reservoir in the lower part. In summer, the air circulation is reversed and relatively cold dense air flows out at the bottom of the slope preventing the ground temperatures from rising significantly above 0 °C. The reverse of the airflow direction is controlled by air temperature and at Dreveneuse d'En Bas this occurs at about 4 °C.

Figure 7.2: Snow melt window at Dreveneuse du Milieu. Photo: C. Lambiel, 08.02.2005.

7.2 Data series

Six GST loggers were installed along a longitudinal profile in November 2004 to characterize the thermal regime of the Dreveneuse d'En Bas talus slope and to investigate the ventilation processes. Additionally, two boreholes were drilled in 2004 and repeated ERT measurements were performed between 2007 and 2015 along a permanently installed vertical profile across the boreholes (see Figure 7.1 for exact locations of the first and last electrodes).

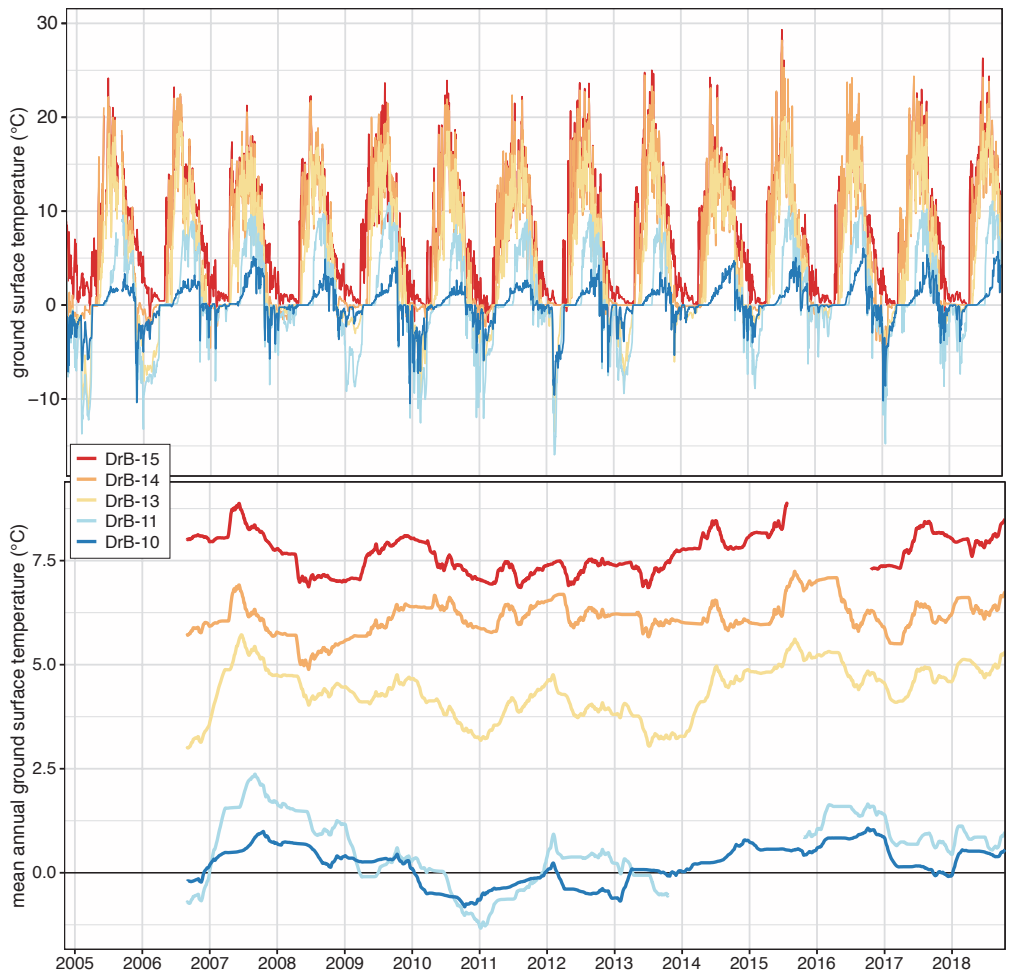

Figure 7.3: *Daily mean (above) and running annual mean (below) ground surface temperatures at five points along the Dreveneuse d'en Bas talus slope (see Figure 7.1 for the exact position of the loggers).*

The influence of the ventilation process on the near surface thermal regime is clearly visible in the GST time series (Figure 7.3). In the upper part of the talus slope, the MAGST remain positive, which shows the outflow of warm air, whereas in the lower part the MAGST are sporadically negative. This particularly depends on the strength of the winter ventilation process. The GST logger in the uppermost part of the talus (DrB-15) shows the highest MAGST of the five loggers. Conversely, the lowermost sensor (DrB-10) generally measures the lowest MAGST due to exceptionally low summer GST (only a few days in October above 5°C in 14 years, see Figure 7.3). At the location 30 m upslope (DrB-11), GST is even lower in winter and the ground subsurface is frozen later in summer (latest melt out date: 29th July 2013). Here, the ground surface significantly warms in late summer or autumn (most days between 5 and 10 °C). The differences in the thermal regime between this logger and the lowest one illustrate the typical asymmetry of the reverted ventilation flow. This pattern has been described in detail at the Creux du Van talus slope by Delaloye (2004).

The last occurrence of permafrost in 2010–2012 (see Morard 2011) is characterized by a long period of MAGST below 0 °C in the lower part of the talus slope (DrB-10 and 11). Following this period, an overall increase of MAGST was observed for all loggers until summer 2016 coinciding with the exceptionally mild winter 2015/16 (see Chapter 2). No significant freezing was observed within the entire talus slope during this period. The relatively high air temperatures during the winter reduced the strength of the internal ventilation and, hence, the cooling of the ground.

The two boreholes at Dreveneuse d'En Bas are located in the lower part of the talus slope, where the ventilation process results in sporadic permafrost occurrence as described in PERMOS (2010). Figure 7.4 shows that permafrost conditions occurred in DRE_0104 (BH 1) at around 11 m depth (that is deeper than the base of the coarse debris layer at 9.5 m) from 2005 to 2007 as well as from 2010 to 2012 (see also Morard 2011). However, since then, no permafrost conditions have been observed. A similar temporal pattern occurred at about 2.5 m depth only in the lower borehole, which is much closer to the surface and drilled in coarser debris (base at 3.5 m).

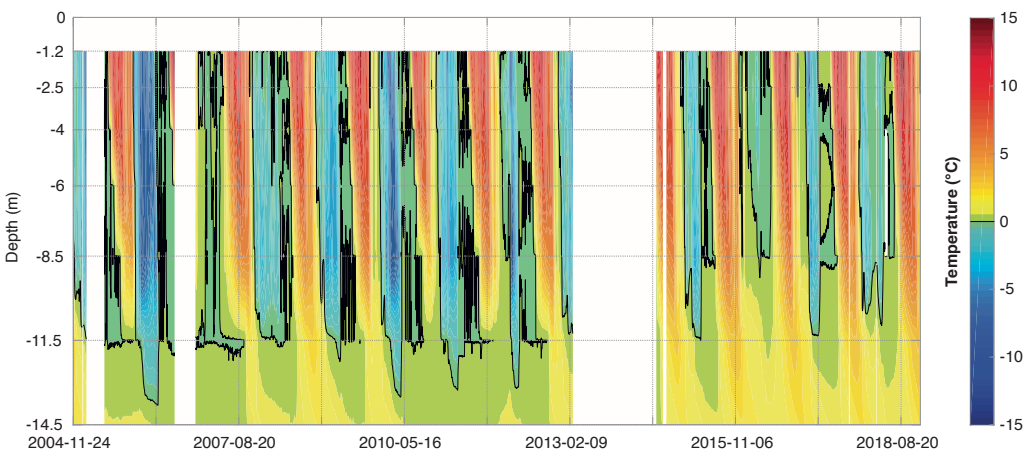

Figure 7.4: Temperature evolution in the borehole DRE_0104 (see Fig. 7.1) between November 2004 and September 2018.

Similarly to the MAGST, temperatures at depth have been warming since 2013. This trend is essentially observed during winter with comparatively high temperatures at all depths and a shallow penetration depth of the 0 °C isotherm. This is due to the higher outside air temperatures during most of the past 7 winters, which limited the strength of the ventilation process and reduced its ground cooling effect.

ERT measurements were carried out at Dreveneuse d'En Bas from 2007 to 2015 to spatially characterize the subsurface composition as well as to document its changes (cf. Mollaret et al. 2018 for the complete time series). The first and last tomograms collected in October 2007 and 2015 at Dreveneuse d'En Bas (Figure 7.5) show resistivity patterns and values that are typical for a talus slope. The clearly delineated resistive zone at depth corresponds to the porous part of the talus slope, which is devided into a highly resitive (>100'000 Ωm) part located in the vicinity of DRE_0104 (BH 1) and a resistive part (~50'000 Ωm) in the upper half of the ERT-profile. This is consistent with the distribution of temperatures resulting from the ventilation process, i.e. the cold reservoir in the lower part of the talus slope. Given the minimum temperatures measured in DRE_0104 (BH 1) at the date of the ERT surveys (0.7 °C in 2007 and 1.6 °C in 2015), it is however very unlikely that the highly resistive zone indicates frozen conditions.

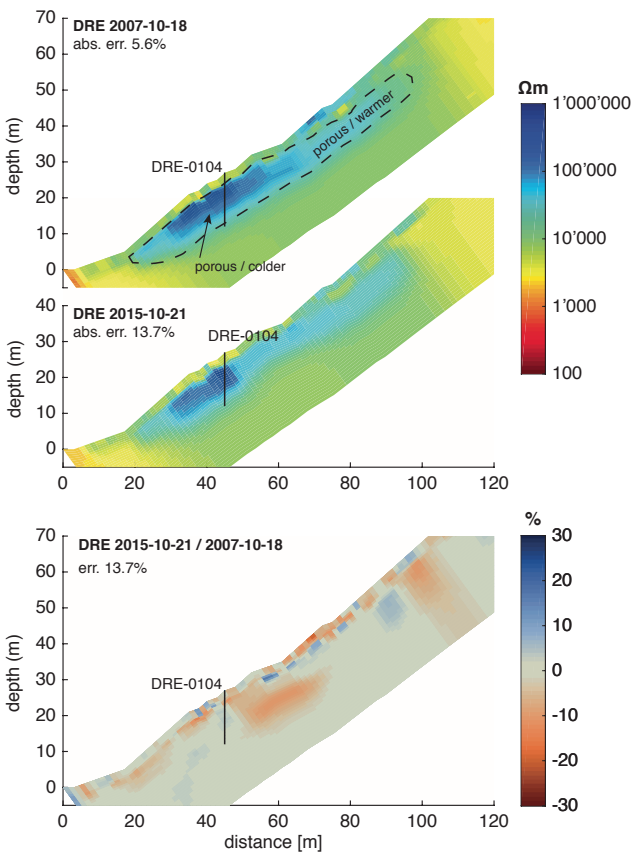

Figure 7.5:
Tomograms showing the resistivity distribution in October (upper panels) and the temporal resistivity change (lower panel) for the years 2007 and 2015 of the ERT profile along the Dreveneuse talus slope.

Between 2007 and 2015, a significant resistivity decrease is observed in the highly resistive zone in middle part of the profile (around 50–70 m) at a depth of 5 to 15 m, which corresponds to the overcooled porous part of the talus slope. Temperature measurements at the surface as well as in the borehole indicate a general increase since 2011 (Figures 7.3 and 7.4). Thus, this anomaly is likely representing differences in temperature and humidity caused by the complex and variable ventilation.

7.3 Summary

The measurements at Dreveneuse d'En Bas illustrate the role of complex ventilation processes and convective/advective heat fluxes for the thermal regime of talus slopes. The most important factor for the thermal conditions in a talus slope is the intensity of winter cooling and the recharge of the cold reservoir, whereas snow cover and summer temperatures play only a minor role.

The data series acquired at Dreveneuse d'En Bas since 2004 confirm the sporadic presence of permafrost in the mid- and lower sections of the talus slope. Since 2012, however, no permafrost conditions have been observed. Furthermore, over the past 5 years, ERT and temperatures measurements consistently show a decreased efficiency of the ventilation process, which is responsible for the important freezing of the ground, as a result of higher winter air temperatures.

8 Synthesis

The reporting period 2014/2015 to 2017/18 was marked by continuously above-average air temperatures but highly variable snow conditions, with the occurrence of both extremely snow-poor (2016/2017) and snow-rich winters (2017/2018). These climatic conditions impacted the evolution of permafrost in the Swiss Alps, which was consistently observed during the 4-year period using three different observation elements (Figure 8.1): ground temperatures, permafrost conductivity (the inverse of the resistivity, see Chapter 4), and creep velocity.

From 2009 until 2015, a consistent general increase of the permafrost temperature at depth, an acceleration of the permafrost creep velocities as well as an increase of the permafrost conductivity were observed. Following this maximum, both the temperatures at cold and snow-influenced permafrost sites (like on Stockhorn or Corvatsch-Murtèl) and the creep velocities decreased until 2017/2018 as a result of the extremely snow-poor winter 2016/2017 (and 2015/2016 in Eastern Switzerland). Conversely, conductivity of the permafrost as well as the boreholes temperatures close to 0 °C (like on Schilthorn) continued to increase and new record values were reached in 2018.

The temporary cooling observed in 2016/2017 ended after the very warm year 2017/2018. During the last year of this report the permafrost conditions are characterized by transient signals varying between sites, observation elements and depths considered: the permafrost creep velocities were stationary or slightly increasing, whereas the permafrost conductivities reached record values at the end of the summer 2018. Ground temperatures similarly show contrasted signals. Conditions near the surface are very warm and GST and ALT reached new record values in summer 2018. Permafrost temperatures at 10 and especially 20m depth, however, still remained under the influence of the snow-poor winter 2016/2017.

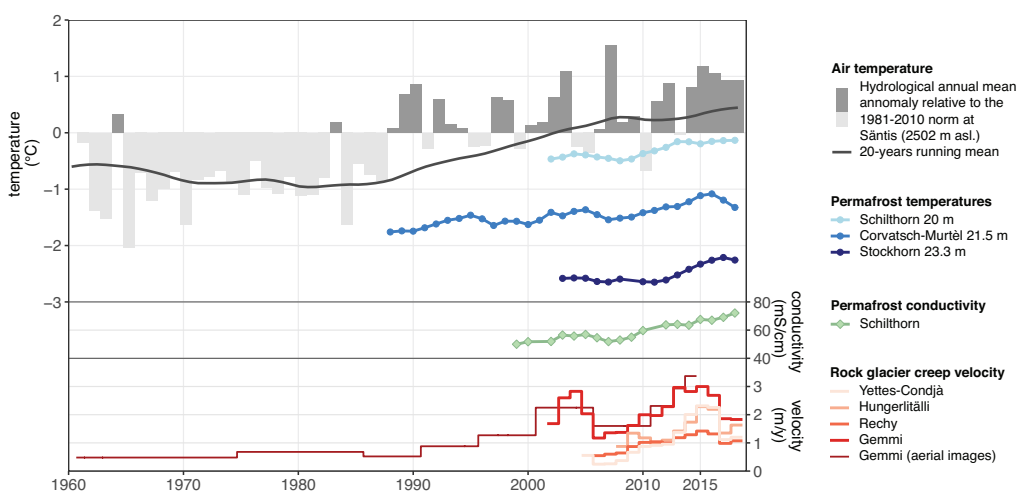

Figure 8.1: Evolution of the three PERMOS observation elements: annual average of permafrost temperatures at around 20 m depth, permafrost conductivity and rock glacier creep velocity, compared to long-term air temperature observations (data source: MeteoSwiss).

Acknowledgements

The Swiss Permafrot Monitoring Network PERMOS is financially supported by an agreement between MeteoSwiss, in the framework of GCOS Switzerland, the Federal Office for the Environment FOEN and the Swiss Academy of Sciences SCNAT.

The equipment and maintenance of the PERMOS sites as well as fieldwork and data preprocessing were performed in the scope of PERMOS and research projects by the six PERMOS partners: The Swiss Federal Institute of Technology (ETH Zurich) through their Institute for Geotechnical Engineering, Laboratory of Hydraulics, Hydrology and Glaciology and Computer Engineering and Networks Laboratory, the WSL Institute for Snow and Avalanche Research SLF, the University of Applied Sciences and Arts of Southern Switzerland (SUPSI) through their Institute of Earth Sciences, the University of Lausanne through the Institute of Earth Surface Dynamics, and the Geography Departments of the Universities of Fribourg and Zurich. The in-kind contributions of the partner institutions as well as the personal commitment are indispensable for the development and maintenance of the PERMOS Network. The present report is a compilation from a large number of contributors collecting, processing and analyzing data, writing text, and providing illustrations and photos as can be seen in the imprint.

The University of Zurich lead the drilling campaign at Corvatsch-Murtèl, which was financed by FOEN, the University of Lausanne coordinated and fincancially supported the drillig at Tsaté, which was additionally supported by PERMOS and MeteoSwiss in the framework of GCOS Switzerland, and the Schilthorn borehole was jointly financed by PERMOS and the University of Fribourg. Important support for the conception and installation of the borehole instrumentation was provided by Alpug GmbH.

SensAlpin GmbH provided professional support for the maintenance of the boreholes and meteo stations as well as the implementation of data flows. In addition, there were numerous field assistants, students and technicians of the PERMOS Partners who came to the field, helped to obtain data and maintained field equipment. Thank you very much for all your efforts! We further like to acknowledge the generous support from Andermatt Gotthard Sportbahnen, Bergbahnen Grächen, Corvatsch-Furtschellas Bahnen, High Altitude Research Station Jungfraujoch, Jungfraubahnen, Schilthorn Bahnen, Téléverbier and Télénendaz.

Finally, our sincere thanks go to all who supported PERMOS in any way and contributed to this report.

References

Arenson, L., Hoelzle, M. and Springman, S. M. 2002. Borehole deformation measurements and internal structure of some rock glaciers in Switzerland. Permafrost and Periglacial Processes, 13(2), 117–135. http://doi.org/10.1002/ppp.414.

Biskaborn, B.K., Smith, S.L., Noetzli, J., Matthes, H., Vieira, G., Streletskiy, D.A., Schoeneich, P., Romanovsky, V.E., Lewkowicz, T., Abramov, A., Allard, M., Boike, J., Cable, W.L., Christiansen, H.H., Delaloye, R., Diekmann, B., Drozdov, D., Etzelmuller, B., Grosse, G., Guglielmin, M., Ingeman- Nielsen, T., Isaksen, K., Ishikawa, M., Johansson, M., Johannsson, H., Joo, A., Kaverin, D., Kholodov, A., Konstantinov, P., Kroger, T., Lambiel, C., Lanckman, J.-P., Luo, D., Malkova, G., Meiklejohn, I., Moskalenko, N., Oliva, M., Phillips, M., Ramos, M., Sannel, A.B.K., Sergeev, D., Seybold, C., Skryabin, P., Vasiliev, A., Wu, Q., Yoshikawa, K., Zheleznyak, M. and Lantuit, H. 2019. Permafrost is warming at a global scale. Nature Communications 10: 264, DOI: 10.1038/s41467-018-08240-4.

Buchli, T., Merz, K., Zhou, X., Kinzelbach, W. and Springman, S. M. 2013. Characterization and Monitoring of the Furggwanghorn Rock Glacier, Turtmann Valley, Switzerland: Results from 2010 to 2012. Vadose Zone Journal, 12(1).

Cicoira, A., Beutel, J., Faillettaz, J., Gärtner-Roer, I. and Vieli, A. 2019. Resolving the influence of temperature forcing through heat conduction on rockglacier dynamics: a numerical modelling approach. The Cryosphere, 13, 927–942, DOI: 10.5194/tc-13-927-2019.

Delaloye, R. 2004. Contribution à l'étude du pergélisol de montagne en zone marginale. PhD thesis, University of Fribourg, Fribourg, 240 pp.

Delaloye, R. and Lambiel, C. 2005. Evidence of winter ascending air circulation throughout talus slopes and rock glaciers situated in the lower belt of alpine discontinuous permafrost (Swiss Alps). Norsk Geografisk Tidsskrift. 59(2). 194–203.

Delaloye, R. and Lambiel, C. 2017. Suivis par GPS et webcam de glaciers rocheux à mouvement rapide. In: Malet, E. and Astrade, L. (eds.), Monitoring en milieux naturels – Retours d'expériences en terrains difficiles. Collection EDYTEM 19, 37–46.

Delaloye, R. and Staub, B. 2016. Seasonal variations of rock glacier creep: time series observations from the Western Swiss Alps. Proceedings of the XI International Conference on Permafrost, https://doi.org/10.2312/GFZ.LIS.2016.001.

Delaloye, R., Lambiel, C. and Gärtner-Roer, I. 2010. Overview of rock glacier kinematics research in the Swiss Alps: seasonal rhythm, interannual variations and trends over several decades. Geographica Helvetica, 65(2), 135–145.

Gruber, S., Hoelzle, M. and Haeberli, W. 2004. Rock-wall temperatures in the Alps: modelling their topographic distribution and regional differences. Permafrost and Periglacial Processes 15: 299–307. DOI: 10.1002/ppp.501.

Harris, C., Haeberli, W., Vonder Mühll, D. and King, L. 2001. Permafrost monitoring in the high mountains of Europe: the PACE Project in its global context, Permafrost and Periglacial Processes 12, 3–11. DOI: 10.1002/ppp.377.

Lambiel, C. 2006. Le pergélisol dans les terrains sédimentaires à forte déclivité: distribution, régime thermique et instabilités. PhD thesis, University of Lausanne, Lausanne, 260 pp.

MeteoSchweiz 2015. Klimareport 2014. Bundesamt für Meteorologie und Klimatologie MeteoSchweiz, Zürich. 80 pp.

MeteoSchweiz 2016. Klimareport 2015. Bundesamt für Meteorologie und Klimatologie MeteoSchweiz, Zürich. 84 pp.

MeteoSchweiz 2017. Klimareport 2016. Bundesamt für Meteorologie und Klimatologie MeteoSchweiz, Zürich. 80 pp.

MeteoSchweiz 2018. Klimareport 2017. Bundesamt für Meteorologie und Klimatologie MeteoSchweiz, Zürich. 84 pp.

MeteoSchweiz 2019. Klimabulletin 2018. Bundesamt für Meteorologie und Klimatologie MeteoSchweiz, Zürich. 12 pp.

Mollaret, C., Hilbich, C., Pellet, C., Flores Orozco, A., Delaloye, R and Hauck, C. 2018. Mountain permafrost degradation documented through a network of permanent electrical resistivity tomography sites. The Cryosphere Discussions 1–34. DOI: 10.5194/tc-2018-272.

Morard, S. 2011. Effets de la circulation d'air par effet de cheminée dans l'évolution du régime thermique des éboulis froids de basse et moyenne altitude. PhD thesis, University of Fribourg, Fribourg, 220 pp.

Morard, S., Delaloye, R. and Dorthe, J. 2008. Seasonal thermal regime of a mid-latitude ventilated debris accumulation. Proceedings of the 9th International Conference on Permafrost, Fairbanks, Alaska. 29. 1233–1238.

Noetzli, J. and Gruber, S. 2009. Transient thermal effects in Alpine permafrost. The Cryosphere, 3, 85–99.

Noetzli, J., Christiansen, H.H., Deline, P., Gugliemin, M., Isaksen, K., Romanovsky, V., Smith, S., Zhao, L. and Streletskiy, D. A. 2018. Permafrost thermal state. In: State of the Climate in 2017. Bulletin of the American Meteorological Society 99 (8), 20–22, doi:10.1175/2018-BAMSStateoftheClimate.1.

PERMOS 2010. Permafrost in Switzerland 2006/2007 and 2007/2008. Noetzli, J. and Vonder Muehll, D. (eds.), Glaciological Report (Permafrost) No. 8/9 of the Cryospheric Commission (CC) of the Swiss Academy of Sciences (SCNAT), 68 pp.

PERMOS 2013. Permafrost in Switzerland 2008/2009 and 2009/2010. Noetzli, J. (ed.), Glaciological Report (Permafrost) No. 10/11 of the Cryospheric Commission (CC) of the Swiss Academy of Sciences (SCNAT), 80 pp.

PERMOS 2016. Permafrost in Switzerland 2010/2011 to 2013/2014. Noetzli, J., Luethi, R. and Staub, B. (eds.), Glaciological Report (Permafrost) No. 12–15 of the Cryospheric Commission (CC) of the Swiss Academy of Sciences (SCNAT), 85 pp.

Staub, B., Hasler, A., Noetzli, J. and Delaloye, R. 2017. Gap-Filling algorithm for ground surface temperature data measured in permafrost and periglacial environments, Permafrost and Periglacial Processes, 28, 275–285. DOI: 10.1002/ppp.1913

Staub, B., Lambiel, C. and Delaloye, R. 2016. Rock glacier creep as a thermally-driven phenomenon: A decade of inter-annual observation from the Swiss Alps. Proceedings of the XI International Conference on Permafrost, Potsdam, Germany, 96–97.

Wakonigg, H. 1996. Unterkühlte Schutthalden. Beiträge zur Permafrostforschung in Österreich. Arbeiten aus dem Inst. f. Geogr. Karl-Franzens-Universität Graz, 33, 209–223.

Weber, S., Beutel, J., Da Forno, R., Geiger, A., Gruber, S., Gsell, T., Hasler, A., Keller, M., Lim, R., Limpach, P., Meyer, M., Talzi, I., Thiele, L., Tschudin, C., Vieli, A., Vonder Mühll, D. and Yücel, M. 2019. A decade of detailed observations (2008–2018) in steep bedrock permafrost at Matterhorn Hörnligrat (Zermatt, CH). Earth System Science Data Discussions, https://doi.org/10.5194/essd-2019-14.

Wirz, V., Beutel, J., Gruber, S., Gubler, S. and Purves, R.S 2014. Estimating velocity from noisy GPS data for investigating the temporal variability of slope movements. Natural Hazards and Earth System Sciences, 14 (9), 2503–2520, https://doi.org/10.5194/nhess-14-2503-2014.

Wirz, V., Geertsema, M., Gruber, S. and Purves, R.S. 2016. Temporal variability of diverse mountain permafrost slope movements derived from multi-year daily GPS data, Mattertal, Switzerland. Landslides, 13(1), 67–83. https://doi.org/10.1007/s10346-014-0544-3.

Appendix A

Aget

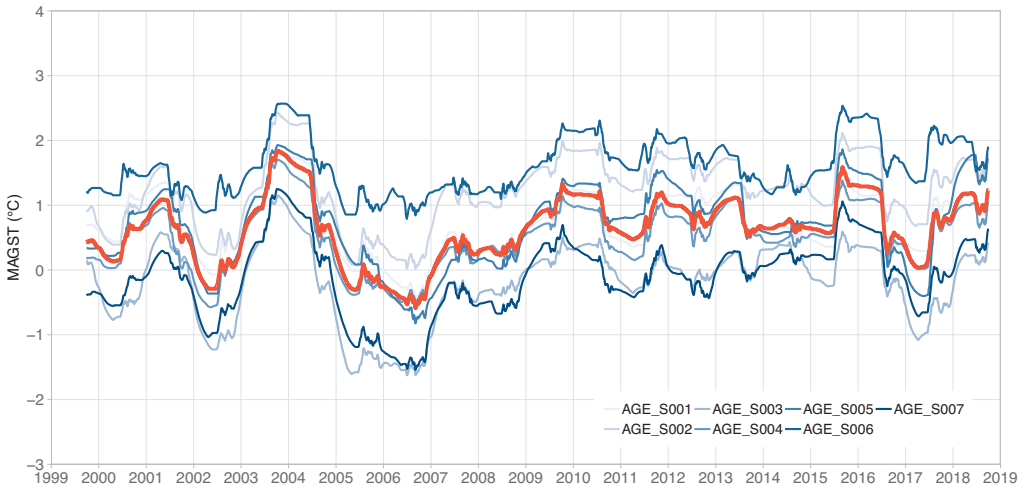

Figure A.1: *Running annual mean of ground surface temperature time series measured at the site Aget. Time series were gap-filled using the method by Staub et al. (2017) and only time series with at least 90% of data were selected. The thick red line is the mean of the indiviudal loggers.*

Alpage de Mille

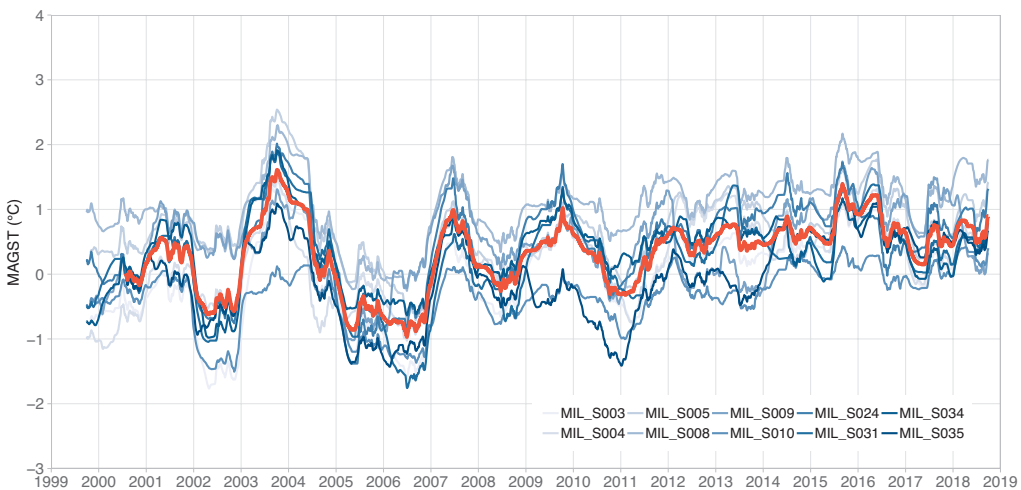

Figure A.2: *Running annual mean of ground surface temperature time series measured at the site Alpage de Mille. Time series were gap-filled using the method by Staub et al. (2017) and only time series with at least 90% of data were selected. The thick red line is the mean of the indiviudal loggers.*

Les Attelas

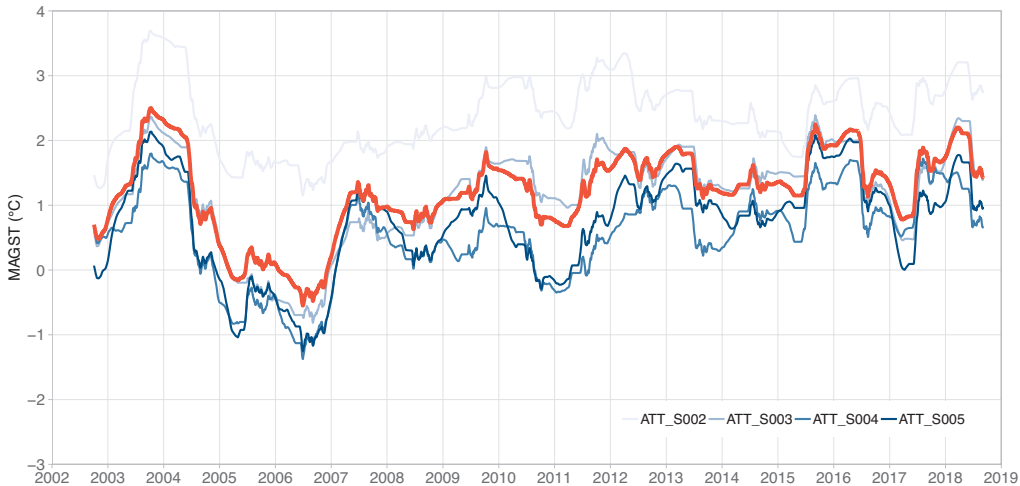

Figure A.3 *Running annual mean of ground surface temperature time series measured at the site Les Attelas. Time series were gap-filled using the method by Staub et al. (2017) and only time series with at least 90% of data were selected. The thick red line is the mean of the indiviudal loggers.*

Corvatsch-Murtèl (rock glacier)

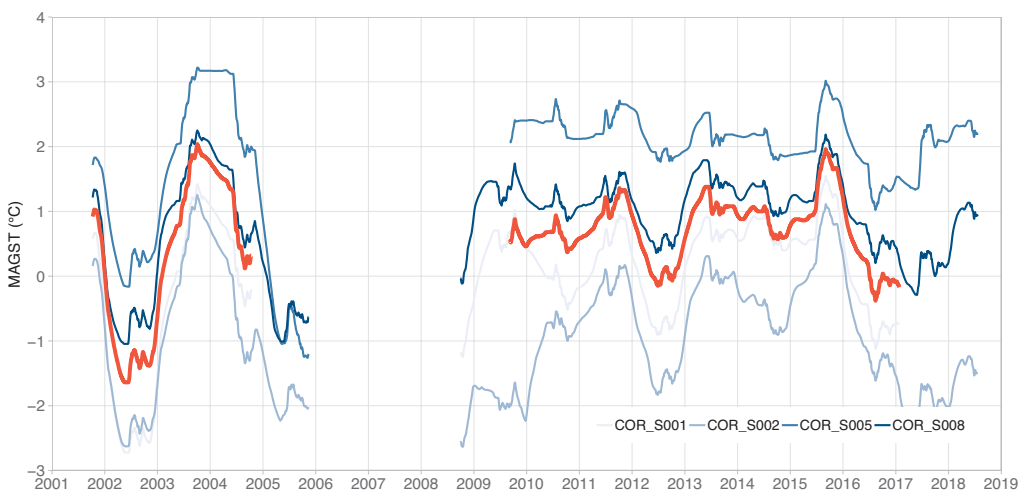

Figure A.4 *Running annual mean of ground surface temperature time series measured at the site Corvatsch-Murtèl. Time series were gap-filled using the method by Staub et al. (2017) and only time series with at least 90% of data were selected. The thick red line is the mean of the indiviudal loggers.*

Corvatsch (flat rock)

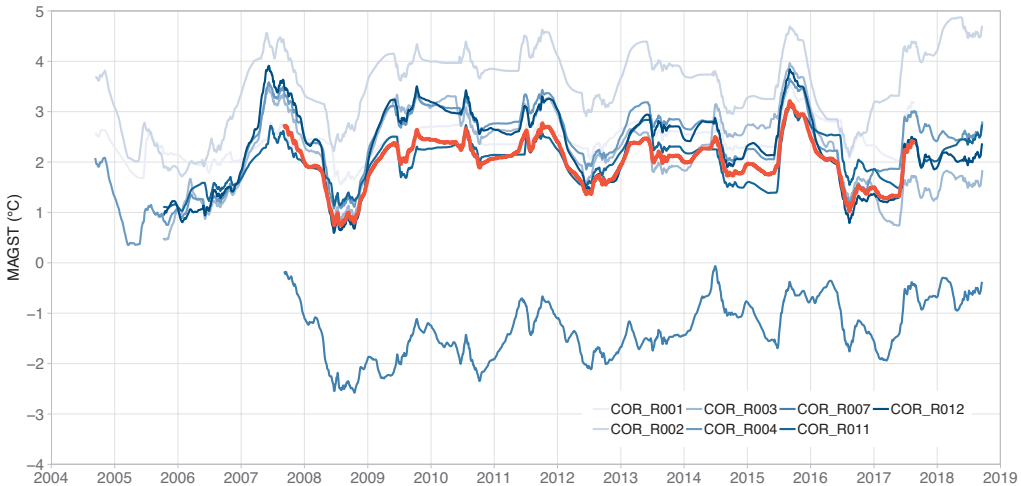

Figure A.5: *Running annual mean of ground surface temperature time series measured at the site Corvatsch on flat rock. Time series were gap-filled using the method by Staub et al. (2017) and only time series with >90% of data were selected. The thick red line is the mean of the indiviudal loggers.*

Corvatsch (steep rock)

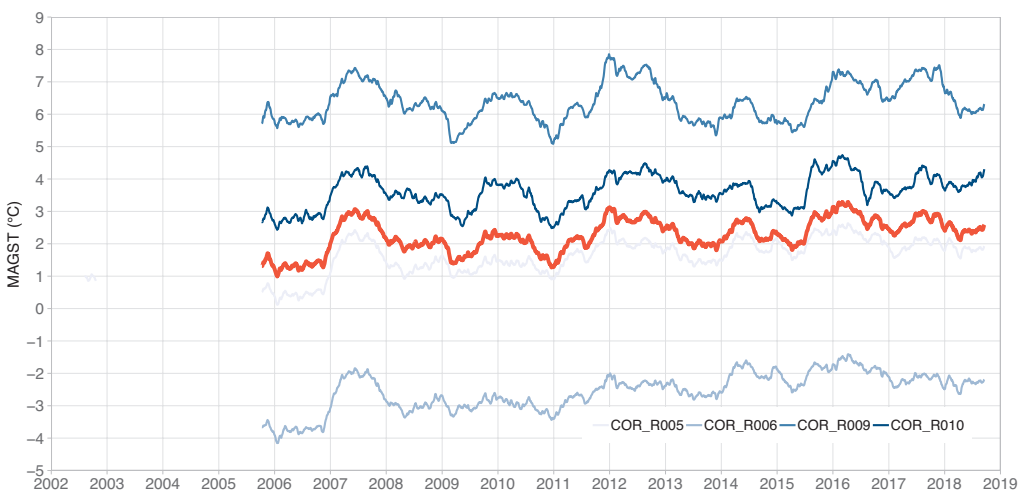

Figure A.6: *Running annual mean of ground surface temperature time series measured at the site Corvatsch in near-vertical rock. Time series were gap-filled using the method by Staub et al. (2017) and only time series with at least 90% of data were selected. The thick red line is the mean of the indiviudal loggers.*

Dreveneuse

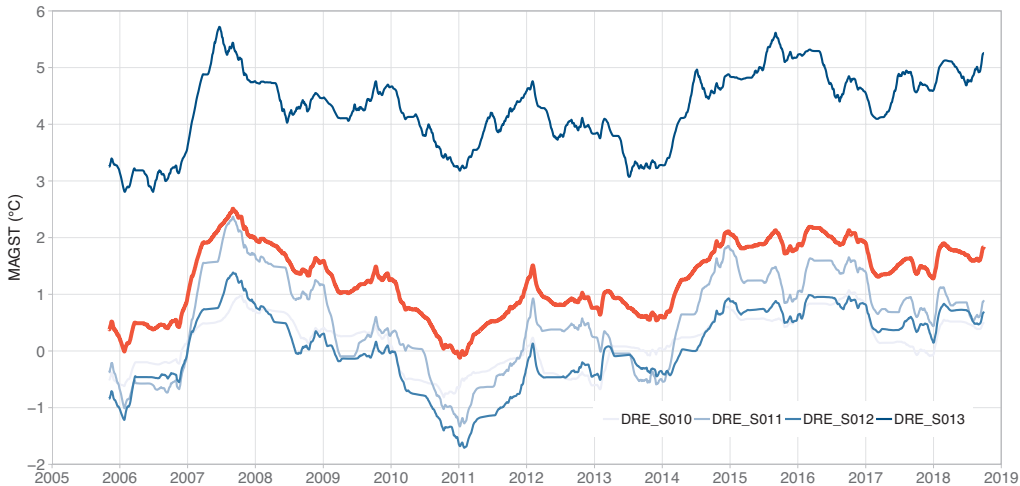

Figure A.7: *Running annual mean of ground surface temperature time series measured at the site Dreveneuse. Time series were gap-filled using the method by Staub et al. (2017) and only time series with at least 90% of data were selected. The thick red line is the mean of the indiviudal loggers.*

Gentianes

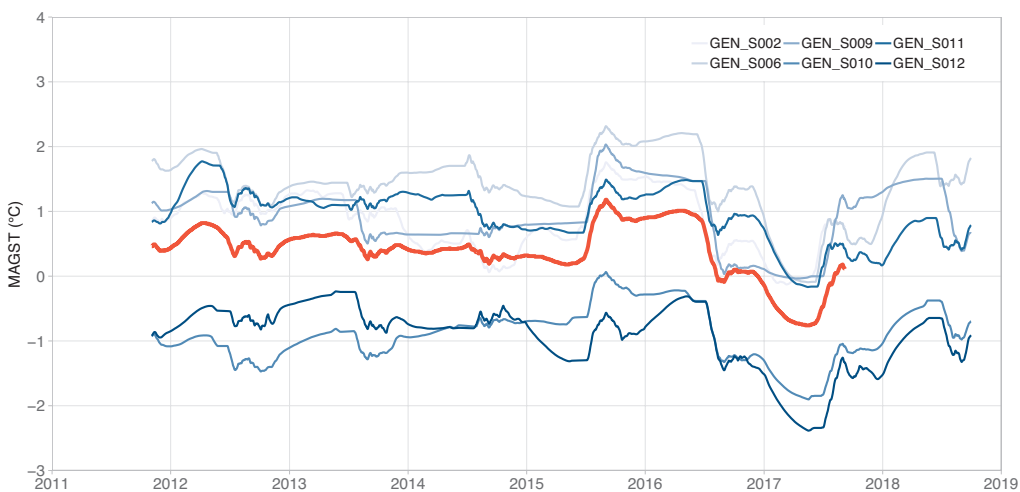

Figure A.8: *Running annual mean of ground surface temperature time series measured at the site Gentianes. Time series were gap-filled using the method by Staub et al. (2017) and only time series with at least 90% of data were selected. The thick red line is the mean of the indiviudal loggers.*

Gemmi-Furggentälti

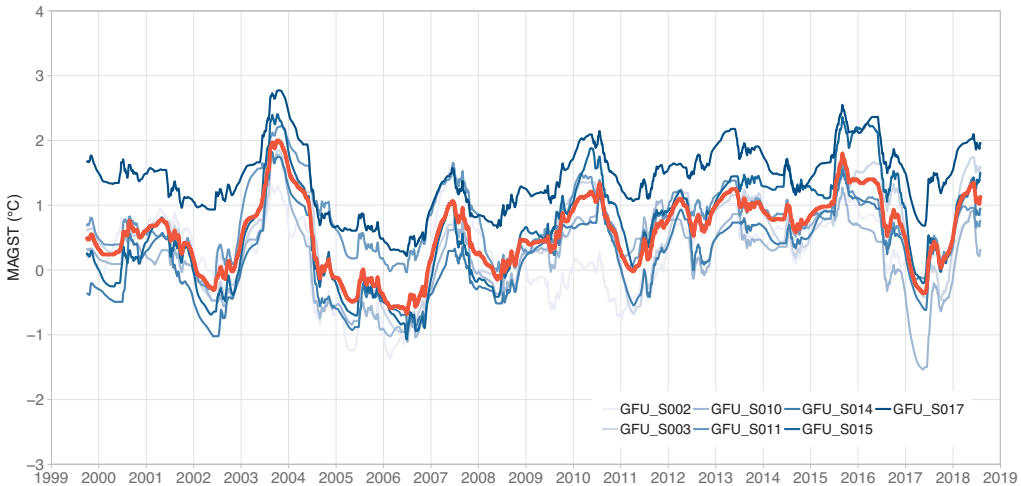

Figure A.9: *Running annual mean of ground surface temperature time series measured at the site Gemmi-Furggentälti. Time series were gap-filled using the method by Staub et al. (2017) and only time series with >90% of data were selected. The thick red line is the mean of the indiviudal loggers.*

Grosses Gufer

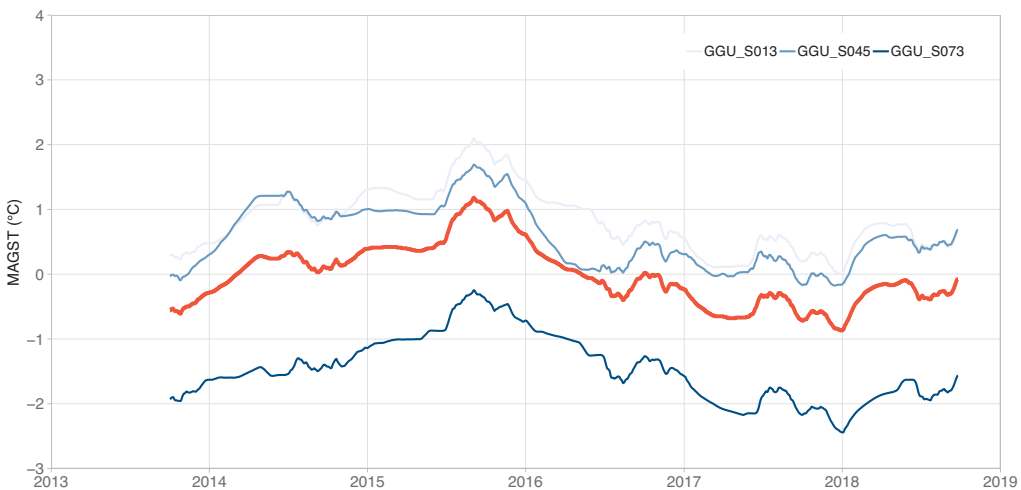

Figure A.10: *Running annual mean of ground surface temperature time series measured at the site Grosses Gufer. Time series were gap-filled using the method by Staub et al. (2017) and only time series with at least 90% of data were selected. The thick red line is the mean of the indiviudal loggers.*

Lapires

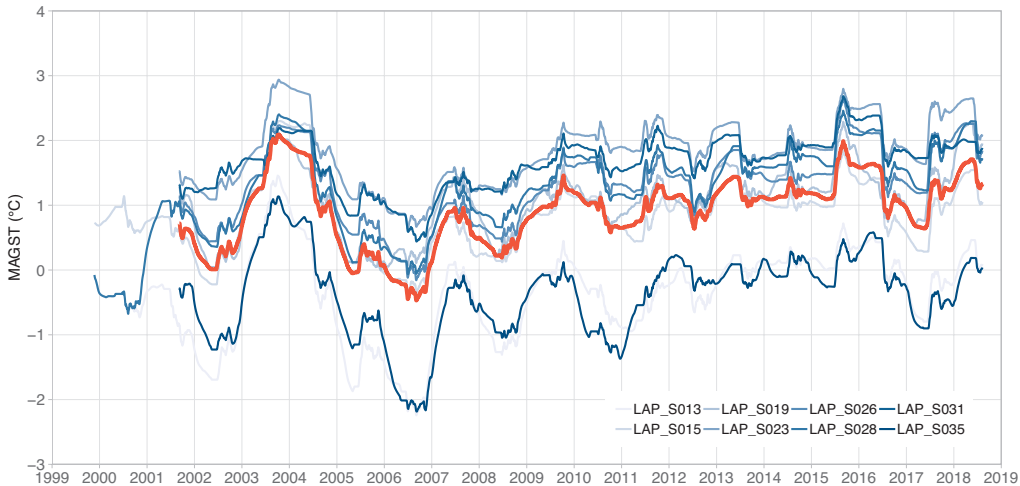

Figure A.11: *Running annual mean of ground surface temperature time series measured at the site Lapires. Time series were gap-filled using the method by Staub et al. (2017) and only time series with at least 90% of data were selected. The thick red line is the mean of the indiviudal loggers.*

Largario

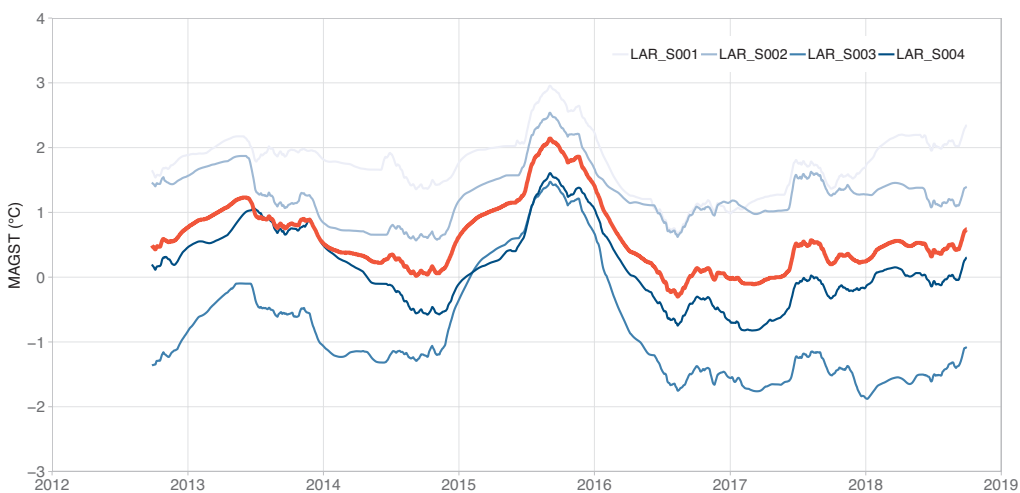

Figure A.12: *Running annual mean of ground surface temperature time series measured at the site Largario. Time series were gap-filled using the method by Staub et al. (2017) and only time series with at least 90% of data were selected. The thick red line is the mean of the indiviudal loggers.*

Monte Prosa

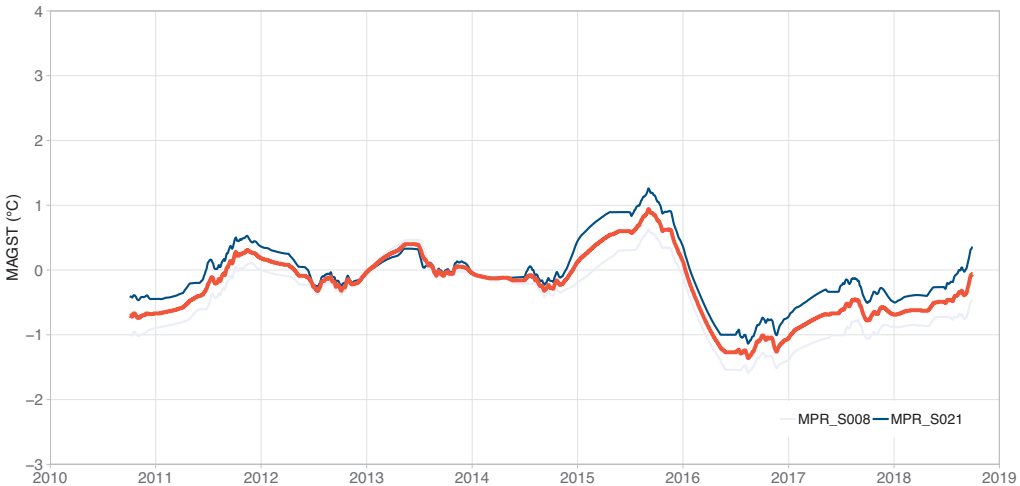

Figure A.13: Running annual mean of ground surface temperature time series measured at the site Monte Prosa. Time series were gap-filled using the method by Staub et al. (2017) and only time series with at least 90% of data were selected. The thick red line is the mean of the indiviudal loggers.

Réchy – Becs de Bosson

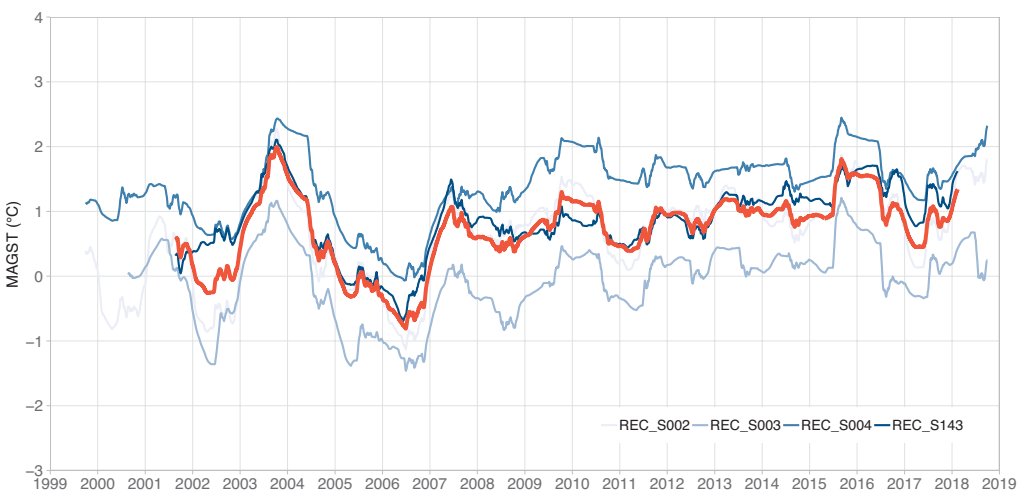

Figure A.14: Running annual mean of ground surface temperature time series measured at the site Réchy – Becs de Bosson. Time series were gap-filled using the method by Staub et al. (2017) and only time series with >90% of data were selected. The thick red line is the mean of the indiviudal loggers.

Réchy – Tsavolires

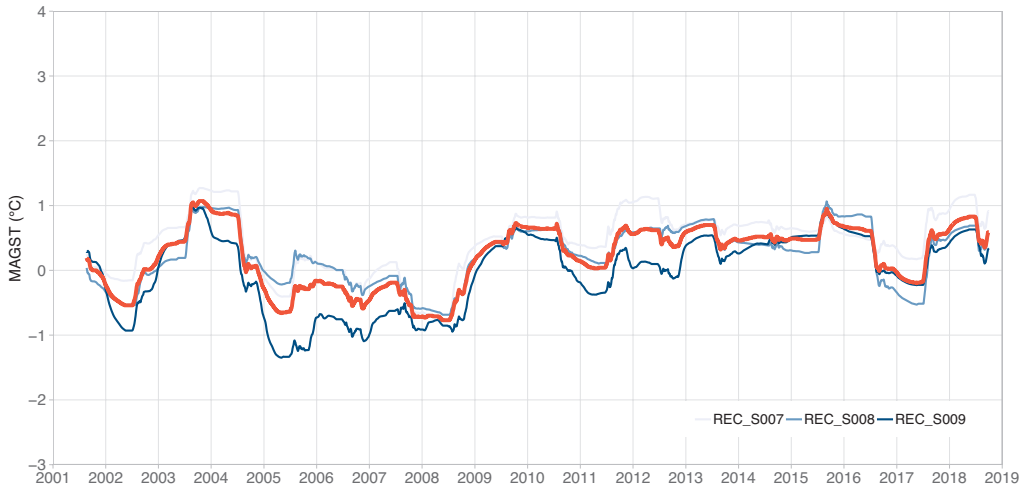

Figure A.15: Running annual mean of ground surface temperature time series measured at the site Réchy – Tsavolires. Time series were gap-filled using the method by Staub et al. (2017) and only time series with >90% of data were selected. The thick red line is the mean of the indiviudal loggers.

Schafberg

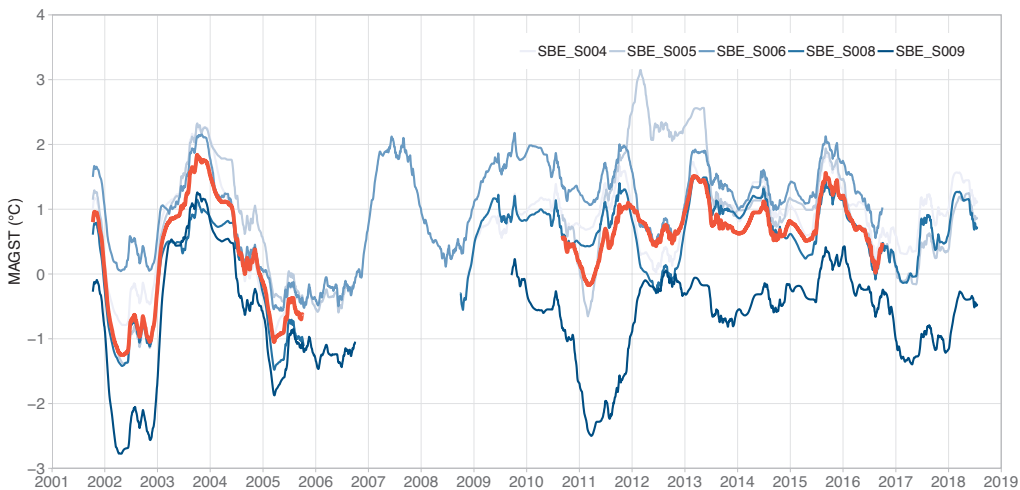

Figure A.16: Running annual mean of ground surface temperature time series measured at the site Schafberg. Time series were gap-filled using the method by Staub et al. (2017) and only time series with at least 90% of data were selected. The thick red line is the mean of the indiviudal loggers.

Schilthorn (north slope)

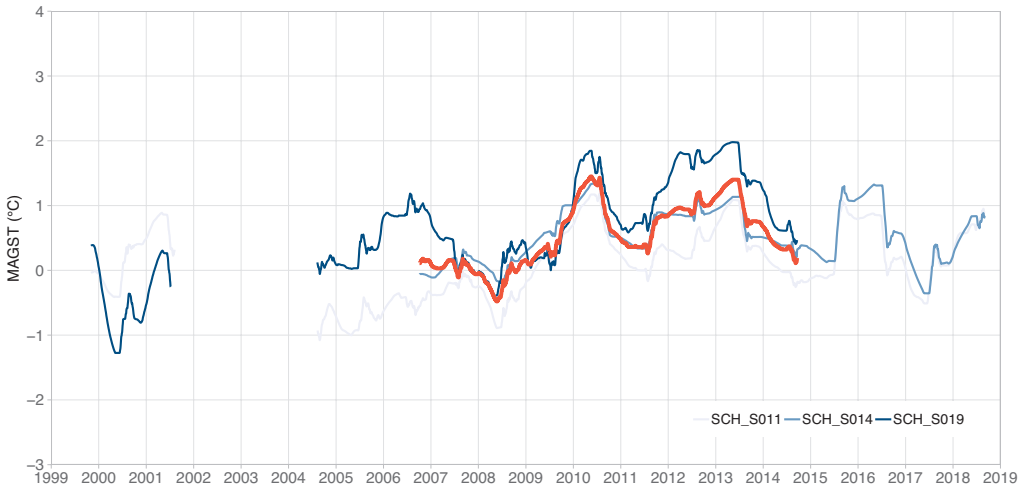

Figure A.17: Running annual mean of ground surface temperature time series measured at the site Schilthorn – North Slope. Time series were gap-filled using the method by Staub et al. (2017) and only time series with >90% of data were selected. The thick red line is the mean of the indiviudal loggers.

Schilthorn (south slope)

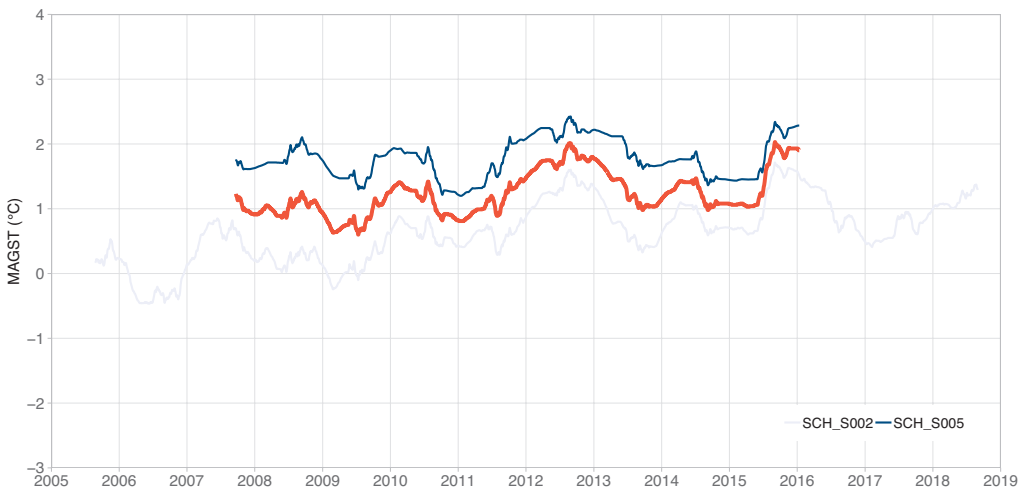

Figure A.18: Running annual mean of ground surface temperature time series measured at the site Schilthorn – South Slope. Time series were gap-filled using the method by Staub et al. (2017) and only time series with >90% of data were selected. The thick red line is the mean of the indiviudal loggers.

Schilthorn (flat rock)

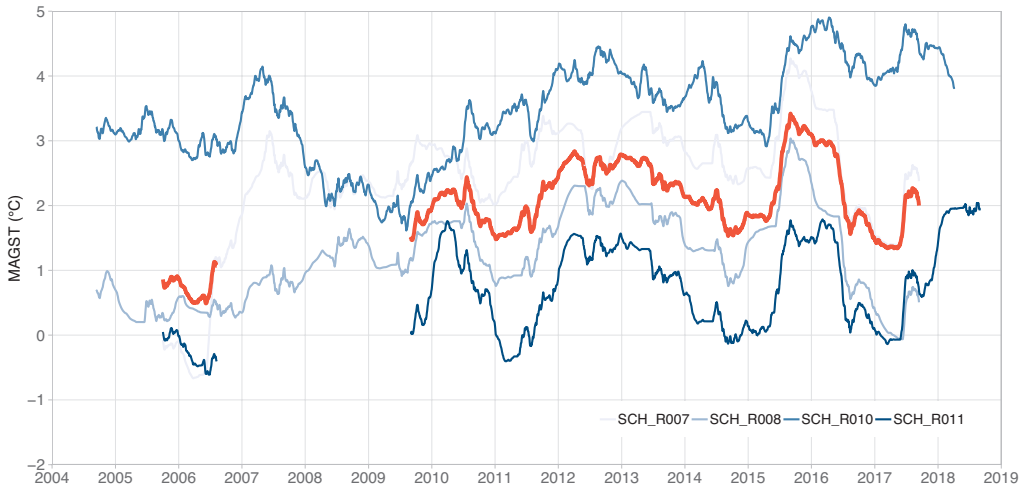

Figure A.19: Running annual mean of ground surface temperature time series measured at the site Schilthorn on flat rock. Time series were gap-filled using the method by Staub et al. (2017) and only time series with >90% of data were selected. The thick red line is the mean of the indiviudal loggers.

Schilthorn (steep rock)

Figure A.20: Running annual mean of ground surface temperature time series measured at the site Schilthorn in near-vertical rock. Time series were gap-filled using the method by Staub et al. (2017) and only time series with at least 90% of data were selected. The thick red line is the mean of the indiviudal loggers.

Tsarmine

Figure A.21: Running annual mean of ground surface temperature time series measured at the site Tsarmine. Time series were gap-filled using the method by Staub et al. (2017) and only time series with at least 90% of data were selected. The thick red line is the mean of the indiviudal loggers.

Tsaté

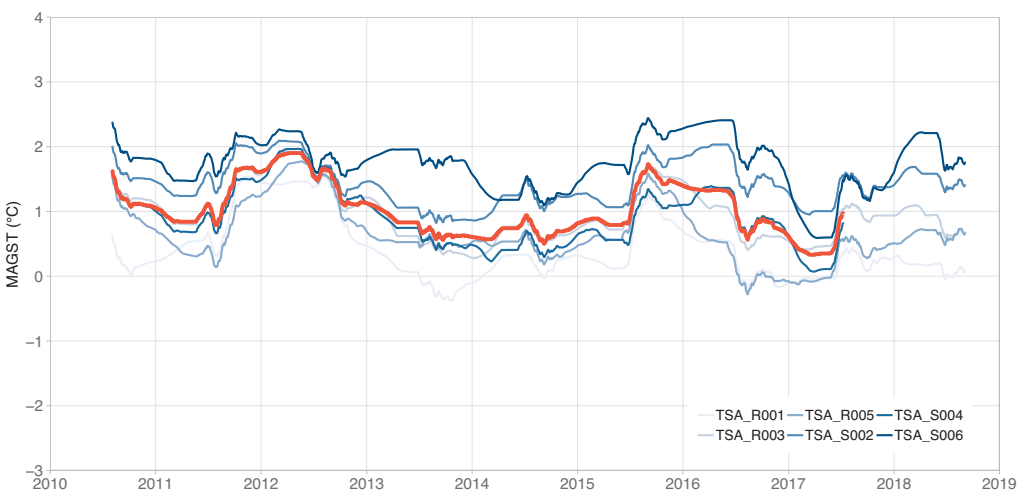

Figure A.22: Running annual mean of ground surface temperature time series measured at the site Tsaté. Time series were gap-filled using the method by Staub et al. (2017) and only time series with at least 90% of data were selected. The thick red line is the mean of the indiviudal loggers.

Valle di Sceru

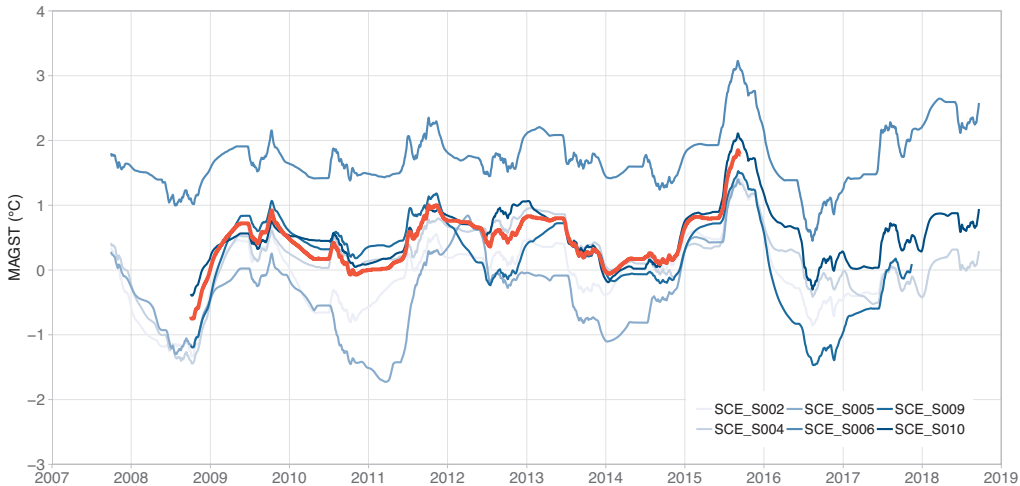

Figure A.23: Running annual mean of ground surface temperature time series measured at the site Valle di Sceru. Time series were gap-filled using the method by Staub et al. (2017) and only time series with at least 90% of data were selected. The thick red line is the mean of the indiviudal loggers.

Yettes Condjà

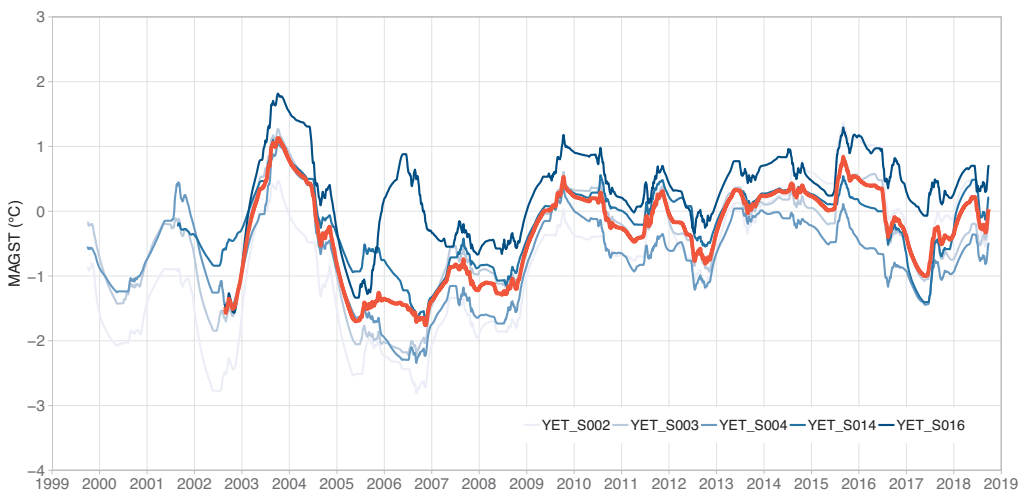

Figure A.24: Running annual mean of ground surface temperature time series measured at the site Yettes Condjà. Time series were gap-filled using the method by Staub et al. (2017) and only time series with at least 90% of data were selected. The thick red line is the mean of the indiviudal loggers.

Appendix B

PERMOS Boreholes

Table B.1a: Location and characteristics of the boreholes.

Borehole	Region	Morphology	X CH1903	Y CH1903	Elev. (m asl.)	Slp. (°)	Asp.	Surface mat.
Corvatsch-Murtèl 0200	Engadine	Rock glacier	783175	144692	2672	10	NW	Coarse blocks
Corvatsch-Murtèl 0287	Engadine	Rock glacier	783160	144720	2670	10	NW	Coarse blocks
Corvatsch-Murtèl 0315	Engadine	Rock glacier	783149	144734	2666	10	NW	Coarse blocks
Dreveneuse 0104	Chablais	Talus slope	557670	124805	1580	30	E	Coarse blocks
Flüela 0102	Engadine	Talus slope	791375	180575	2394	26	NE	Debris
Gemsstock 0106	Urner Alps	Crest	689781	161780	2940	50	NW	Bedrock
Gentianes 0102	Lower Valais	Moraine	589467	103586	2888	20	E	Debris
Jungfraujoch 0195	Bernese Oberland	Crest	641000	155120	3590	55	N	Bedrock
Lapires 0198	Lower Valais	Talus slope	588070	106080	2500	25	NE	Coarse blocks
Lapires 1108	Lower Valais	Talus slope	588099	106092	2500	25	NE	Coarse blocks
Lapires 1208	Lower Valais	Talus slope	588028	106027	2535	25	NE	Coarse blocks
Les Attelas 0108	Lower Valais	Talus slope	587196	105043	2661	30	W	Coarse blocks
Les Attelas 0208	Lower Valais	Talus slope	587243	105040	2689	30	W	Debris
Matterhorn 0205	Upper Valais	Crest	618399	92334	3295	0	–	Bedrock
Muot da Barba Peider 0196	Engadine	Talus slope	791314	152493	2946	38	NW	Debris
Muot da Barba Peider 0296	Engadine	Talus slope	791339	152513	2941	38	NW	Debris
Muragl 0199	Engadine	Rock glacier	791025	153726	2536	15	NW	Coarse blocks
Muragl 0299	Engadine	Rock glacier	790989	153687	2539	15	NW	Coarse blocks
Muragl 0499	Engadine	Rock glacier	791017	153688	2549	15	SW	Coarse blocks
Ritigraben 0105	Upper Valais	Rock glacier	631755	113775	2690	0	–	Coarse blocks
Schafberg 0190	Engadine	Rock glacier	790944	152590	2754	0	–	Coarse blocks
Schafberg 0290	Engadine	Rock glacier	790855	152745	2732	0	–	Coarse blocks
Schilthorn 5198	Bernese Oberland	Crest	630365	156410	2909	30	NE	Debris
Schilthorn 5000	Bernese Oberland	Crest	630350	156410	2910	30	NE	Debris
Schilthorn 5200	Bernese Oberland	Crest	630350	156410	2910	30	NE	Debris
Schilthorn 5318	Bernese Oberland	Crest	630343	156416	2910	30	NE	Debris
Stockhorn 6000	Upper Valais	Crest	629878	92876	3410	8	S	Debris
Stockhorn 6100	Upper Valais	Crest	629867	92850	3410	8	S	Debris
Tsaté 0104	Lower Valais	Crest	608499	106417	3050	30	W	Bedrock
Tsaté 0117	Lower Valais	Crest	608500	106416	3050	30	W	Bedrock

Table B.1b: Instrumentation of the boreholes.

Borehole	Since	Depth	Lowest S.	#Therm.	Sensors	Access	Calib.	Institution
	(m)	(m)						
Corvatsch-Murtèl 0200	2000	63.20	62.00	30	YSI 44006	remote	2000	ETHZ
Corvatsch-Murtèl 0287	1987	62.00	57.95	46	YSI 44006	remote	1997	UZH
Corvatsch-Murtèl 0315	2015	60.50	60.00	38	YSI 44031	remote	2015	UZH
Dreveneuse 0104	2004	15.00	14.50	12	MAAD	on site	2006	UNIFR
Flüela 0102	2002	23.00	20.00	12	YSI 46006	on site	2002	SLF
Gemsstock 0106	2006	40.00	39.50	27	YSI 44008	on site	2005	SLF
Gentianes 0102	2002	20.04	20.04	11	MAAD	on site	2002	UNIL
Jungfraujoch 0195	1995	19.7	19.70	9	YSI 46008	remote	2009	SLF
Lapires 0198	1998	19.60	19.60	12	YSI 44031	remote	1998	UNIFR
Lapires 1108	2008	40.00	39.00	28	YSI 44031	remote	2008	UNIFR
Lapires 1208	2008	35.00	34.00	18	YSI 44031	remote	2008	UNIFR
Les Attelas 0108	2008	26.00	24.00	12	YSI 44031	on site	2008	UNIL
Les Attelas 0208	2008	21.00	20.00	11	YSI 44031	on site	2008	UNIL
Matterhorn 0205	2005	53.00	52.90	12	YSI 44008	on site	2005	SLF
Muot da Barba Peider 0196	1996	18.00	17.50	10	YSI 44008	on site	1996	SLF
Muot da Barba Peider 0296	1996	18.00	17.50	10	YSI 44008	on site	1996	SLF
Muragl 0199	1999	70.20	69.70	18	YSI 44006	on site	1999	ETHZ
Muragl 0299	1999	64.00	60.00	22	YSI 44006	on site	1999	ETHZ
Muragl 0499	1999	72.00	69.59	22	YSI 44006	on site	1999	ETHZ
Ritigraben 0105	2002	30.00	14.00	30	YSI 44006	remote	2002	SLF
Schafberg 0190	1990	67.00	15.90	15	YSI 46006	on site	2005	SLF
Schafberg 0290	1990	37.00	25.20	10	YSI 46006	on site	1997	SLF
Schilthorn 5198	1998	14.00	13.00	14	YSI 44006	remote	1998	UNIFR
Schilthorn 5000	2000	101.00	100.00	30	YSI 44006	remote	1999	UNIFR
Schilthorn 5200	2000	100.00	87.00	19	YSI 44006	remote	1999	UNIFR
Schilthorn 5318	2018	30.00	30.00	26	YSI 44031	remote	2019	UNIFR
Stockhorn 6000	2000	100.00	98.30	30	YSI 44006	remote	2000	UNIFR
Stockhorn 6100	2000	31.00	17.00	18	YSI 44006	remote	2000	UNIFR
Tsaté 0104	2004	20.00	19.50	11	MAAD	on site	2006	UNIL
Tsaté 0117	2017	20.00	20.00	15	YSI 44031	remote	2017	UNIL

Attelas 0108

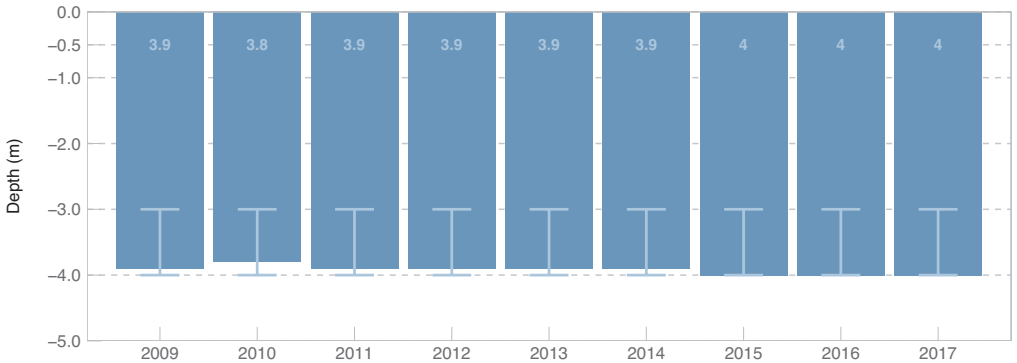

Figure B.1: *Active layer thickness determined at the borehole ATT 0108. The error bars indicate the depth of the thermistors used for the interpolation.*

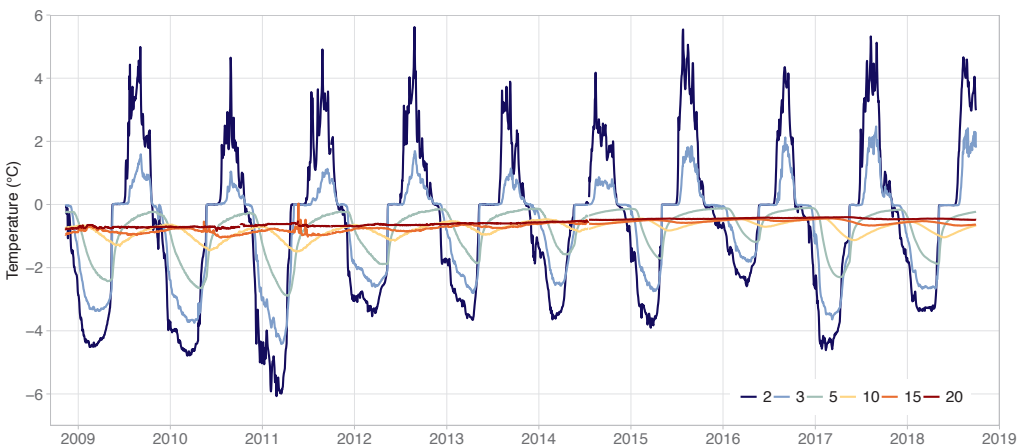

Figure B.2: *Temperature-time series measured in the Attelas 0108 borehole at depths of 2, 3, 5, 10, 15 and 20 metres.*

Attelas 0208

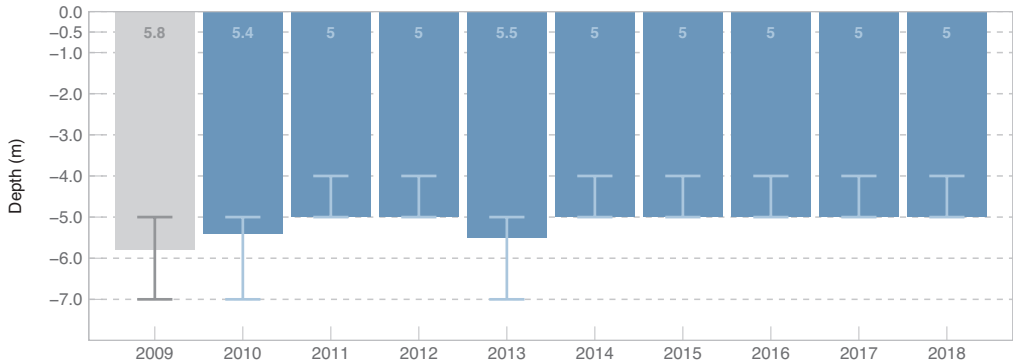

Figure B.3: *Active layer thickness determined at the borehole ATT 0208. The error bars indicate the depth of the thermistors used for the interpolation. Grey bars indicate years with reduced data quality.*

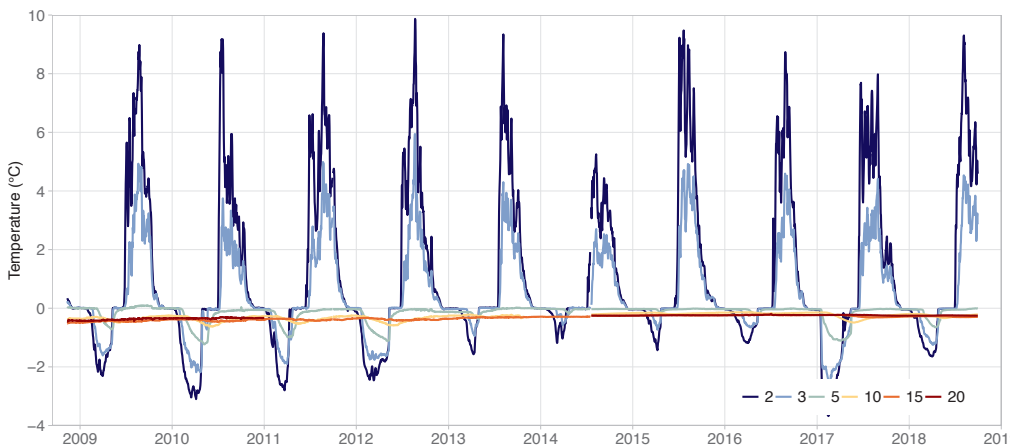

Figure B.4: *Temperature-time series measured in the Attelas 0208 borehole at depths of 2, 3, 5, 10, 15, and 20 metres.*

Corvatsch 0200

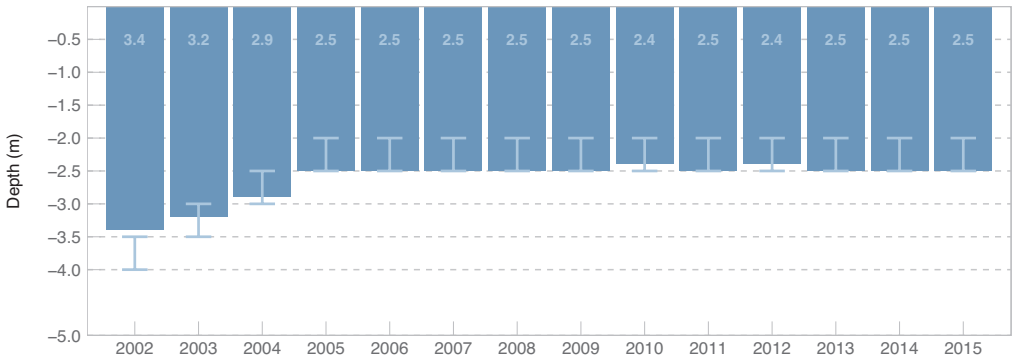

Figure B.5: *Active layer thickness determined at the borehole COR 0200. The error bars indicate the depth of the thermistors used for the interpolation.*

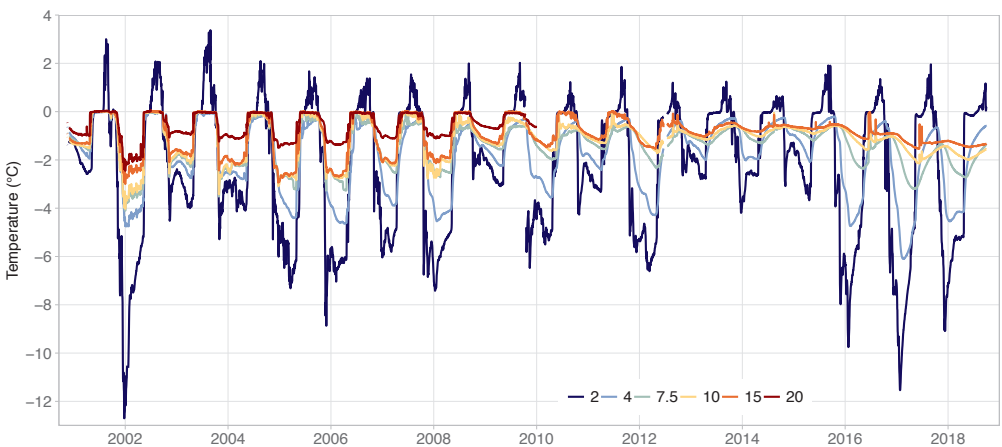

Figure B.6: *Temperature-time series measured in the borehole COR 0200 at depths of 2, 4, 7.5, 10, 15, and 20 metres.*

Corvatsch 0287

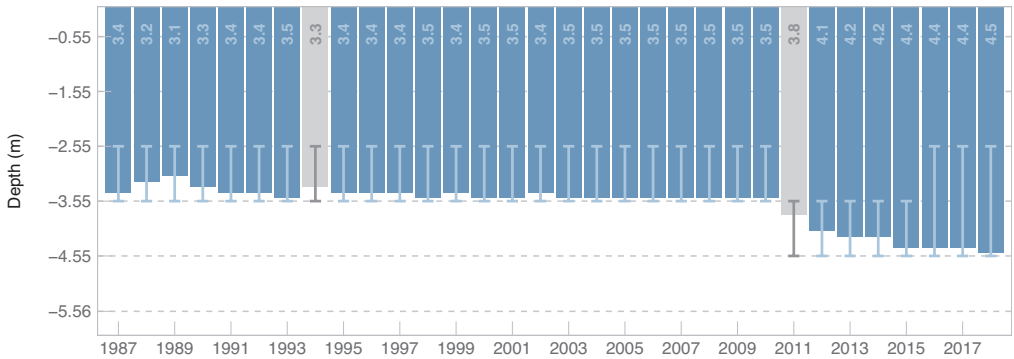

Figure B.7: *Active layer thickness determined at the borehole COR 0287. The error bars indicate the depth of the thermistors used for the interpolation. Grey bars indicate years with reduced data quality.*

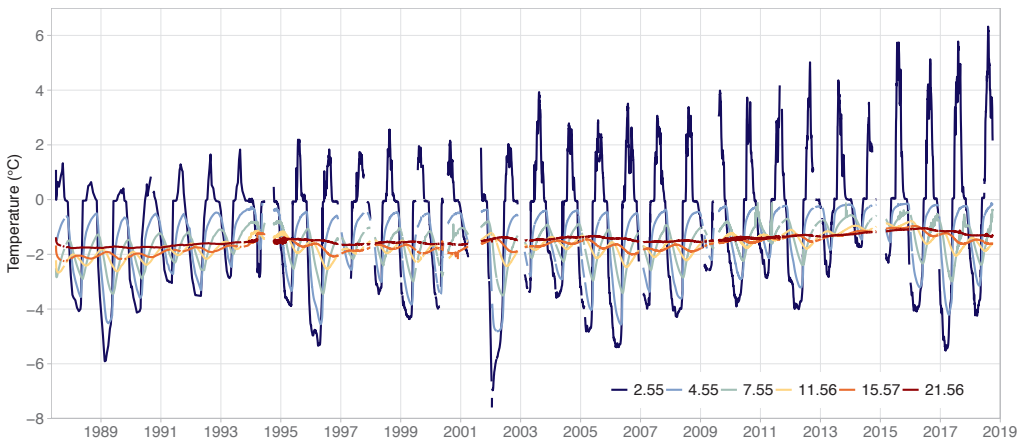

Figure B.8: *Temperature-time series measured in the borehole COR 0287 at depths of 2.55, 4.55, 7.55, 11.56, 15.57, and 21.56 metres.*

Corvatsch 0315

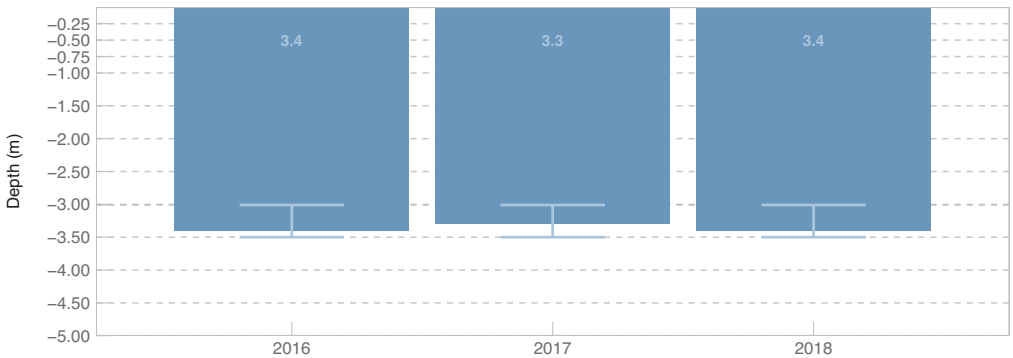

Figure B.9: *Active layer thickness determined at the borehole COR 0315. The error bars indicate the depth of the thermistors used for the interpolation.*

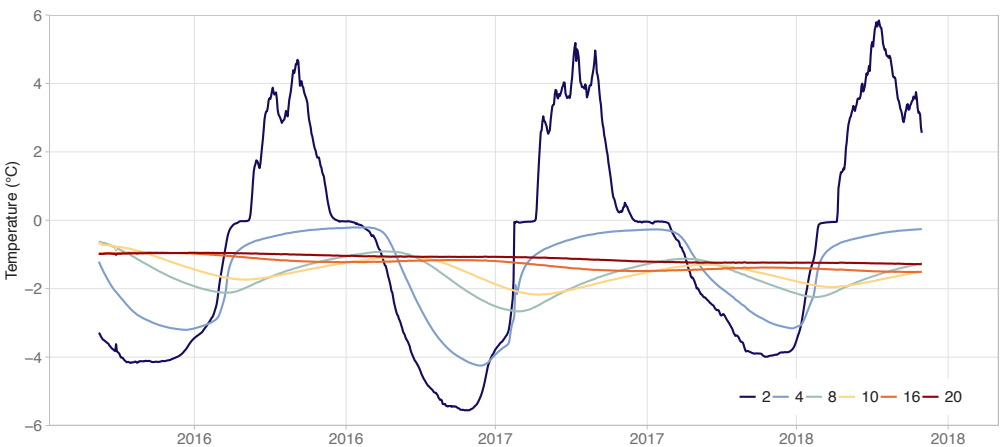

Figure B.10: *Temperature-time series measured in the borehole COR 0315 at 2, 4, 8, 10, 16 and 20 m depth.*

Dreveneuse 0104

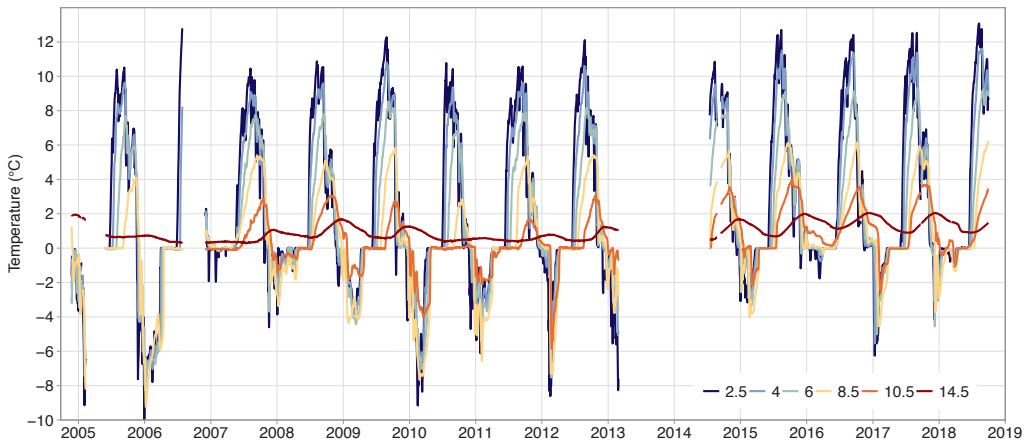

Figure B.11: Temperature-time series measured in the borehole DRE 0104 at 2.5, 4, 6, 8.5, 10.5 and 14.5 m depth.

Flüela 0102

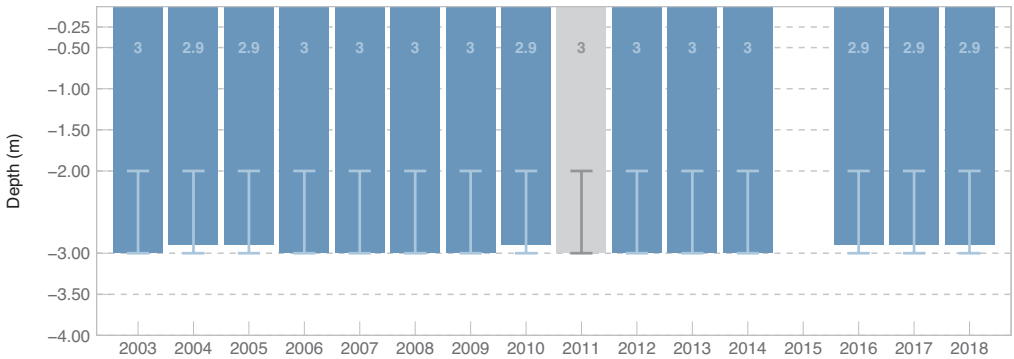

Figure B.12: Active layer thickness determined at the borehole FLU 0102. The error bars indicate the depth of the thermistors used for the interpolation. Grey bars indicate years with reduced data quality.

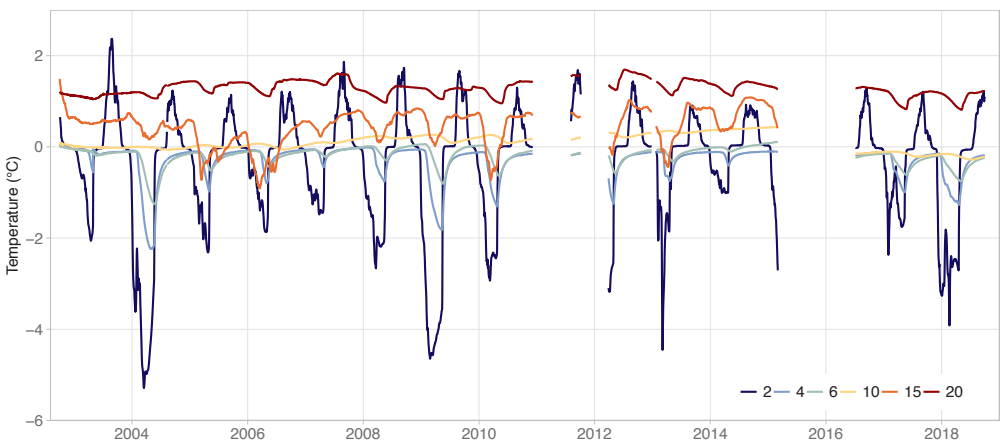

Figure B.13: Temperature-time series measured in the borehole FLU 0102 at 2, 4, 6, 10, 15 and 20 m depth.

Gemsstock 0106

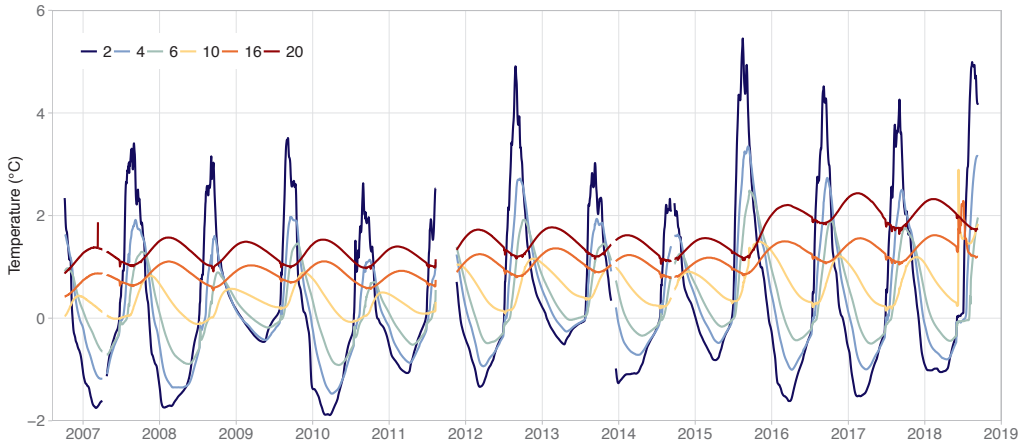

Figure B.14: Temperature-time series measured in the borehole GEM 0106 at 2, 4, 6, 10, 16 and 20 m depth. The borehole is drilled horizontally through the ridge from the north side.

Jungfraujoch 0195

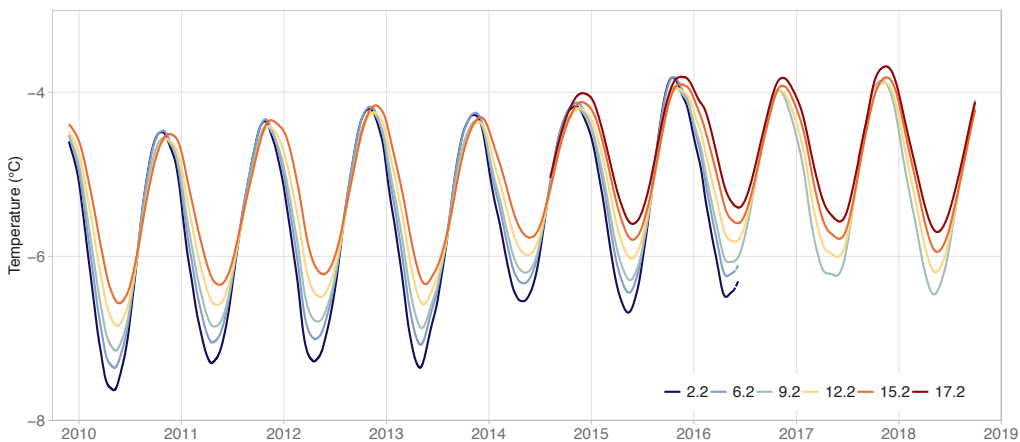

Figure B.15: Temperature-time series measured in the borehole JFJ 0195 at 2.2, 6.2, 9.2, 12.2, 15.2 and 17.2 m depth. The borehole is drilled from a tunnel towards the outside. Therefore larger thermistor depths are located closer to the surface.

Gentianes 0102

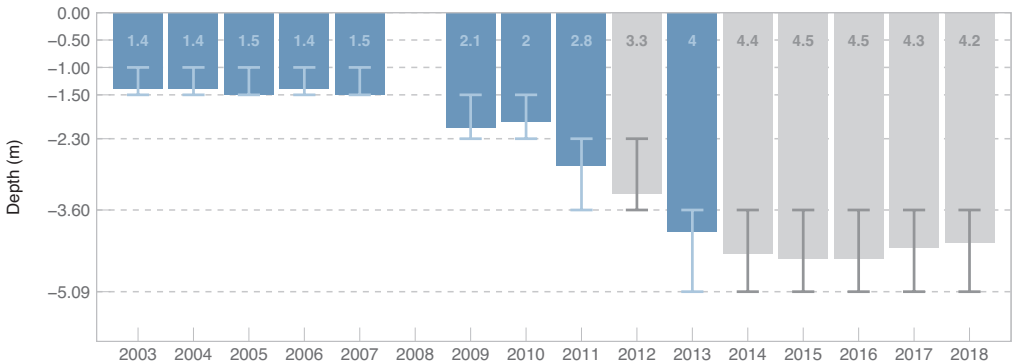

Figure B.16: *Active layer thickness determined at the borehole GEN 0102. The error bars indicate the depth of the thermistors used for the interpolation. Grey bars indicate years with reduced data quality.*

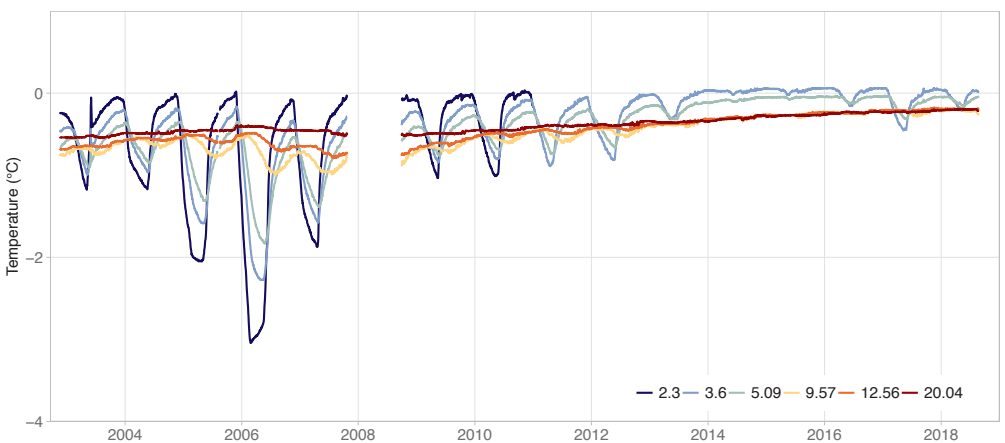

Figure B.17: *Temperature-time series measured in the borehole GEN 0102 at 2.3, 3.6, 5.09, 9.57, 12.56 and 20.04 m depth.*

Lapires 0198

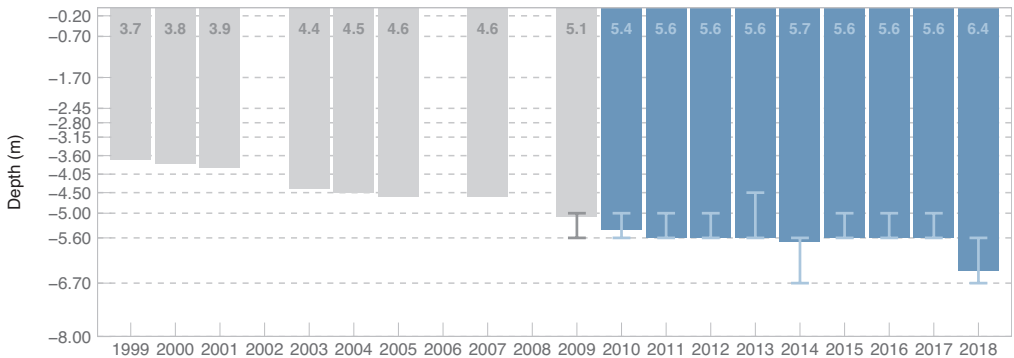

Figure B.18: Active layer thickness determined at the borehole LAP 0198. The error bars indicate the depth of the thermistors used for the interpolation. Grey bars indicate years with reduced data quality.

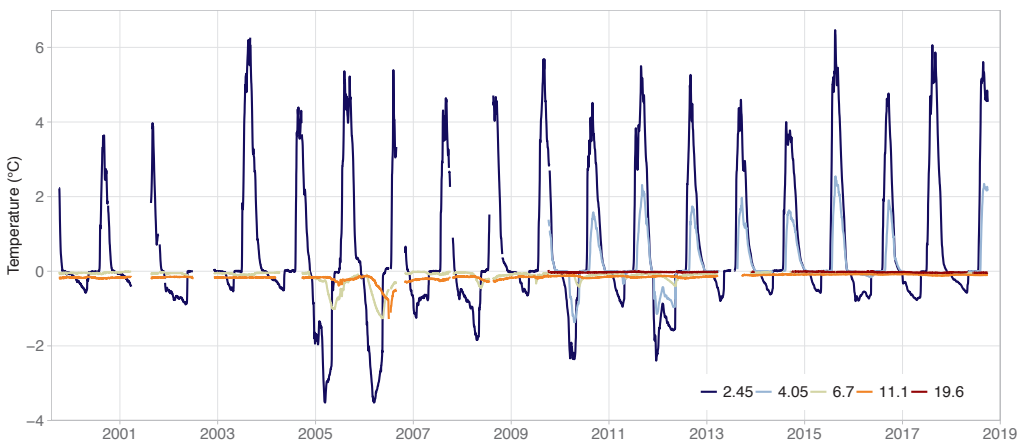

Figure B.19: Temperature-time series measured in the borehole LAP 0198 at 2.45, 4.05, 6.7, 11.1 and 19.6 m depth.

Lapires 1108

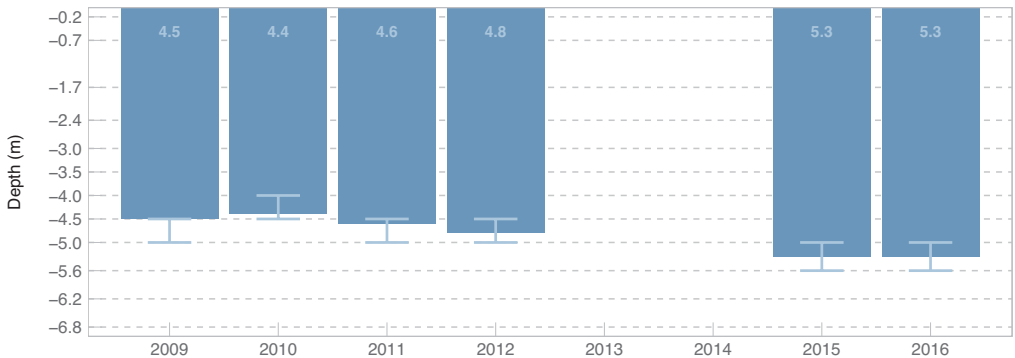

Figure B.20: *Active layer thickness determined at the borehole LAP 1108. The error bars indicate the depth of the thermistors used for the interpolation.*

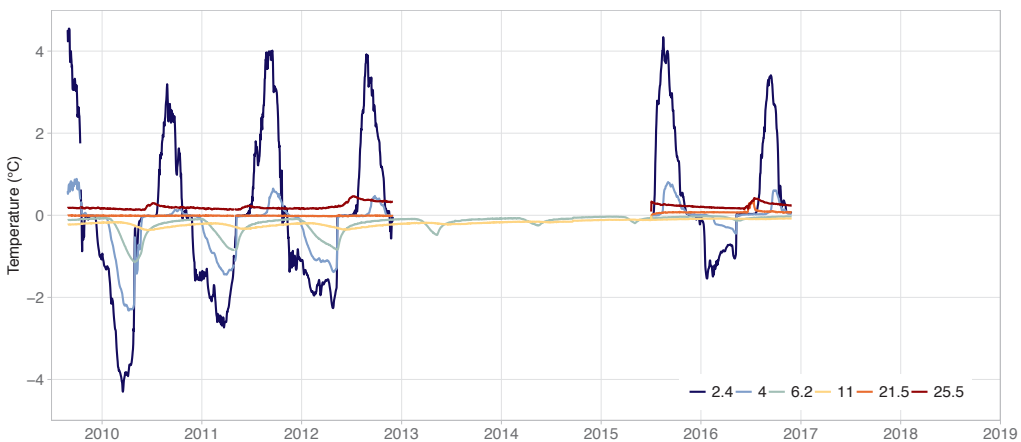

Figure B.21: *Temperature-time series measured in the borehole LAP 1108 at 2.4, 4, 6.2, 11, 21.5 and 25.5 m depth.*

Lapires 1208

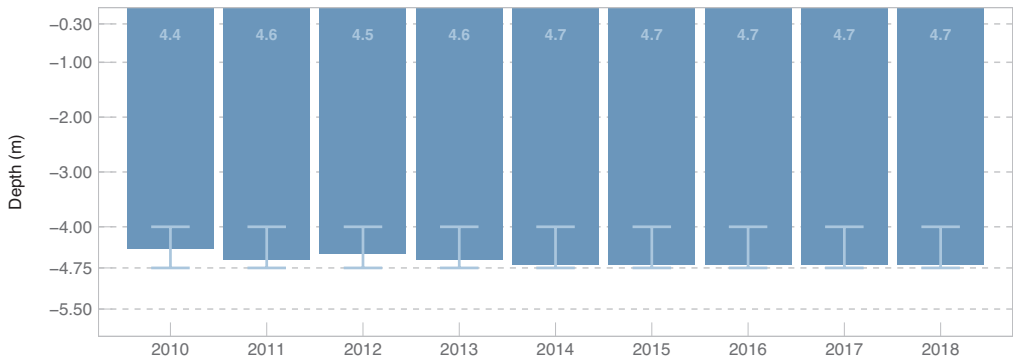

Figure B.22: Active layer thickness determined at the borehole LAP 1208. The error bars indicate the depth of the thermistors used for the interpolation.

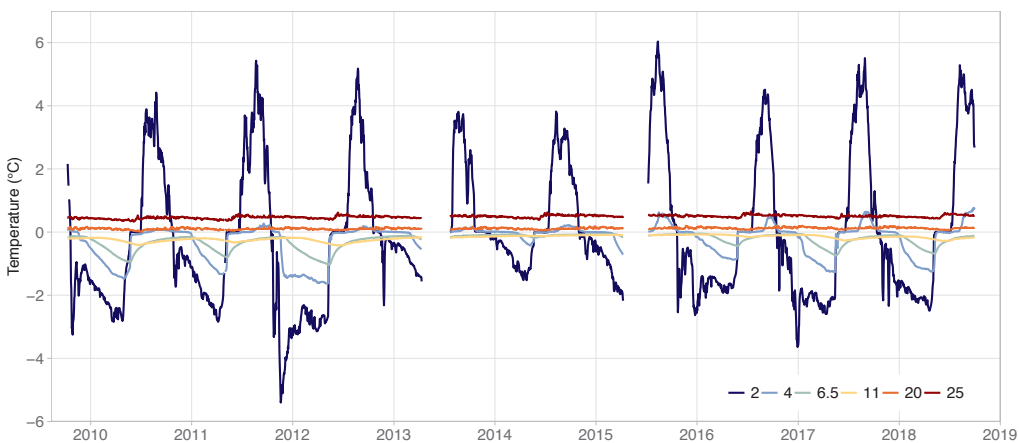

Figure B.23: Temperature-time series measured in the borehole LAP 1208 at 2, 4, 6.5, 11, 20 and 25 m depth.

Matterhorn 0205

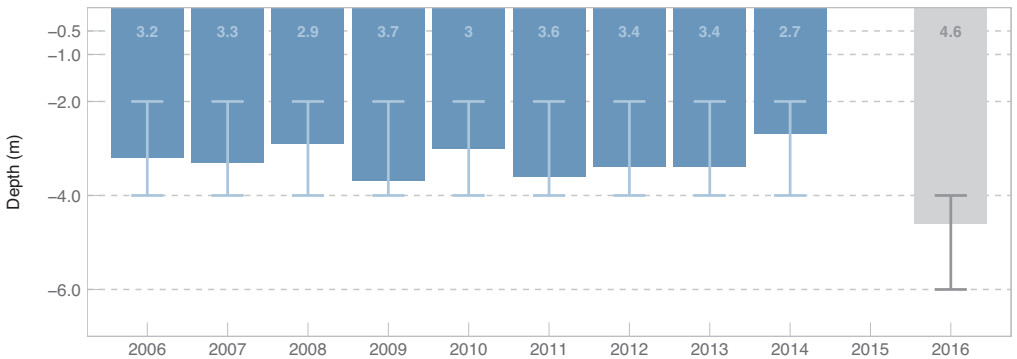

Figure B.24: *Active layer thickness determined at the borehole MAT 0205. TThe error bars indicate the depth of the thermistors used for the interpolation. Grey bars indicate years with reduced data quality.*

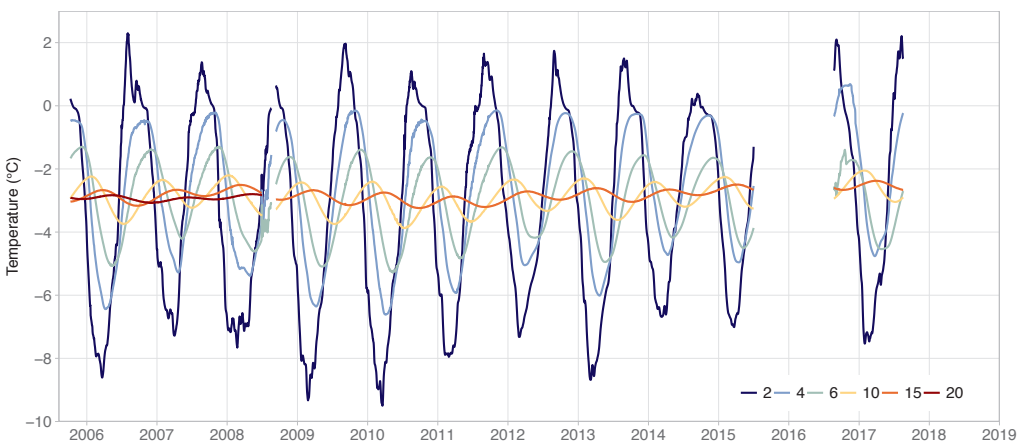

Figure B.25: *Temperature-time series measured in the borehole MAT 0205 at 2, 4, 6, 10, 15 and 20 m depth.*

Muot da Barba Peider 0196

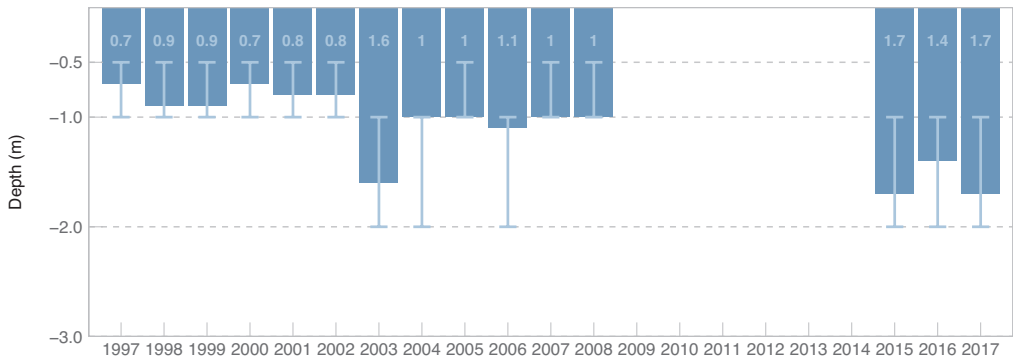

Figure B.26: Active layer thickness determined at the borehole MBP 0196. The error bars indicate the depth of the thermistors used for the interpolation.

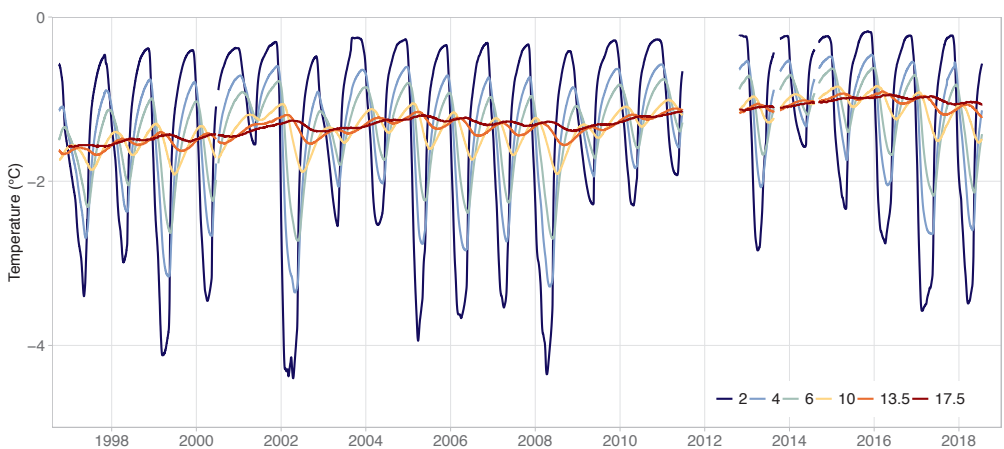

Figure B.27: Temperature-time series measured in the borehole MBP 0196 at 2, 4, 6, 10, 13.5 and 17.5 m depth.

Muot da Barba Peider 0296

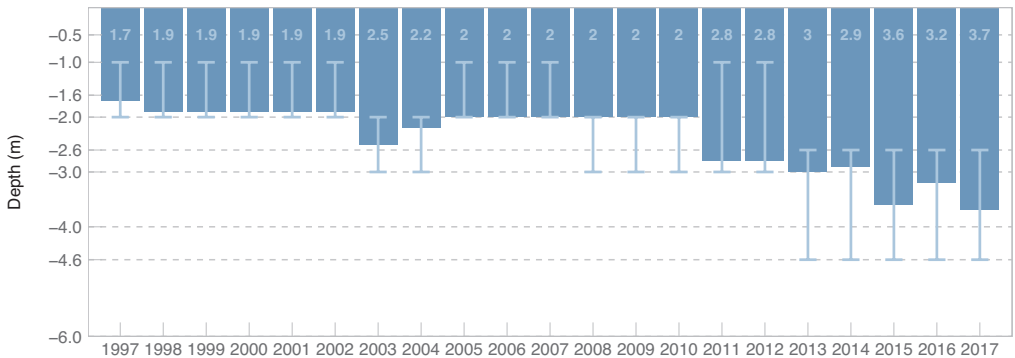

Figure B.28: *Active layer thickness determined at the borehole MBP 0296. The error bars indicate the depth of the thermistors used for the interpolation.*

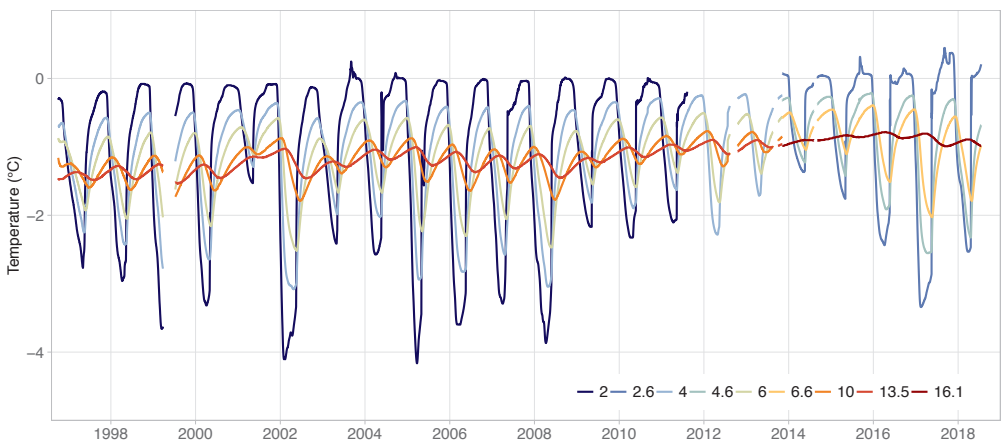

Figure B.29: *Temperature-time series measured in the borehole MBP 0296 at 2 , 4, 6, 10, 13.5 and 17.5 m depth.*

Muragl 0199

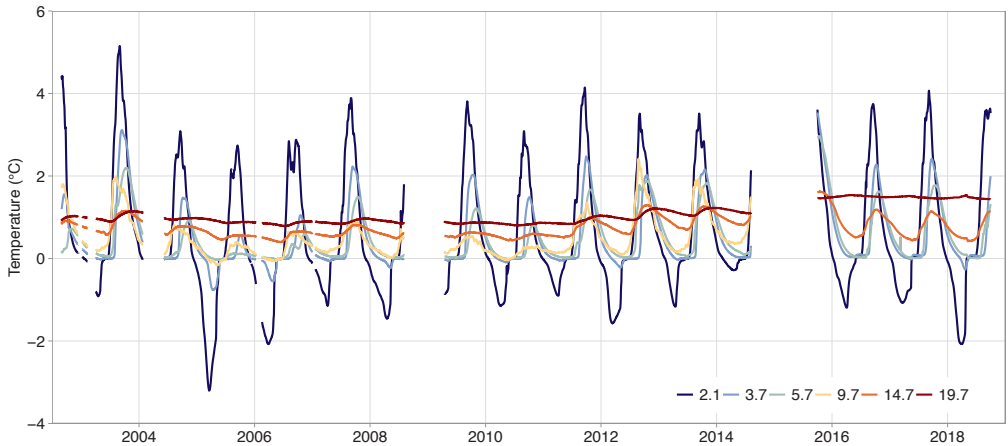

Figure B.30: Temperature-time series measured in the borehole MUR 0199 at 2.1, 3.7, 5.7, 9.7, 14.7 and 19.7 m depth.

Muragl 0299

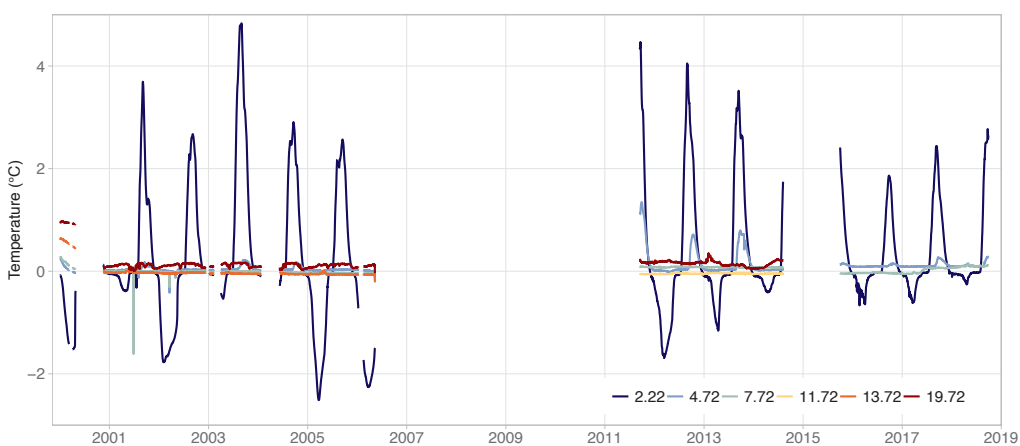

Figure B.31: Temperature-time series measured in the borehole MUR 0299 at 2.22, 4.72, 7.72, 11.72, 13.72 and 19.72 m depth.

Muragl 0499

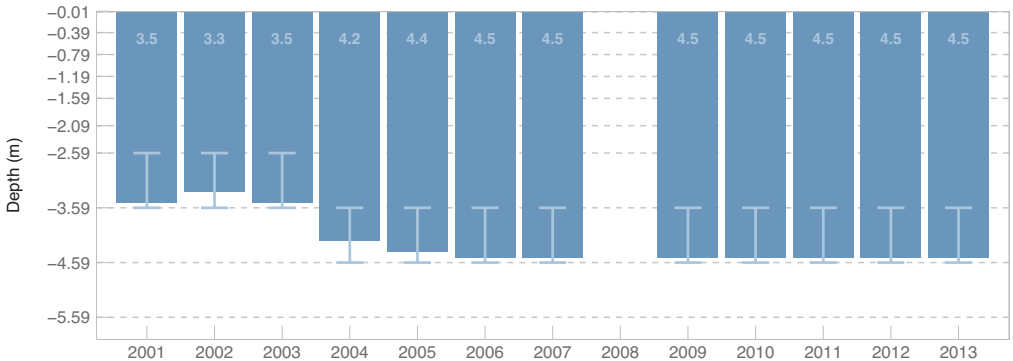

Figure B.32: Active layer thickness determined at the borehole MUR 0499. The error bars indicate the depth of the thermistors used for the interpolation.

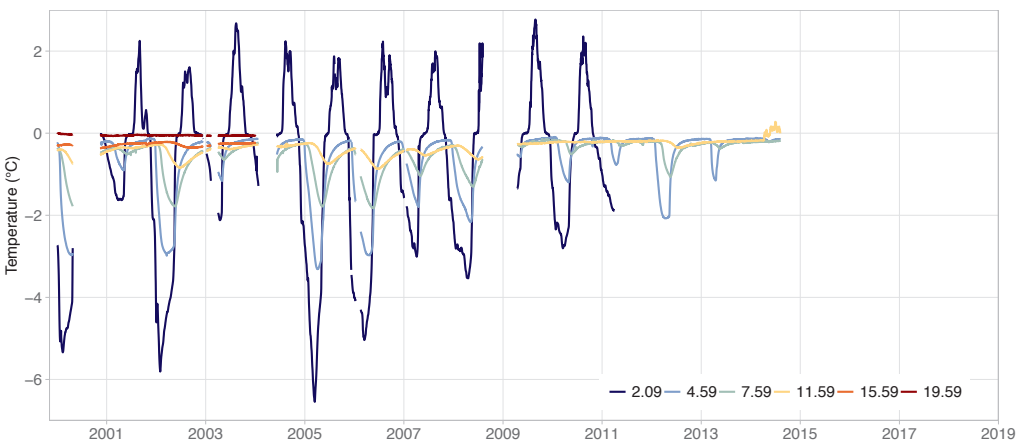

Figure B.33: Temperature-time series measured in the borehole MUR 0499 at 2.09, 4.59, 7.59, 11.59, 15.59 and 19.59 m depth.

Ritigraben 0102

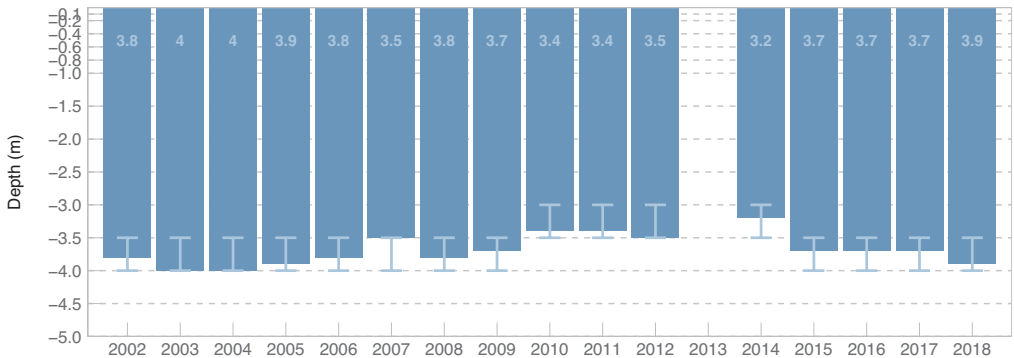

Figure B.34: Active layer thickness determined at the borehole RIT 0102. The error bars indicate the depth of the thermistors used for the interpolation.

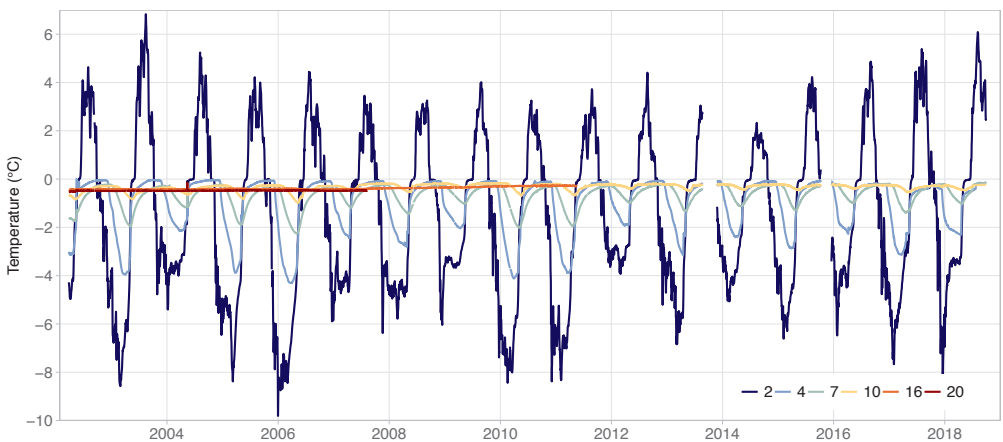

Figure B.35: Temperature-time series measured in the borehole RIT 0102 at 2, 4, 7, 10, 16 and 20 m depth.

Schafberg 0190

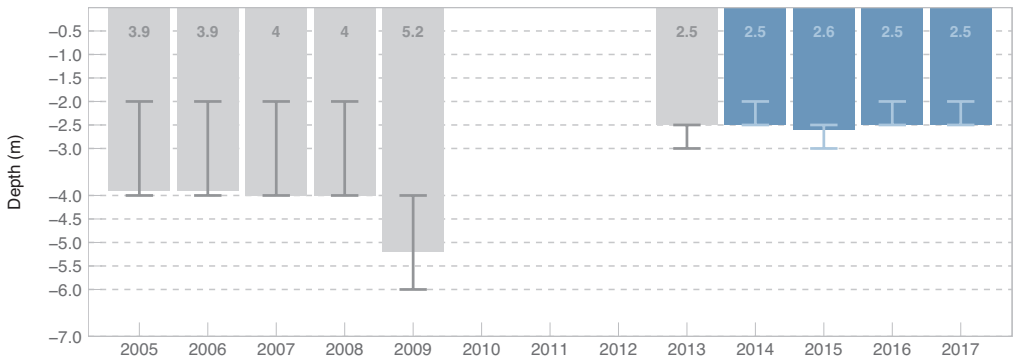

Figure B.36: *Active layer thickness determined at the borehole SBE 0190. The error bars indicate the depth of the thermistors used for the interpolation. Grey bars indicate years with reduced data quality.*

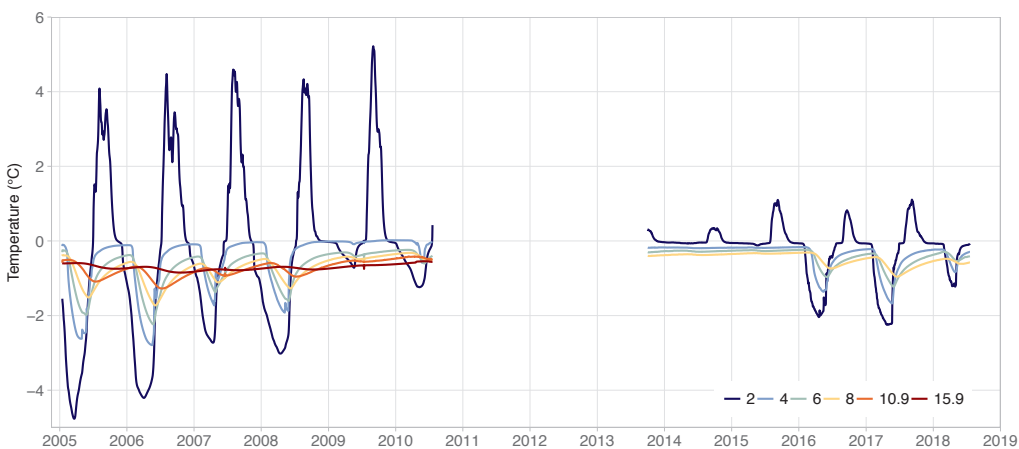

Figure B.37: *Temperature-time series measured in the borehole SBE 0190 at 2, 4, 6, 8, 10.9 and 15.9 m depth.*

Schafberg 0290

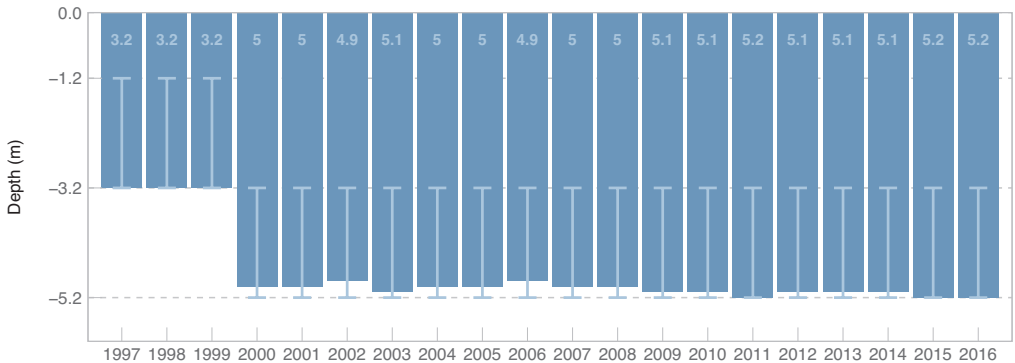

Figure B.38: Active layer thickness determined at the borehole SBE 0290. The error bars indicate the depth of the thermistors used for the interpolation.

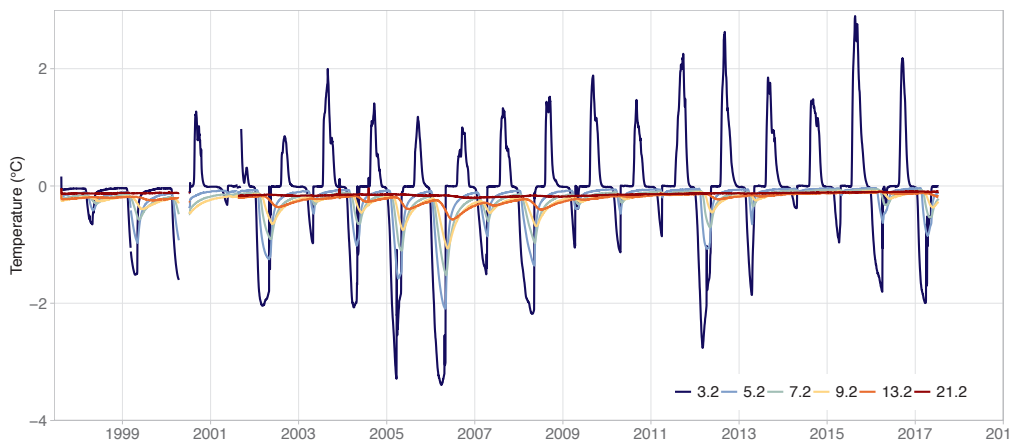

Figure B.39: Temperature-time series measured in the borehole SBE 0290 at 3.2, 5.2, 7.2, 9.2, 13.2 and 21.2 m depth.

Schilthorn 5000

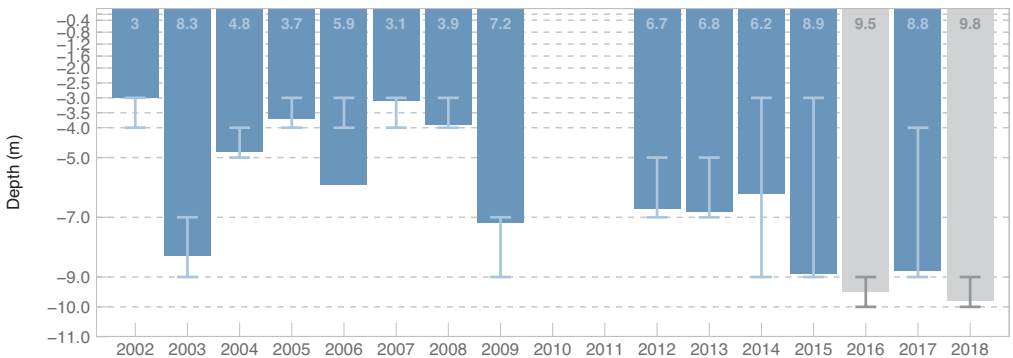

Figure B.40: *Active layer thickness determined at the borehole SCH 5000. The error bars indicate the depth of the thermistors used for the interpolation. Grey bars indicate years with reduced data quality.*

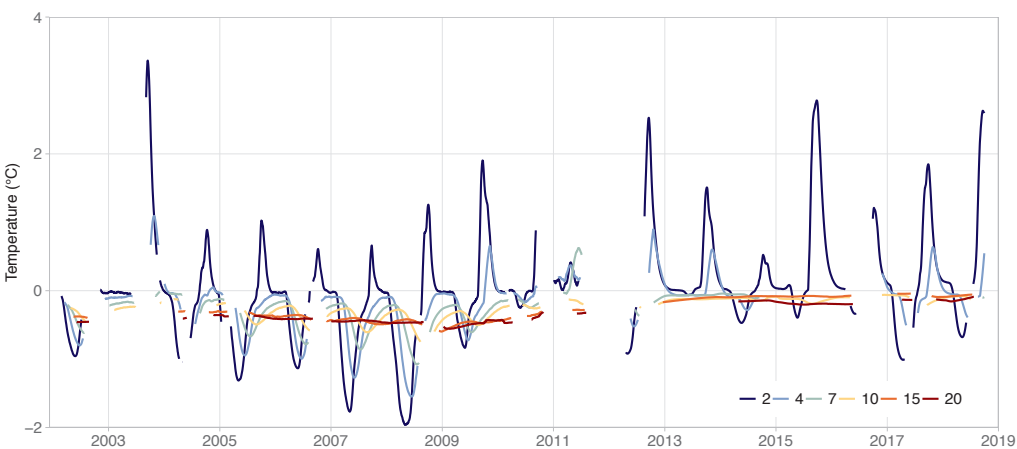

Figure B.41: *Temperature-time series measured in the borehole SCH 5000 at 2, 4 , 7, 10, 15 and 20 m depth.*

Schilthorn 5198

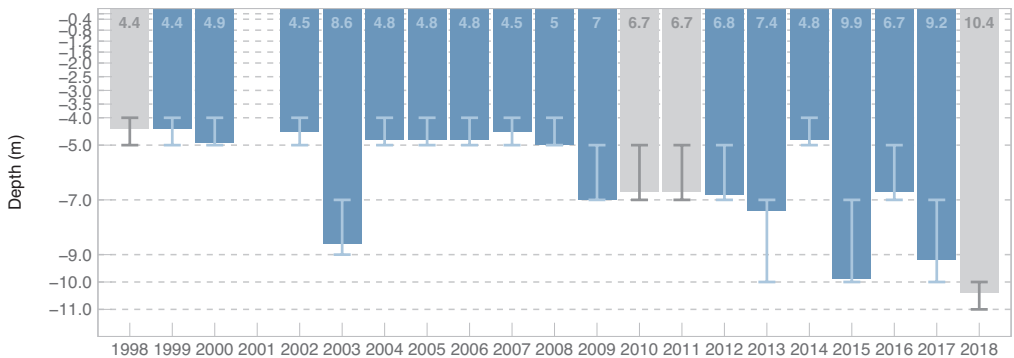

Figure B.42: *Active layer thickness determined at the borehole SCH 5198. The error bars indicate the depth of the thermistors used for the interpolation. Grey bars indicate years with reduced data quality.*

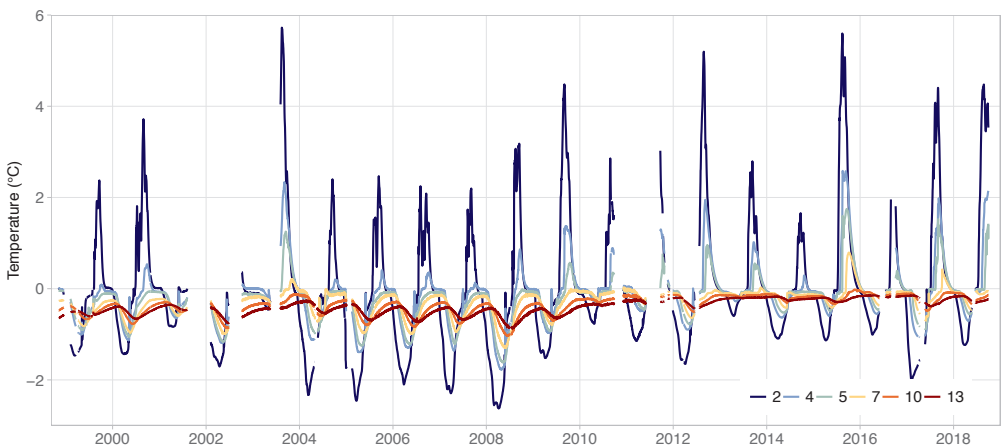

Figure B.43: *Temperature-time series measured in the borehole SCH 5198 at 2, 4, 5, 7, 10 and 13 m depth.*

Schilthorn 5200

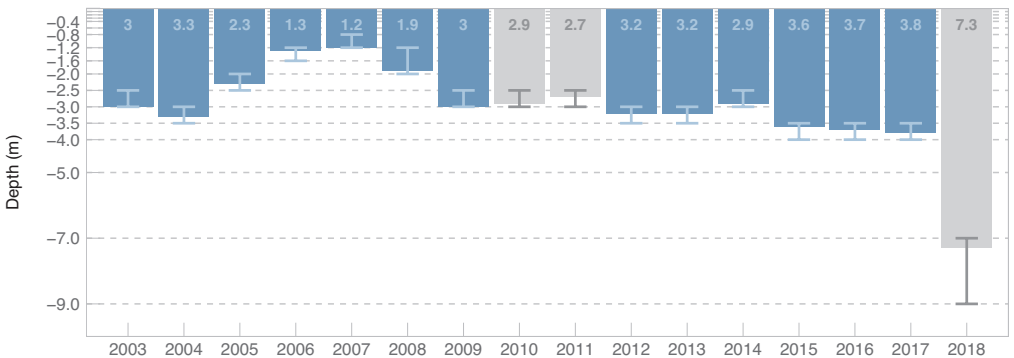

Figure B.44: Active layer thickness determined at the borehole SCH 5200. The error bars indicate the depth of the thermistors used for the interpolation. Grey bars indicate years with reduced data quality.

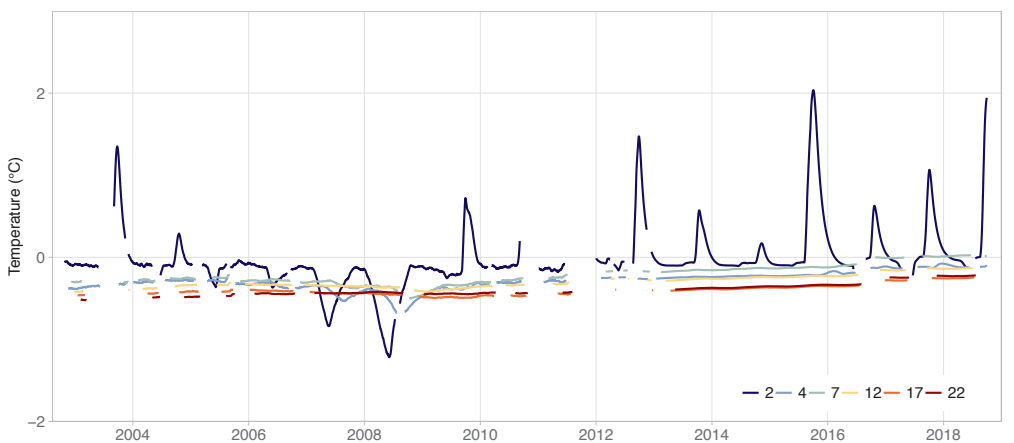

Figure B.45: Temperature-time series measured in the borehole SCH 5200 at 2, 4 , 7, 12, 17 and 22 m depth.

Stockhorn 6000

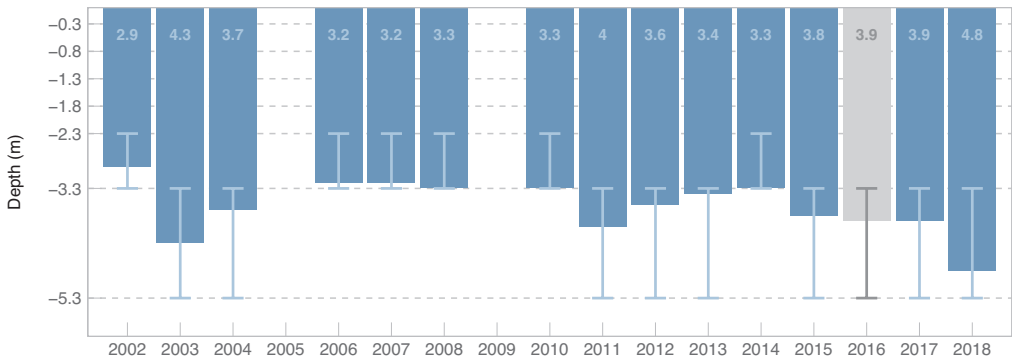

Figure B.46: Active layer thickness determined at the borehole STO 6000. The error bars indicate the depth of the thermistors used for the interpolation. Grey bars indicate years with reduced data quality.

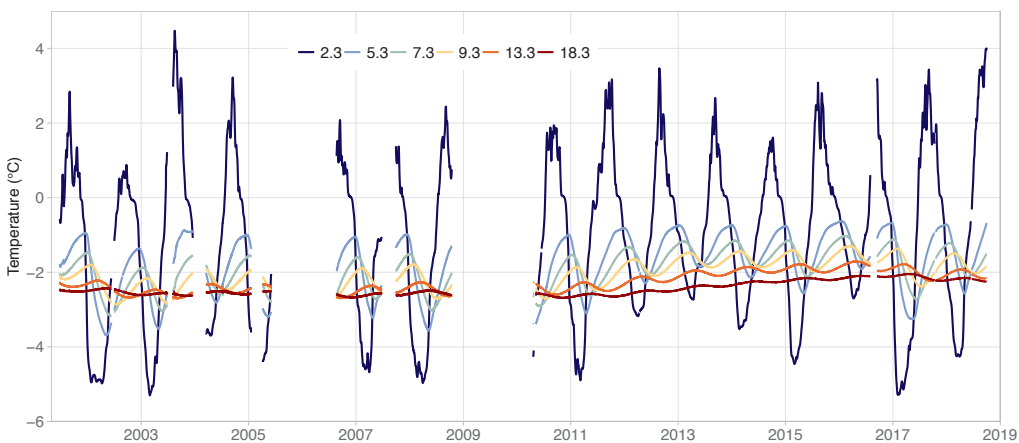

Figure B.47: Temperature-time series measured in the borehole STO 6000 at 2.3, 5.3 , 7.3, 9.3, 13.3 and 18.3 m depth.

Stockhorn 6100

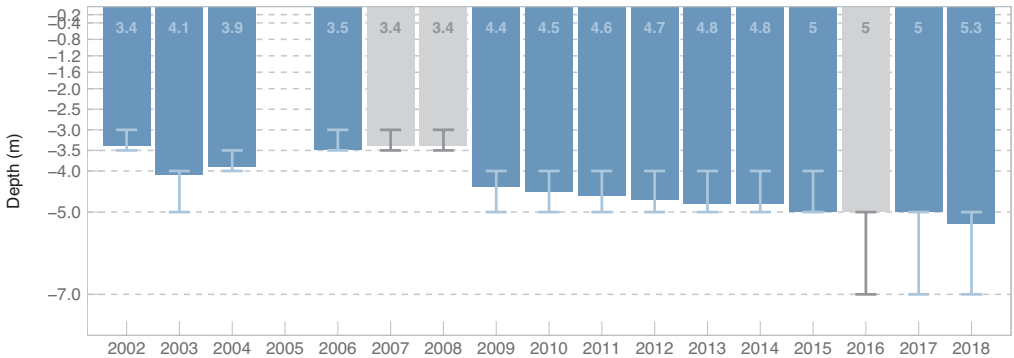

Figure B.48: Active layer thickness determined at the borehole STO 6100. The error bars indicate the depth of the thermistors used for the interpolation. Grey bars indicate years with reduced data quality.

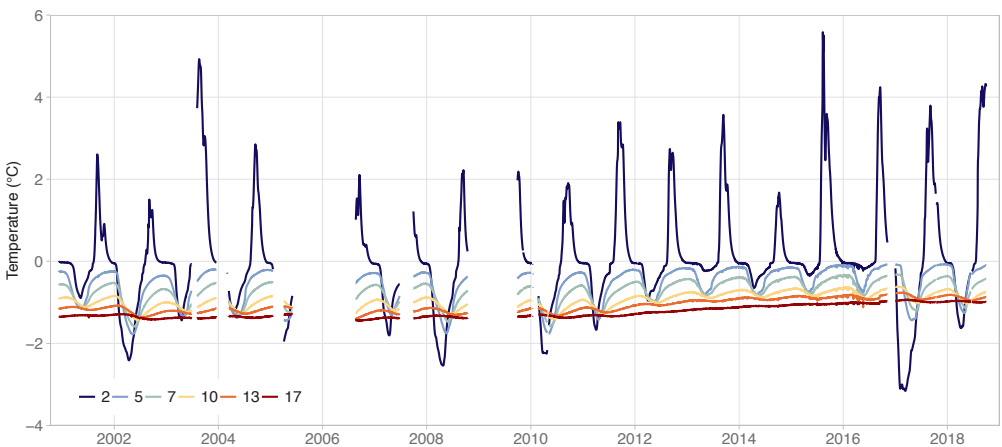

Figure B.49: Temperature-time series measured in the borehole STO 6100 at 2, 5 , 7, 10, 13 and 17 m depth.

Tsaté 0104

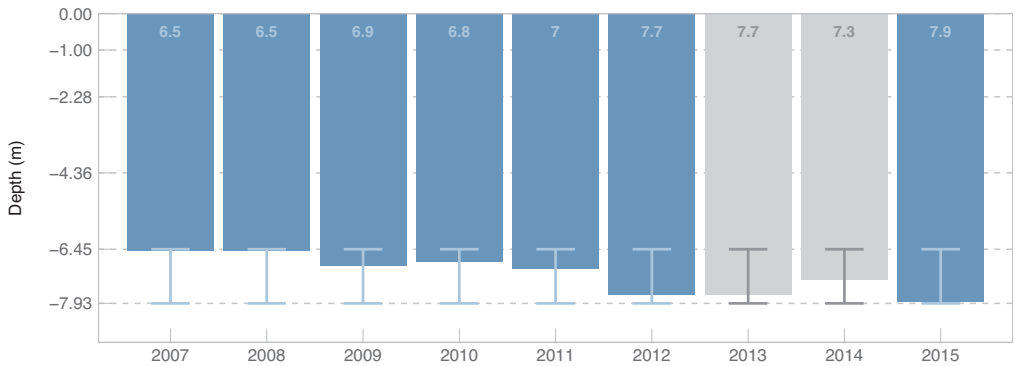

Figure B.50: *Active layer thickness determined at the borehole TSA 0104. The error bars indicate the depth of the thermistors used for the interpolation. Grey bars indicate years with reduced data quality.*

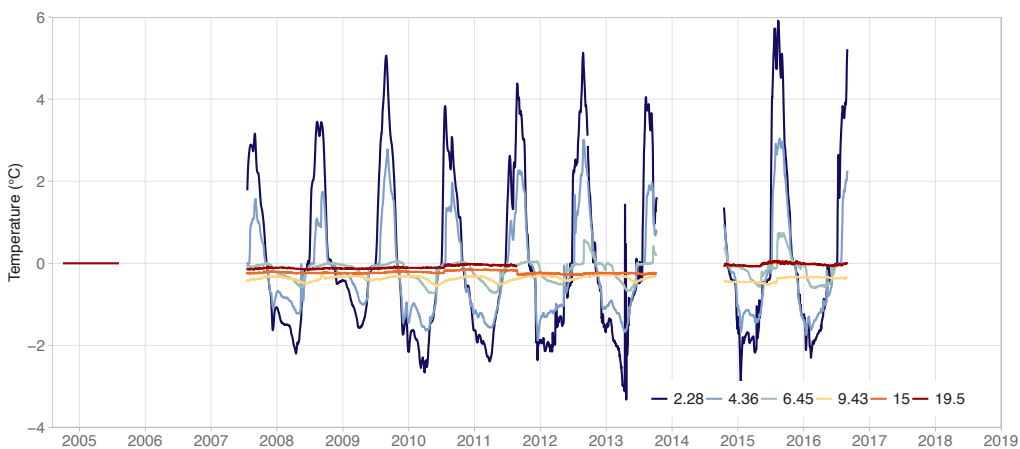

Figure B.51: *Temperature-time series measured in the borehole TSA 0104 at 2.28, 4.36, 6.45, 9.43, 15 and 19.5 metres.*

Tsaté 0117

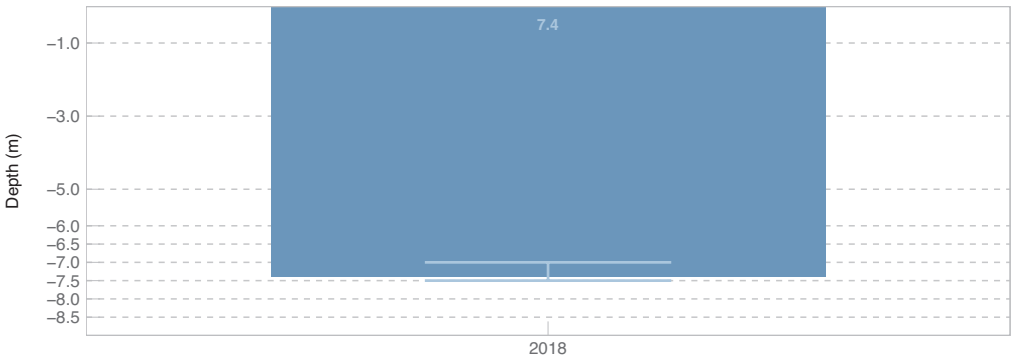

Figure B.52: Active layer thickness determined at the borehole TSA 0117. The error bars indicate the depth of the thermistors used for the interpolation.

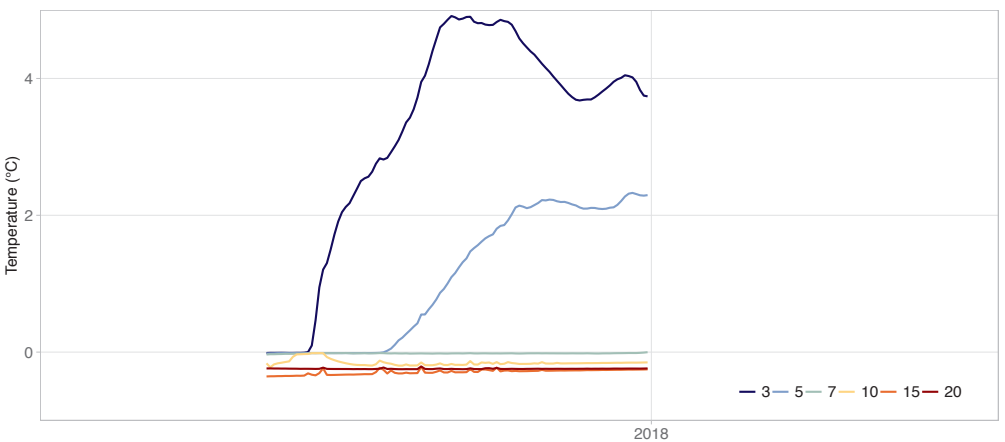

Figure B.53: Temperature-time series measured in the borehole TSA 0117 at 3, 5, 7, 10, 15 and 20 metres.

Appendix C

PERMOS Geophysics Sites

Table C.1: Sites where Electrical Resistivity Tomography surveys are conducted.

Site	Region	Aspect	Elevation (m asl.)	Start	Institution
Attelas	Lower Valais	W	2643–2729	2007	UniL
Lapires	Lower Valais	NE	2506–2510	2006	UniFR
Corvatsch-Murtèl	Engadine	NW	2623–2675	2005	UniFR
Schilthorn	Bernese Oberland	NE	2911–2913	1999	UniFR
Stockhorn	Upper Valais	S	3379–3415	2005	UniFR

Geophysics Attelas

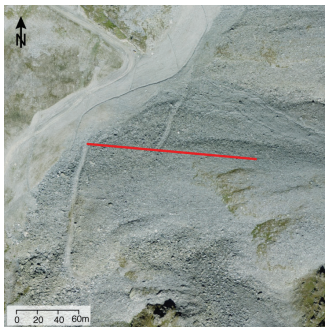

Source: Swiss Federal office for Topography

Location:	Attelas
Region:	Lower Valais
Type:	Talus slope
Lithology:	Micaschists
Length (m):	188
Spacing (m):	4
Number of electrodes:	48
Mean elevation (m asl.):	2686
Average slope (°):	25
Exposition:	W
Measurement begin:	2007
Institution:	UniL

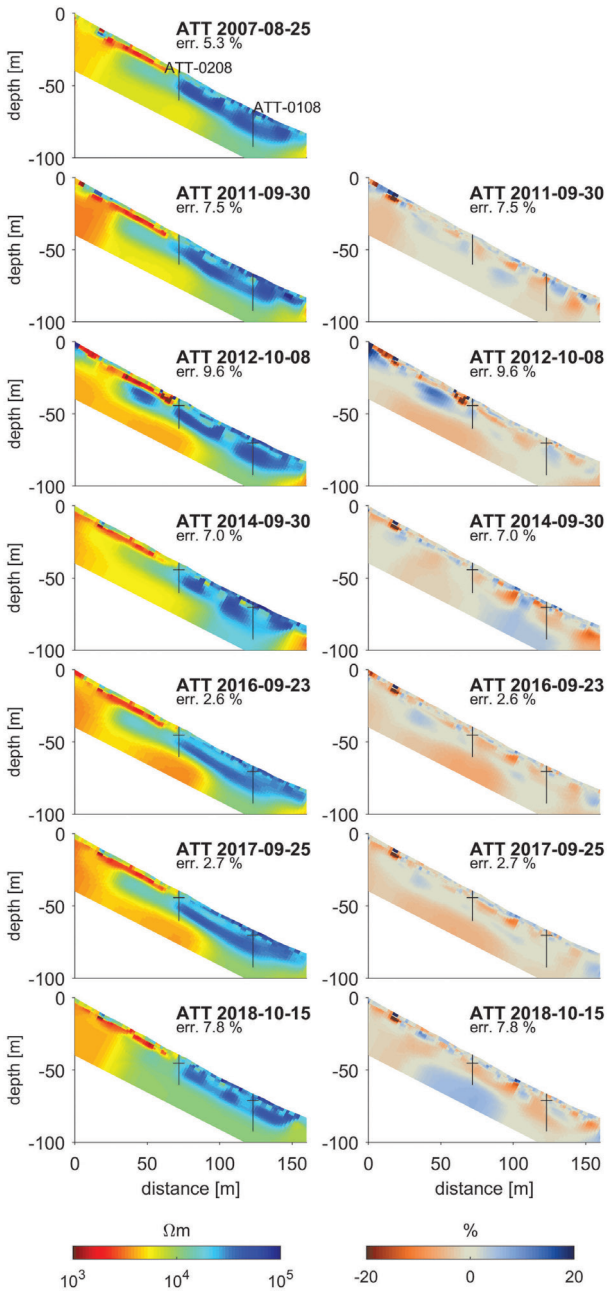

Figure C.1: Tomograms showing the resistivity distribution (left) and the temporal resistivity change (right) for the years 2007 to 2018 of the ERT profile in the Attelas talus slope. The vertical lines indicate the location of the boreholes and the horizontal ones the depth of the thaw layer

Geophysics Lapires

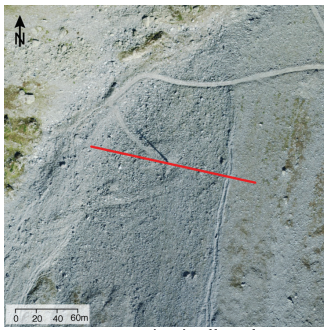

Source: Swiss Federal office for Topography

Location:	Lapires
Region:	Lower Valais
Type:	Talus slope
Lithology:	Paragneiss
Length (m):	168/136
Spacing (m):	4
Number of electrodes:	43/35
Mean elevation (m asl.):	2507
Average slope (°):	25
Exposition:	NE
Measurement begin:	2006/2013
Institution:	UniFR

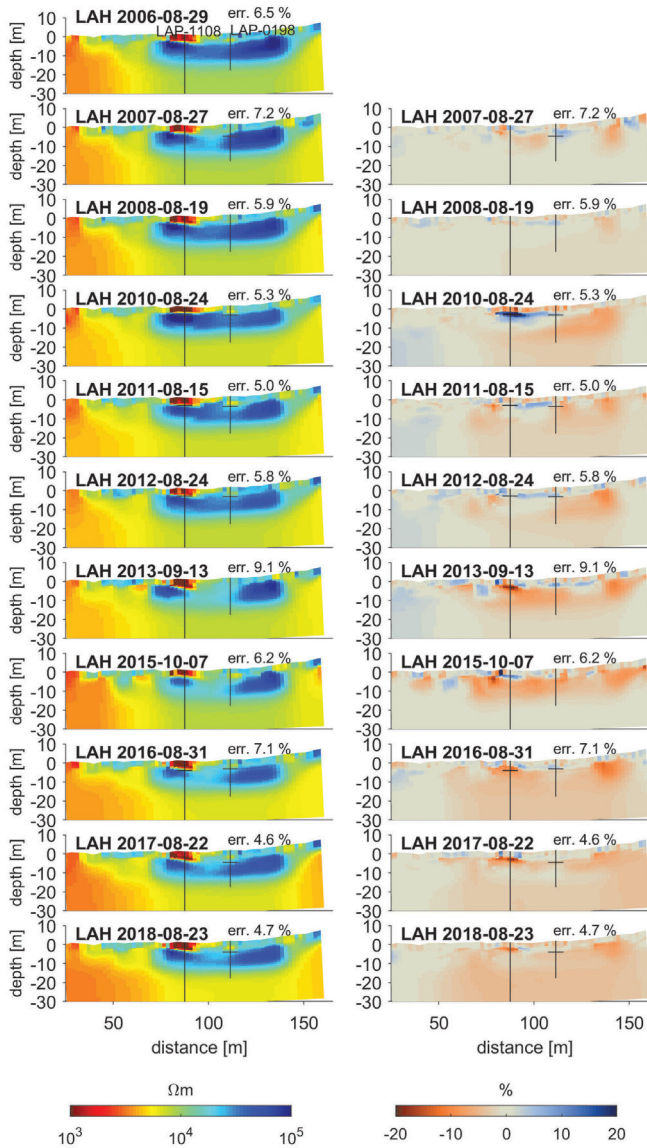

Figure C.2: Tomograms showing the resistivity distribution (left) and the temporal resistivity change (right) for the years 2006 to 2018 of the ERT profile in the Lapires talus slope. The vertical lines indicate the location of the boreholes and the horizontal ones the depth of the thaw layer

Geophysics Corvatsch-Murtèl

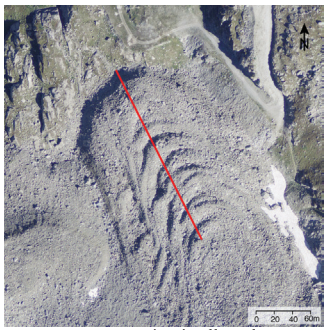

Source: Swiss Federal office for Topography

Location:	Corvatsch-Murtèl
Region:	Engadine
Type:	Rock glacier
Lithology:	Gneiss
Length (m):	235
Spacing (m):	5
Number of electrodes:	48
Mean elevation (m asl.):	2649
Average slope (°):	10
Exposition:	NW
Measurement begin:	2005
Institution:	UniFR

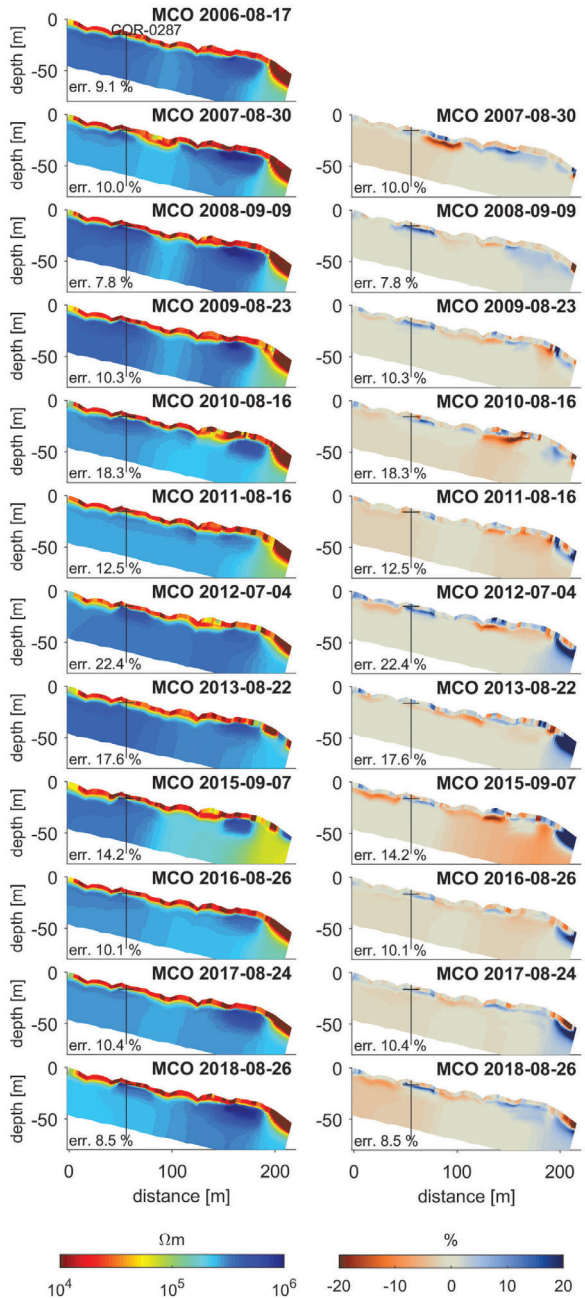

Figure C.3: Tomograms showing the resistivity distribution (left) and the temporal resistivity change (right) for the years 2006 to 2018 of the ERT profile in the Murtèl Corvatsch rock glacier. The vertical line indicates the location of the borehole and the horizontal one the depth of the thaw layer

Geophysics Schilthorn

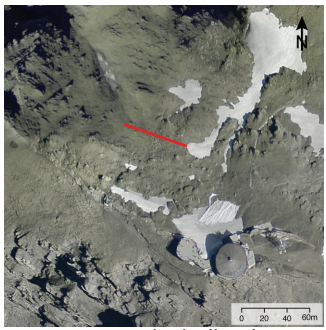

Source: Swiss Federal office for Topography

Location:	Schilthorn
Region:	Bernese Oberland
Type:	Crest
Lithology:	Limestone schists
Length (m):	58/96
Spacing (m):	2
Number of electrodes:	30/49
Mean elevation (m asl.):	2912
Average slope (°):	30
Exposition:	NE
Measurement begin:	1999/2012
Institution:	UniFR

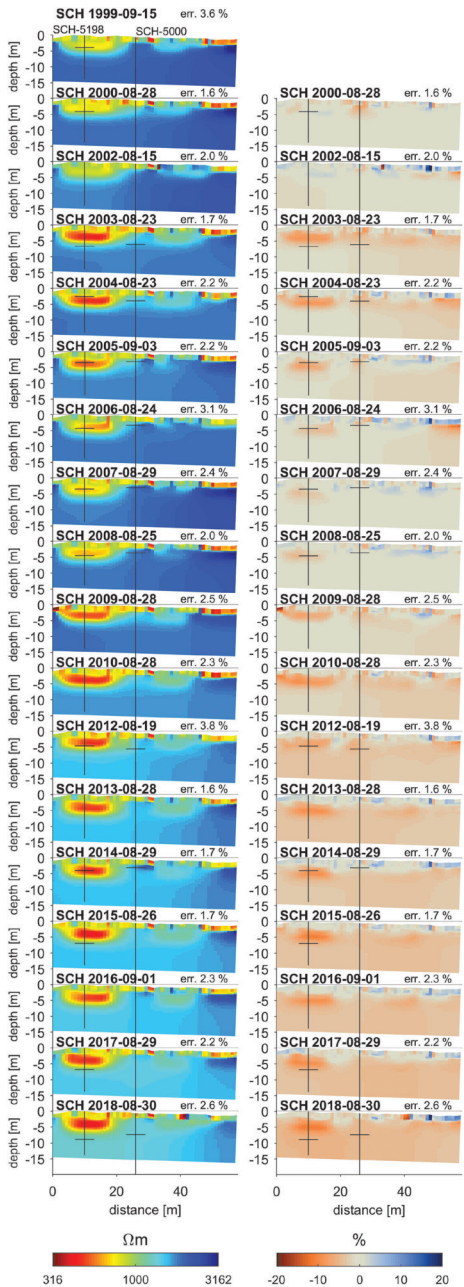

Figure C.4: Tomograms showing the resistivity distribution (left) and the temporal resistivity change (right) for the years 1999 to 2018 of the ERT profile in the Schilthorn mountain slope. The vertical lines indicate the location of the boreholes and the horizontal ones the depth of the thaw layer

Geophysics Stockhorn

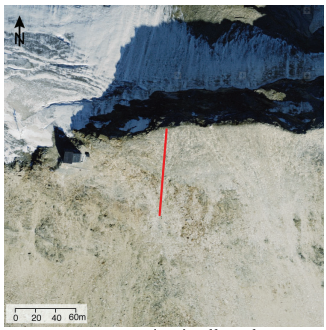

Source: Swiss Federal office for Topography

Location:	Stockhorn
Region:	Upper Valais
Type:	Crest
Lithology:	Albit-Muskovit schists
Length (m):	94/108
Spacing (m):	2
Number of electrodes:	48/55
Mean elevation (m asl.):	3397
Average slope (°):	8
Exposition:	S
Measurement begin:	2005/2007
Institution:	UniFR

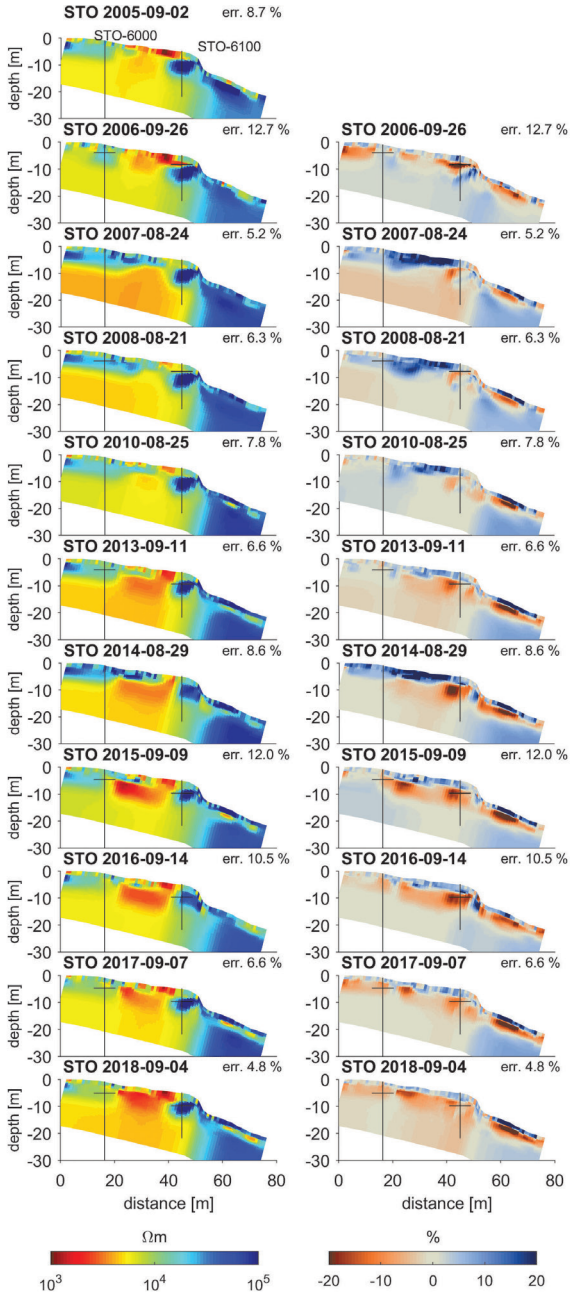

Figure C.5: Tomograms showing the resistivity distribution (left) and the temporal resistivity change (right) for the years 2005 to 2018 of the ERT profile on the Stockhorn crest. The vertical lines indicate the location of the boreholes and the horizontal ones the depth of the thaw layer